

UNIVERSITÀ DI PISA

Dipartimento di Fisica
Corso di Laurea Magistrale in Fisica

TESI DI LAUREA

Experimental methods for Rydberg Atomtronics

Relatore:
Prof. Oliver Morsch

Candidato:
Valerio Amico

Anno Accademico 2022/2023

Contents

1	Introduction	6
1.1	Rydberg Atomtronics	9
1.2	Dipole traps	10
1.2.1	Far-Off-Resonance optical dipole Trap: FORT	12
1.3	Atom and interactions	13
1.3.1	Rydberg atoms	14
1.3.2	Excite an atom on a Rydberg state	16
1.3.3	Van der Waals interaction between Rydberg atoms	20
1.3.4	Incoherent dynamics in the many-body system	21
1.3.5	Photoionization	26
1.4	The Mandel-Q factor	27
1.4.1	Mandel-Q with a noisy laser source.	31
2	Experimental set-up	36
2.1	Laser cooling	36
2.2	Dipole trap	39
2.3	Lasers for internal state control	40
2.3.1	Blue laser	40
2.3.2	Infrared laser	40
2.4	Detection	44
2.4.1	Detector limits	44
3	Characterization of the FORT	53
3.1	Experiment description	53
3.2	How many atoms?	57
3.2.1	A model for the number of atoms in the FORT	60
3.3	Estimation of the Photoionization rate	63

3.4	Loading of the FORT	65
3.4.1	Loading time experiment	66
3.4.2	A model for FORT loading	66
3.4.3	How to trap a single atom	72
4	Facilitation and dissipation for Rydberg Atomtronics	76
4.1	Facilitation on a many-body disordered system	81
4.1.1	A <i>facilitation</i> signature: the fluctuations	83
4.2	The artificial dissipation channel	86
4.2.1	Double dissipation experiment	88

A mamma, papà e Gabriele

Chapter 1

Introduction

The second quantum revolution is beginning. As transistors and other similar devices changed the world in the second half of the 1900s, today's new quantum technologies are paving the way for a new era of inventions that will revolutionize human life in the coming decades. *Atomtronics* and *Rydberg Atomtronics* [14], together with other disciplines such as quantum computing [26], fits into this scenario.

Atomtronics is a young research field which explores the use of matter-wave in the building of electronic-like circuits and devices. Differently from traditional electronic circuits, where electrons move on a conductor guide, in an *Atomtronics* device, atoms are cooled to very low temperatures (nK), and then coherently moved in either optical or magnetic guides [14]. In *Rydberg Atomtronics*, instead, the aim is to establish a new concept of quantum circuits in which Rydberg¹ excitations, instead of matter, can flow in atomic networks created using light-induced traps [19]. Rydberg atoms were chosen for their peculiar properties such as strong polarizability, long-range dipole interactions, and long lifetimes. Long-range interactions [6] between Rydberg atoms are proposed to be used to control the propagation of the Rydberg excitation through the atom array [20].

Many applications are possible for this new technology. In *Atomtronics*, analogues of basic electronic devices have been proposed and realized, such as batteries, capacitors, transistors, and diodes [21] [22]. Analogues to superconducting SQUIDS,

¹A Rydberg atom is an atom in a state with a high principal quantum number [4].

called AQUIDs, have been realized [23]. There are proposals and experiments for quantum sensing devices [24] [25] used for high-precision measurements of electric and magnetic fields (the polarizability of Rydberg atoms strongly depends on the principal quantum number), which could help in answering the most challenging questions of fundamental physics [25]. Hybrid *Rydberg Atomtronics* / *Atomtronics* devices, in which both the internal and external states of the atoms are artificially controlled, could be developed, resulting in more versatile devices. This work is the first step of a long-term project that aims to realize a *Rydberg Atomtronics* circuit. The first target of this long-term project is to set up a ring-shaped network of ^{87}Rb atoms, which then are driven by lasers to Rydberg states. Moreover, using microwaves, it is possible to drive transitions between close Rydberg states [35]. With this set up different processes can be explored. In [20] it was proposed to study chiral currents of Rydberg excitations along the ring of Rydberg atoms, to develop new methods to transport information in atomic networks. Ref. [12] experimentally shows a signature of the *absorbing-state phase transition* on a cold-atoms many-body system demonstrating that such a system belongs to the directed percolation universality class [10], where a system switches from an absorbing inactive to a fluctuating active phase.

The goal of this thesis is to prepare the necessary tools and methods for a long-term project that aims to achieve a Rydberg Atomtronics circuit experimentally. The essential tools required for this project include dipole traps for trapping atoms, lasers for driving them from ground to Rydberg state and vice versa, and a detection system. During the course of my thesis, I was involved in building and characterizing a dipole trap. In this process, I aimed to determine the loading time and the number of atoms trapped. Our readout system consists of ionizing (either through photoionization or Rydberg excitation followed by field-ionization) the atoms to allow us to accelerate the resulting ions towards the detector² with the help of an electrostatic field. I proposed and tested an experimental method to efficiently estimate the number of atoms in the dipole trap using photoionization readout, which proved to be challenging due to ions repulsion resulting in loss (of the ions) during the detection process, so that only measurements of a few ions could be possible. The loading time of the trap is another relevant quantity be-

²The detector is a charge multiplier. For each arriving ion it sends a spike to an oscilloscope, which counts them.

cause it permits us to optimize the experiment by decreasing its duration without affecting the results. Furthermore, I also proposed and tested a model to describe the loading of a dipole trap and used this model to discuss how a single atom could be trapped. Additionally, I noticed that the same method used for estimating the number of trapped atoms could be used to determine the photoionization rate, which enabled us to calibrate our detection system when a photoionization readout is used.

To fulfill the ultimate goal, we need three channels³ to control the state of the atoms. One that is resonant with the ground-Rydberg transition, thus allowing us to excite an atom in the Rydberg state (*excitation channel*). One, which is detuned from the transition, so it can be used for conditioned excitations (*facilitation channel*). In fact, thanks to *facilitation* [13], we can excite a ground-state atom with an off-resonant driving laser only if another Rydberg atom is in close proximity. Finally, we required a last (*dissipation*) channel, which allows us to artificially control the lifetime of the Rydberg state, and so speed up the dynamics. Recently, it was observed that black body radiation induced transitions becomes relevant after $\sim 100 \mu s$ in our set-up [32]. Since the timescales of the system dynamics are governed by the Rydberg atom lifetime⁴, in order to make the black-body transitions negligible, we need to speed up the dynamics; in other words, we need an artificial *dissipation channel*. *Dissipation* and *facilitation* had already been studied independently in the same lab where I conducted this thesis. Particularly, *dissipation* was studied by G. Cichelli [38] and *facilitation* by C. Simonelli [37]. One of the aims of this thesis is to combine both channels in a unique setup and test them together. As there is no atom array yet, we will use a many-body disordered system of cold atoms to test these channels.

In this chapter I will introduce the theory behind dipole traps and Rydberg atoms. The experimental set-up is explained in the second chapter. The third chapter is about the characterization of our dipole trap: loading and number of trapped atoms are investigated experimentally, followed by a discussion on how a single atom could be trapped. In the last chapter, two experiments on the dissipation and interaction of Rydberg atoms are presented with the aim of testing the *dissipation*

³I call *channel* a laser (or more), which drives the atoms in a certain transition.

⁴For our target state, $|70s_{1/2}\rangle$ the lifetime is $\tau = 151 \mu s$.

and *facilitation* channels.

1.1 Rydberg Atomtronics

This thesis is the beginning of a series of experiments that aim to build a Rydberg Atomtronic device able to demonstrate some proposed applications, such as electronic-like diodes and transistors. In figure 1.1 two examples of device are graphically represented. To understand these schemes one has to imagine that each point is an atom trapped with optical tweezers. Then each atom is driven by a laser beam. The colours of the point represents the detuning (reported in the figure as well) of the driving laser. The red points (source) correspond to atoms that are resonantly coupled to a Rydberg state by a driving laser. The light blue points (drain), instead, are driven by an off-resonant (blue-detuned) laser, which is chosen to be resonant with the shifted Rydberg level because of the Van der Waals interaction. As I will show in section 1.3 of this chapter, the interactions play a role only if at least one of the interacting atoms is in the excited (Rydberg) state. So, you will have a propagation of the Rydberg excitation through the drain only if the last right atom in the source region is excited, otherwise no propagation of the excitation will be observed at all. If one put an atom more between the source and the drain (figure 1.1 top) it will be possible to use this atom as a gate: by choosing the detuning of the driving laser it will be possible to control the excitation propagation through the chain. The study of the Rydberg excitation transport through an atoms chain is beyond the scope of this thesis. This introduction is a qualitative overview that aims to intuitively introduce the final long-term project.

To realize such devices, first of all, it is necessary to trap atoms. There are several ways to restrict atoms in a chosen position in space, such as doppler and sub-doppler cooling, dipole traps (blue and red detuned), optical lattices, and magnetic cooling. They have been studied in the last few decades and merits and defects have been explored. To realize a *Rydberg Atomtronics* device we need a technique which permits us to have a good control of the number of trapped atoms, particularly that would permit us to trap a single atom. Dipole traps are the best candidates for this aim, several works already have proposed and realized methods to use dipole traps to isolate a single atom [1]. Those methods also allow one to fine control the distance between two atoms, to make them interact efficiently.

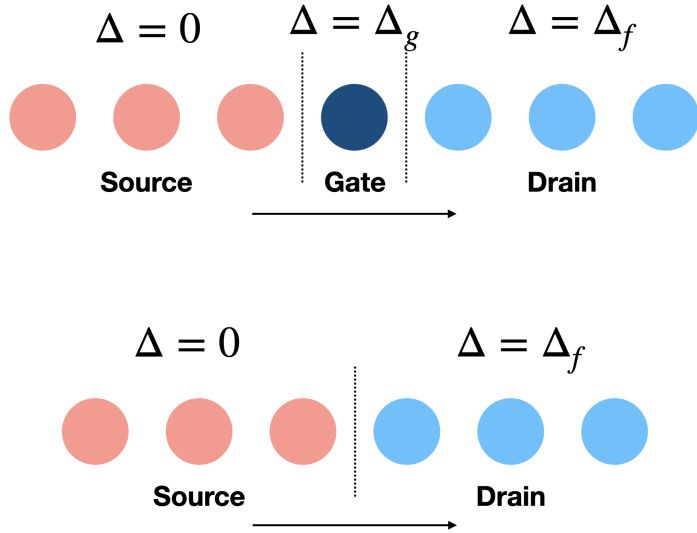


Figure 1.1: *Graphics representation of simple Rydberg Atomtronics devices. Electronic-like transistor (top) and source-drain gate (bottom).*

In fact, they are also used in neutral atoms quantum computing [26]. I introduce the theory of dipole traps in the next section.

1.2 Dipole traps

This section presents an introduction to dipole traps, with the purpose of finding the potential profile induced by a Gaussian beam. The following treatment is adapted from [27]. Neutral atoms have a total charge equal to zero, so, in first approximation if we locate one in an oscillating electric field it shouldn't feel any force. But, since the electric field can induce a dipole in the atom, actually the atom will feel a force due to the induced dipole and light interaction. The atomic dipole moment is related to an oscillating electric field (with frequency ω) with

$$\mathbf{E} = \tilde{E} e^{-i\omega t} \hat{\mathbf{e}} + c.c. ; \quad \mathbf{p} = \tilde{p} e^{-i\omega t} \hat{\mathbf{e}} + c.c.$$

$$\tilde{p} = \alpha \tilde{E}$$

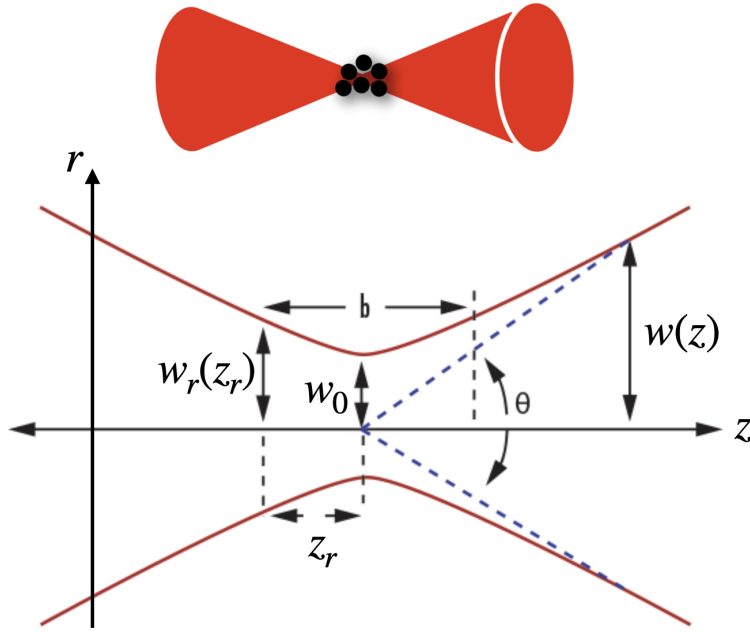


Figure 1.2: Schematic representation of a Gaussian beam in the focal point.

where α is the complex *polarizability*, \tilde{E} is the amplitude of the electric field, and \tilde{p} is the amplitude of the dipole. The interaction energy of the system is given by

$$U_{dip} = -\frac{1}{2}\langle \mathbf{p} \cdot \mathbf{E} \rangle = -\frac{1}{2\epsilon_0 c} \text{Re}(\alpha) I$$

where $I = 2\epsilon_0 c |\tilde{E}|^2$ is the intensity of the electric field, c is the speed of light, ϵ_0 is the vacuum permittivity, and $\langle \cdot \rangle$ is the temporal average on the fast oscillating terms. The real part of the polarizability describes the *in-phase* component of the dipole with respect the driving field. To get the force due to a given potential we can calculate the gradient of it.

$$\mathbf{F}(\mathbf{r}) = -\nabla U_{dip}(\mathbf{r}) = \frac{1}{2\epsilon_0 c} \text{Re}(\alpha) \nabla I(\mathbf{r})$$

From this simple relation we see that the force is proportional to the gradient of the intensity profile of the laser beam.

Classically an oscillating electric dipole emits radiation with a power given by the following expression:

$$P_{abs} = \langle \dot{\mathbf{p}} \cdot \mathbf{E} \rangle = \frac{\omega}{\epsilon_0 c} \text{Im}(\alpha) I$$

In quantum mechanics light is quantized, so this power corresponds to an amount of emitted photons per unit time. Since we know the energy of a photon ($\hbar\omega$), if we divide the power by this energy we can have the rate of scattered photons.

$$\Gamma_{sc} = \frac{P_{abs}}{\hbar\omega} = \frac{1}{\hbar\epsilon_0 c} \text{Im}(\alpha) I$$

By semi-classical considerations it can be shown [27] that *polarizability* and Γ are given by

$$\alpha = 6\pi\epsilon_0 c^3 \frac{\Gamma/\omega_0^2}{\omega_0^2 - \omega^2 - i(\omega^3/\omega_0^2)\Gamma} ; \quad \Gamma = \frac{e^2\omega_0^2}{6\pi\epsilon_0 m_e c^3}$$

Where e is the elementary charge and m_e is the mass of the electron. These expressions hold only if the laser, with frequency ω , is far detuned from the atomic transition ω_0 .

1.2.1 Far-Off-Resonance optical dipole Trap: FORT

It is possible to show that for large detunings and thus small scattering rates ($\Gamma_{sc} \ll \Gamma$) this classical derivation of the *polarizability* is an excellent approximation of the quantum one [27]. Using this result we can rewrite the expression for the interaction potential

$$U_{dip} = -\frac{3\pi c^2}{2\omega_0^2} \left(\frac{\Gamma}{\omega_0 - \omega} + \frac{\Gamma}{\omega_0 + \omega} \right) I(\mathbf{r})$$

since experimentally we always choose a detuning ($\Delta = \omega - \omega_0$) much smaller than the natural frequency of the reference transition ($\Delta \ll \omega_0$) we can neglect the *counter-rotating* term (rotating wave approximation). Thus we finally obtain

$$U_{dip} = \frac{3\pi c^2}{2\omega_0^2} \frac{\Gamma}{\Delta} I(\mathbf{r})$$

The sign of the potential depends on the detuning Δ . For *red-detuned* beam ($\Delta < 0$) the point of maximum intensity corresponds to the lowest energy, so the resulting force is attractive toward high intensity regions. On the other hand, in a *blue-detuned* beam ($\Delta > 0$) the resulting force is directed toward lower intensity regions. Both the possibilities have been tested and studied [27], in our experiment we will use a *red-detuned* dipole trap.

If we use a Gaussian beam the intensity profile is a Gaussian:

$$I(z, r) = \frac{2P}{\pi w(z)^2} e^{-\frac{2r^2}{w(z)^2}} \quad (1.1)$$

where $w(z)$ is the waist of the beam in the z position (figure 1.2), r is the radial coordinate, and P is the beam power.

$$w(z) = w_0 \sqrt{1 + \left(\frac{z}{z_R}\right)^2}$$

$$z_R = \frac{\pi w_0^2}{\lambda}$$

So, finally the potential is given by the following expression:

$$U_{dip}(z, r) = \frac{3c^2 P}{\omega_0^3 w(z)^2} \frac{\Gamma}{\Delta} e^{-\frac{2r^2}{w(z)^2}} \quad (1.2)$$

To get an idea of the order of magnitude of the quantities in expression 1.2, I report in figure 1.3 a contour plot of fixed-potential curves, where I used the following parameters: $P = 100 \text{ mW}$, $\lambda = 840 \text{ nm}$, $w_0 = 5 \mu\text{m}$, $\Delta = 30 \text{ THz}$, which are typical for our experimental setup.

Once one manages to trap atoms in a dipole trap, the second step is to understand how to artificially control their internal state and how to make them interact with each other. In the next section, I will introduce Rydberg atoms and their peculiar properties.

1.3 Atom and interactions

The atomic species that we will use in all our experiments is the ^{87}Rb , which is an alkali atom, so in the periodic table it occupies the first column. Alkali atoms are interesting for their simple electronic structure, in which there is only one valence electron. Such a structure is easy to control by optical driving, and for high excited states, it becomes analogous to the hydrogen atom system, which has been deeply studied, and explicit solutions for the electron wave function are well known. In fact, when the valence electron occupies a high energy state, which corresponds to long-radius orbits (high principal quantum number n), it sees the nucleus and

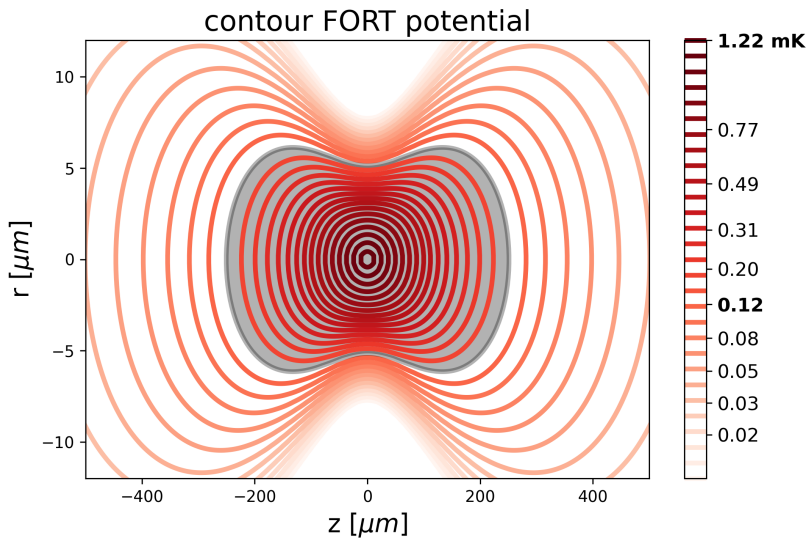


Figure 1.3: Fixed-potential curves from expression 1.2, with intensity profile from expression 1.1. $P = 100 \text{ mW}$, $\lambda = 840 \text{ nm}$, $w_0 = 5 \mu\text{m}$, $\Delta \simeq 30 \text{ THz}$. x and y axes are longitudinal and radial axis of the dipole trap (see figure 1.2). The maximum depth is bold in the top of the colorbar $U_{\max} = 1.22 \text{ mK}$. The grey shadow region indicates the trapping volume if the temperature of the system is $T = 120 \mu\text{K}$.

the other electrons as a single proton (charge $+e$), since the total charge must be zero. This condition occurs when the radius of the internal electronic cloud is much smaller than the radius of the valence electron orbit. When an atom is in such a state, it is called *Rydberg Atom*. Otherwise, if the valence electron is within a distance comparable to the core size, this approximation doesn't hold anymore, and different approaches are necessary. To give some numbers for these quantities, I report a semi-classical approach proposed by Bohr in 1913.

1.3.1 Rydberg atoms

Let me consider an hydrogen atom in a stable electronic configuration. The electron, with a circular orbit around the nucleus, must have a quantized angular momentum, given in unit of \hbar ($mvr = n\hbar$). Moreover, to be in a stable orbit, the centripetal force must be equal to the Coulomb force.

$$m_e \frac{v^2}{r} = k \frac{e^2}{r^2}$$

where m_e is the mass of the electron, e is the elementary charge, v the velocity of the electron and $k = \frac{1}{4\pi\epsilon_0}$ is the Coulomb constant. Substituting $m_evr = n\hbar$, and solving for the radius r of the circular orbit we get the following expression

$$r = \frac{n^2\hbar^2}{km_e e^2} = \frac{n^2 h^2 \epsilon_0}{\pi m_e e^2} = n^2 a_0 \quad (1.3)$$

where a_0 is the Bohr radius and n is the principal quantum number. Knowing the radius, we can give an expression for the energy that is equal to the kinetic energy plus the Coulomb potential.

$$E = \frac{1}{2}m_e v^2 - \frac{ke^2}{r} = -\frac{k^2 e^4 m_e}{2n^2 \hbar^2} = -\frac{Ry}{n^2} \quad (1.4)$$

Where Ry is the Rydberg constant. In equation 1.3 the radius of circular orbits of the hydrogen atom is proportional to the square of the principal quantum number n . So, an atom in the ground state, $n = 1$, has an orbit of radius $r \simeq 0.052 \text{ nm}$, while for higher excited states, for example $n = 70$, the radius is $r \simeq 0.26 \mu\text{m}$. If now we substitute the proton with a core composed by 37 protons (rubidium) and 36 electrons, we will have the alkali atom rubidium. be in presence of an alkali atom, more precisely rubidium⁵. For such an alkali atom the expression 1.3 is a good approximation only if $n \gg 1$, which is true when the radius of the core is much smaller than the radius of the valence electron orbit.

The expression of the energy given in equation 1.4 is the energy of the bound states of the hydrogen atom, since to obtain it we have assumed that the core charge is point-like and with the charge of a proton. In alkali atoms this core is not located in a point but is distributed in space, and how it is distributed changes the potential on the valence electron, and hence its energy. To take into account this energy difference the principal quantum number is corrected by a quantity named *quantum defect*, δ_{nl} , that depends on the value of the quantum numbers n and l . In other words, the *quantum defect* is a measure of how the energy of the valence electron is affected by the distribution of the core electrons in the atom. It is a correction factor that accounts for the non-uniformity of the potential energy

⁵In nature two isotopes of rubidium exists. ⁸⁵Rb with abundance 72.2% stable, and ⁸⁷Rb with abundance 27.8% and lifetime $\sim 10^{10}$ years. We use ⁸⁷Rb.

experienced by the valence electron due to the distribution of the core electrons.

$$n \rightarrow n^* = n - \delta_{nl} \quad (1.5)$$

Using eq. 1.5 in eq. 1.4 the corrected expression of the energy of the Rydberg states is given

$$E = -\frac{Ry^*}{(n^*)^2} \quad (1.6)$$

where Ry^* is the Rydberg constant corrected for the mass M of the atom nucleus

$$Ry \rightarrow Ry^* = \frac{Ry}{1 + m_e/M} \quad (1.7)$$

The *quantum defect* is determined for each atomic species experimentally by spectroscopy measurements [5] and approximated by the empirical Rydberg-Ritz formula [4].

In the table 1.1 I report the dependencies on n^* of some Rydberg atoms properties.

property	n^* dependence
Binding energy	$(n^*)^{-2}$
Orbital radius	$(n^*)^2$
Polarizability	$(n^*)^7$
Radiative life-time	$(n^*)^3$
Van der Waals int.	$(n^*)^{11}$

Table 1.1: *Dependence on n^* of some properties of Rydberg atoms. Adapted from [7]*

Let me now dress the atom with a laser beam and see how to experimentally reach a Rydberg state. In the next section, I will show how a rubidium atom can be driven to a Rydberg state, focusing on the target state which we will use in the experiments.

1.3.2 Excite an atom on a Rydberg state

Our target Rydberg state is the $|70s\rangle = |r\rangle$, which can be reached, from the ground state $|5s\rangle = |g\rangle$, via a two photon process, because, for the *selection rules*, a single photon dipole process must respect $\Delta l = \pm 1$. We use the state $|6p\rangle = |i\rangle$ as

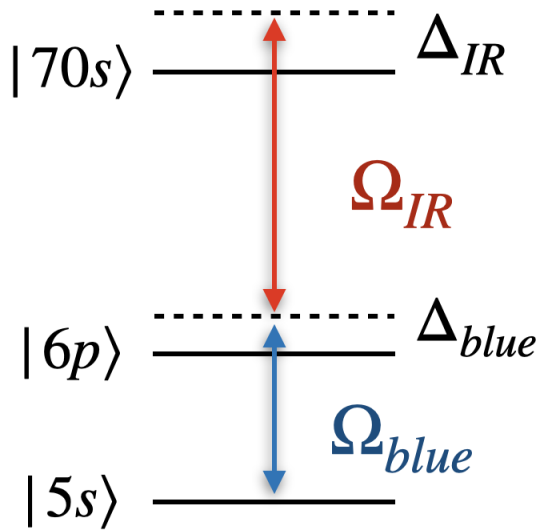


Figure 1.4: Scheme of a two photon process.

intermediate state. So, we need a laser beam that couples the ground with the intermediate state and another for the second transition, a blue beam ($\lambda = 420 \text{ nm}$) and an IR beam ($\lambda = 1013 \text{ nm}$) fit for this scope.

Let's consider the hamiltonian of an atom interacting with a laser beam.

$$H = H_0 + H_{int} = H_{atom} + H_{lasers} + H_{int}$$

The hamiltonian of the bare atom, H_{atom} , is a diagonal matrix with the energy of all the states in which the atom can be. Since we already know which states we will populate using the light we can restrict the bare hamiltonian to the these three states.

$$H_{atom} = E_g|g\rangle\langle g| + E_i|i\rangle\langle i| + E_r|r\rangle\langle r|$$

in matrix form can be written as

$$H_{atom} = \begin{pmatrix} E_g & 0 & 0 \\ 0 & E_i & 0 \\ 0 & 0 & E_r \end{pmatrix}$$

Suppose now to have N_1 and N_2 photons for the two lasers, with respective frequency ω_1 and ω_2 such that $\hbar\omega_1 = E_i - E_g + \Delta_{blue}$ and $\hbar\omega_2 = E_r - \hbar\omega_1 + \Delta_{IR}$

(figure 1.4). I will write the number (fock) state of the lasers as

$$|N_1, N_2\rangle$$

with energy

$$E = \hbar(N_1\omega_1 + N_2\omega_2)$$

where ω_1 and ω_2 are the frequencies of the two lasers, near to the atomic transitions ($|g\rangle \rightarrow |i\rangle$ and $|i\rangle \rightarrow |r\rangle$). If the atom is initially in the ground state, it is possible that one or two photons are absorbed, so during the evolution of the system the field could be in other two states. Neglecting the spontaneous emission⁶ the states of the fields are

$$|N_1, N_2\rangle ; |N_1 - 1, N_2\rangle ; |N_1, N_2 - 1\rangle$$

which correspond to the following hamiltonian

$$H_{lasers} = \hbar(N_1\omega_1 + N_2\omega_2)\mathbb{I} + \hbar \begin{pmatrix} 0 & 0 & 0 \\ 0 & -\omega_1 & 0 \\ 0 & 0 & -\omega_1 - \omega_2 \end{pmatrix}$$

The non-interacting hamiltonian of the system **atom+field** can be written as

$$H_0 = H_{atom} \otimes \mathbb{I} + \mathbb{I} \otimes H_{lasers}$$

that in general is a 9×9 matrix. But, if we neglect the energetically unlikely states (rotating wave approximation), we restrict the space on only three states

$$|g, N_1, N_2\rangle ; |i, N_1 - 1, N_2\rangle ; |r, N_1 - 1, N_2 - 1\rangle$$

Arbitrarily imposing the zero of the energy to $E_g = 0$, the final hamiltonian is

$$H_0 = \hbar \begin{pmatrix} 0 & 0 & 0 \\ 0 & -\Delta_{blue} & 0 \\ 0 & 0 & -\Delta_{IR} \end{pmatrix}$$

⁶If an atom absorbs a photon from the field and then spontaneously decays, it will emits a photon which doesn't belong to the laser mode.

where $\Delta_{blue} = \hbar\omega_1 - E_i + E_g$ and $\Delta_{IR} = \hbar\omega_2 - E_r + \hbar\omega_1$. The **atom+field** interaction Hamiltonian H_{int} can be written as

$$H_{int} = -\mathbf{d} \cdot (\mathbf{E}_1 + \mathbf{E}_2)$$

where \mathbf{d} is the electric dipole moment of the atom with matrix element $\langle i | d_z | g \rangle = d_{ig}$ (for the transition $|g\rangle \rightarrow |i\rangle$), and $\mathbf{E}_1 = E_1 \mathbf{e}_z \cos(\omega_1 t)$ is a classic electric field for the laser of the lower transition (\mathbf{E}_2 is for the higher transition). Defining the Rabi frequencies as

$$\hbar\Omega_{blue} = d_{ig}E_1 ; \quad \hbar\Omega_{IR} = d_{ri}E_2$$

we obtain the total hamiltonian

$$H = \hbar \begin{pmatrix} 0 & \Omega_{blue}/2 & 0 \\ \Omega_{blue}/2 & -\Delta_{blue} & \Omega_{IR}/2 \\ 0 & \Omega_{IR}/2 & -\Delta_{IR} \end{pmatrix}$$

The electric field amplitudes, E_1 and E_2 , can be expressed in measurable quantities as

$$E_i = \sqrt{\frac{4P_i}{\pi w_i^2 \epsilon_0 c}}$$

where P_i and w_i are the power and the waist of the Gaussian beam ($i = 1$ or 2), ϵ_0 the vacuum permittivity, and c is the speed of light.

The two photon Rabi frequency

It can be shown that for large detunings of the intermediate state and for small detunings of the Rydberg state ($\Delta_{blue} \gg \Omega_{blue}, \Omega_{IR}, \Delta_{IR}$) the the dynamics is reduced to a two level system with only the ground state and the Rydberg state with the *two photon Rabi frequency* given by

$$\Omega_{2ph} = \frac{\Omega_{blue}\Omega_{IR}}{2\Delta_{blue}}$$

and hamiltonian

$$H = \hbar \begin{pmatrix} 0 & \Omega_{2ph}/2 \\ \Omega_{2ph}/2 & -\Delta_{IR} \end{pmatrix}$$

A scheme is reported in figure 1.6 (a). For a more complete treatment see [16].

As discussed in the introduction these peculiar properties, such as long lifetime, strong polarizability and long range interactions (table 1.1), make Rydberg atoms excellent candidates for many applications in quantum information technologies. The next property of Rydberg atoms I will introduce briefly is the Van der Waals interaction, which is of primary importance in the understanding of the results of this work, and to realize a working *Rydberg Atomtronics* device.

1.3.3 Van der Waals interaction between Rydberg atoms

The following introduction to Rydberg atoms Van der Waals interaction is adapted from [7]. Let me consider two atoms with a relative distance $\mathbf{R} = \mathbf{R}_1 - \mathbf{R}_2$, where \mathbf{R}_1 and \mathbf{R}_2 are the position of the centres of the two atoms. If this distance, \mathbf{R} , is much greater than the size of the electronic cloud of the two atoms then the dominant term of the interaction is the *dipole-dipole* interaction

$$V_{int} = \frac{1}{4\pi\epsilon_0} \frac{\mathbf{d}_1 \cdot \mathbf{d}_2 - 3(\mathbf{d}_1 \cdot \mathbf{n})(\mathbf{d}_2 \cdot \mathbf{n})}{R^3} \quad (1.8)$$

where \mathbf{d}_i is the electric dipole operator of the atom i and $\mathbf{n} = \mathbf{R}/R$. Let's consider the eigenstates of the single atom ($|\alpha_1\rangle, |\alpha_2\rangle, \dots, |\alpha_i\rangle, \dots$) and their relative eigenvalues (E_1, E_2, \dots), where i indexes all the possible quantum numbers configurations (n, l, j, m_j). The eigenstates of the two atoms system with no interactions are all the states $|\alpha_i\alpha_k\rangle = |\alpha_i\rangle \otimes |\alpha_k\rangle$ with energies $E_{ik} = E_i + E_k$. To calculate the interaction energy between two states a second order perturbation theory can be used, where 1.8 is the perturbation. In my specific case I'm interested in the case which the two atoms are in the same state (in the experiments we excite the atoms on the same state, $|70s\rangle$), so let's consider the state $|\alpha_i\alpha_i\rangle$, the perturbation is given by equation 1.9.

$$\Delta E_{ii} = \sum_{rk} \frac{|\langle \alpha_i\alpha_i | V_{int} | \alpha_r\alpha_k \rangle|^2}{E_{ii} - E_{rk}} = \frac{C_6}{R^6} \quad (1.9)$$

from this expression it is easy to see that the energy shift due to this interaction is proportional to R^{-6} since it depends on the squared of the potential that goes with R^{-3} . In the experiments presented in this thesis the Rydberg state considered is

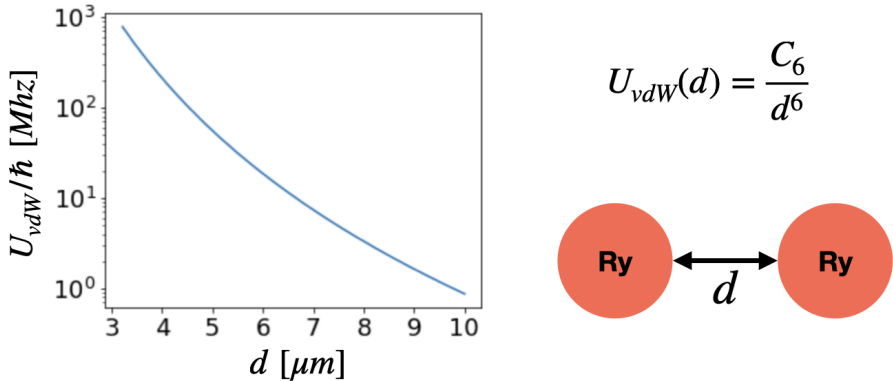


Figure 1.5: *Interacting potential (in MHz) of two ^{87}Rb atoms in the $|70s\rangle$ Rydberg state with a relative distance d .*

always the $|70s\rangle$. For this particular state the Van der Waals coupling constant is $C_6 = h \times 870 \text{ GHz } \mu\text{m}^6$ [12]. In figure 1.5 a plot of the interaction potential (in MHz) is reported versus the distance between two atoms in the $|70s\rangle$ state.

In some experiments discussed in the present thesis, disordered many-body systems of ^{87}Rb atoms are treated. With a MOT⁷ we trap a sample of 10^4 to 10^6 atoms and than we switch on the laser beams to control their state. So, next I will consider a system composed by more than two atoms and introduce a bit of theory about the dynamics of such a systems.

1.3.4 Incoherent dynamics in the many-body system

The following derivation was adapted from ref. [8]. Let's consider a system of N disordered atoms in the ground state. A laser beam dress all the many-body system, and drive the atoms to an excited state with a detuning Δ (a single atom is a two-level system see figure 1.6 a). To describe the dynamics of the system let me first of all write the hamiltonian.

$$H = \frac{\Omega}{2} \sum_k \sigma_k^x + \Delta \sum_k n_k + \frac{1}{2} \sum_{k \neq i} \frac{C_6}{R_{ki}^6} n_k n_i \quad (1.10)$$

where Ω is the Rabi frequency, Δ is the detuning of the laser, R_{ki} is the distance between the atoms k and i , and $n_k = |r\rangle^k \langle r|^k$ is the projector on the Rydberg state of the k^{th} atom. The Schrödinger equation, which governs the evolution

⁷Magneto Optical Trap.

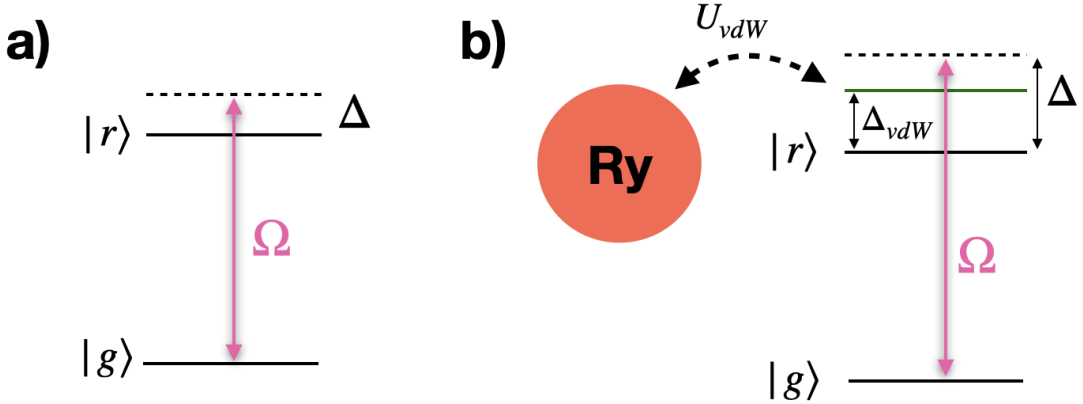


Figure 1.6: a) the two levels system of a non-interacting single atom. b) the two levels system of an atom that is interacting with a rydberg atom. Δ_{vdW} is the shift due to the interaction. Δ is the detuning of the driving laser.

of the system, in the density matrix formalism is given by the following master equation.

$$\frac{d}{dt}\rho(t) = -\frac{i}{\hbar}[H, \rho(t)] \quad (1.11)$$

The equation 1.11 holds only for closed systems. That means systems that have no interaction with an external environment. In our case the spontaneous emission (interaction with the surrounding vacuum field) and the dephasing of the coherences, γ (given by Doppler broadening, line-width of the laser and spurious interactions with background atoms) are not negligible, $\gamma > \Omega$. To take into account the interaction with the environment is possible to correct the equation 1.11 with a new term [9] [10]. Giving in equation 1.12 the *Lindblad master equation*.

$$\frac{d}{dt}\rho(t) = -\frac{i}{\hbar}[H, \rho(t)] + \sum_{\alpha,\beta,k} L(\hat{S}_{\alpha \rightarrow \beta,k}, \rho(t)) \quad (1.12)$$

where the superoperator L is defined as follows

$$L(\hat{O}, \rho) = \hat{O}\rho\hat{O}^\dagger - \frac{1}{2}(\hat{O}^\dagger\hat{O}\rho + \rho\hat{O}^\dagger\hat{O})$$

and the operator $\hat{S}_{\alpha \rightarrow \beta,k}$ is a *jump operator* of the atom k , which describes the transition $\alpha \rightarrow \beta$. There will be two jump operators in the two-level system that describe each atom, one describing the spontaneous emission from the excited

state $|r\rangle$ to the ground $|g\rangle$, $\hat{S}_{r\rightarrow g,k}$, and the other the dephasing, $\hat{S}_{r\rightarrow r,k}$.

$$\hat{S}_{r\rightarrow g,k} = \sqrt{\Gamma_{rg}}|g\rangle^k\langle r|^k ; \quad \hat{S}_{r\rightarrow r,k} = \sqrt{\gamma}|r\rangle^k\langle r|^k$$

where Γ_{rg} is the spontaneous decay rate of the considered Rydberg state and γ is the decoherence rate.

In our experiment, the dynamics of the system is strongly incoherent, that means that the dephasing of the quantum state is much larger than the Rabi frequency of the ground-Rydberg transition, $\gamma \gg \Omega, \Gamma_{rg}$. In this limit the out of diagonal elements of the density matrix go rapidly to zero and the system can be described by a probability vector \mathbf{v} which evolves classically [10] [8]. The dynamics follows the equation 1.13, with $\sigma_k^- = (\sigma_k^+)^{\dagger} = |g\rangle^k\langle r|^k$ and $p_k = 1 - n_k$.

$$\dot{\mathbf{v}} = \sum_k \Gamma_k [\sigma_k^+ - p_k] \mathbf{v} + \sum_k (\Gamma_{rg} + \Gamma_k) [\sigma_k^- - n_k] \mathbf{v} \quad (1.13)$$

where Γ_k is the rate for the k^{th} atom to be excited.

$$\Gamma_k = \frac{\Omega^2}{2\gamma} \frac{1}{1 + \frac{1}{\gamma^2} \left(\Delta + \sum_{q \neq k} \frac{C_6}{R_{kq}} v_q \right)^2} \quad (1.14)$$

To get an idea of the order of magnitude of these quantities, I report the example for the two atoms case. In figure 1.7 the excitation rate of an atom with a distance d to a Rydberg atom is reported for different values of the detuning of the driving laser. The excitation rate of an atom with no interaction is

$$\Gamma_{exc} = \frac{\Omega^2}{2\gamma} \frac{1}{1 + \frac{\Delta^2}{\gamma^2}} \quad (1.15)$$

and for one atom with a Rydberg atom at a distance d is

$$\Gamma_{fac} = \frac{\Omega^2}{2\gamma} \frac{1}{1 + \frac{1}{\gamma^2} \left(\Delta - \frac{C_6}{d^6} \right)^2} \quad (1.16)$$

Rydberg blockade

The curve obtained in figure 1.7 with $\Delta = 0$ (dark blue) goes to 1 for distances greater than almost $10 \mu m$, and goes to zero for lower distances. This behaviour

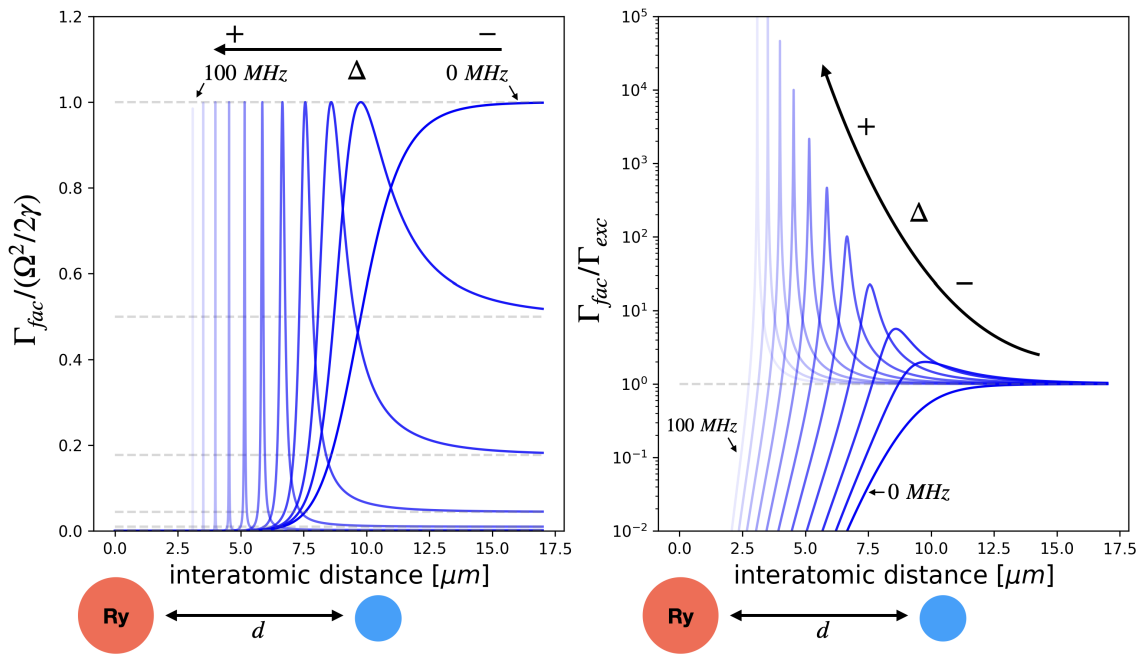


Figure 1.7: Excitation rate of an atom with a distance d to a Rydberg atom $|70s\rangle$ is reported for different values of the detuning of the driving laser $\Delta \in [0, 10, 20, \dots, 100]$ MHz. $\gamma = 1$ MHz. $C_6 = h \times 870$ GHz μm^6 . Δ is graphically introduced in figure 1.6, when $\Delta = \Delta_{vdW}$ a maximum of Γ_{fac} is observed.

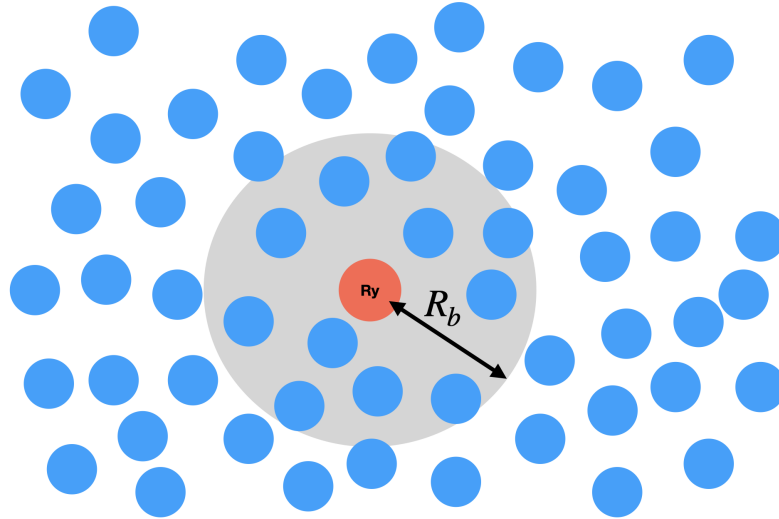


Figure 1.8: The blue balls are atoms in the ground state. The red ball is a Rydberg atom. Gray shadow is the blockaded region. If a ground state atom is in the gray region it can't be excited in the Rydberg state, because of interactions. R_b is the blockade radius.

is named *Rydberg blockade effect*. When the energy shift induced by the interaction is larger than the width of the atomic transition the probability to excite the non-excited atom drops dramatically. The distance for which this effect becomes relevant is called *blockade radius*, which in the incoherent regime ($\gamma \gg \Omega$) can be obtained imposing

$$\hbar\gamma > U_{vdW} \Rightarrow R_b = \left(\frac{C_6}{\hbar\gamma}\right)^{\frac{1}{6}}$$

From the figure 1.7 one can see that the *Rydberg blockade radius* for the state $|70s\rangle$ is about $\sim 10 \mu m$. In figure 1.8 a schematic illustration is reported for the understanding of the idea in a many-atoms case.

Facilitation

If the detuning of the driving laser is grater than zero, than there is a point where the energy shift due to the interaction is equal to the energy associated to the detuning (see figure 1.6 b).

$$\Delta = U_{vdW}/\hbar \Rightarrow r_{fac} = \left(\frac{C_6}{\hbar\Delta}\right)^{\frac{1}{6}}$$

This point corresponds to a maximum in the rate given in the expression 1.16, which is shown in figure 1.7. Thanks to the interactions is it possible to resonantly drive an atom to the Rydberg state even with an off-resonant laser. This process is called *facilitation*. The width of the resonances (fig. 1.7) is given by

$$\delta r_{fac} = \frac{r_{fac}}{6\Delta} \gamma.$$

1.3.5 Photoionization

In the experiments for the characterization of the dipole trap we used the photoionization process as a measurement protocol. The *photoionization* is a process that consists in the excitation of an atom, by a photon, to a state in the continuum, so in a non-bound state (figure 1.9). When this happens the valence electron is ejected from the atom and the atom becomes an ion. Differently than neutral atoms, ions are accelerated in the presence of an electric field. This permits us to be able to detect them with the channeltron (see chapter 2). This process is possible only if the energy of the absorbed photon is higher than the ionization energy E_i of the state the atom is in.

$$E_{ph} \geq E_i$$

for ^{87}Rb , the ionization energy of the state that we populate during the experiments ($|5s\rangle$, $|6p\rangle$, $|70s\rangle$) are reported in table 1.2.

state	$ 5s_{1/2}\rangle$	$ 6p_{3/2}\rangle$	$ 70s_{1/2}\rangle$
E_i (eV)	4.18	1.23	3.04×10^{-3}
λ (nm)	297	1010	407×10^3

Table 1.2: Ionization threshold and corresponding wavelength for ^{87}Rb state used in the present work.

To calculate the photoionization life-time of the states the *Fermi Golden Rule* can be used, which for unbound states is written as equation 1.17.

$$P_{i \rightarrow f} = \frac{2\pi}{\hbar} |V_{fi}|^2 \delta(E_f - E_i) \quad (1.17)$$

where $E_f - E_i$ is the difference of energy between the starting and arriving states

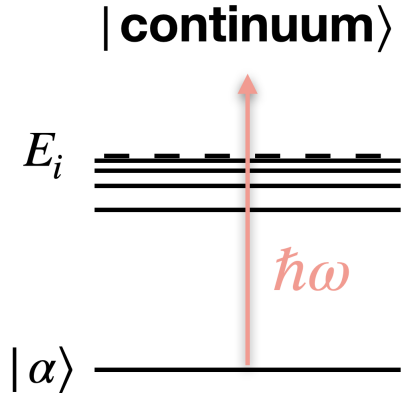


Figure 1.9: Graphic representation of the photoionization process. The states are bound if their energy is less than the ionization energy E_i . α is a generic bound state. $\hbar\omega$ is the energy of the absorbed photon.

and

$$V_{fi} = \langle \psi_f | \hat{V} | \psi_i \rangle$$

is the matrix element of the interaction hamiltonian of the atom-field system, and $|\psi_f\rangle$ and $|\psi_i\rangle$ are the starting and arriving states. See ref. [34] for a more detailed explanation.

1.4 The Mandel-Q factor

One of the aim of this thesis is to experimentally show that with our setup we can observe a strongly interacting many-body system of atoms. One way of testing this is by measuring the counting statistics of Rydberg excitations. In this section, I will show qualitatively that we expect a Poissonian behaviour when a non-interacting system is considered and a super(sub)-Poissonian one when atoms interact with each other. Moreover, I will show that the *Mandel-Q* factor is a good candidate to discriminate between these different regimes (figure 1.10). The *Mandel-Q* factor is defined as the ratio between sample variance (s^2) and sample mean (\bar{N}) minus 1:

$$Q = \frac{s^2}{\bar{N}} - 1 \quad (1.18)$$

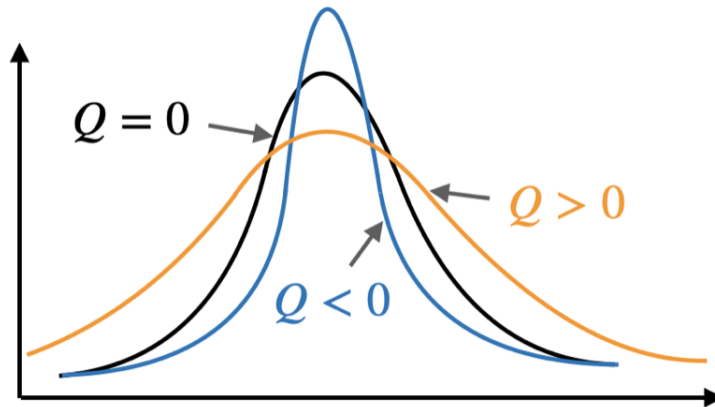


Figure 1.10: For a Poisson distribution $Q = 0$. $Q < 0$ for sub-Poissonian distributions and $Q > 0$ for super-Poissonians.

with

$$s^2 = \frac{1}{n-1} \sum_i^n (N_i - \bar{N})^2 ; \quad \bar{N} = \frac{1}{n} \sum_i^n N_i$$

where n is the number of identical experiments and N_i is the number of atoms measured in the i^{th} experiment.

Non-interacting system

Let's consider N non-interacting atoms, where each one has a certain probability λ to be excited in an amount of time Δt . Let's suppose to repeat several times the experiment where the laser beam are kept on for a time Δt . How many atoms will be excited? and how this number is distributed? This problem is analogous to distributing N identical balls in two boxes with labels r and g . The probability for a single ball to go in the box r is λ , while $1 - \lambda$ is the probability to go in the box g . The distribution of the number of balls k in the box r is a binomial distribution, which in the limit $N \gg k$, $\lambda \ll 1$ and $\lambda N = \mu$, becomes a Poisson distribution.

$$p(k|\mu) = \frac{\mu^k e^{-\mu}}{k!} \quad (1.19)$$

where $p(k|\mu)$ is the probability to excite k atoms in the Rydberg state given a mean value μ . In each experiment the number of atoms in the ground state is $\sim 10^4$ in the interaction volume, and we usually excite not more than ~ 50 atoms. The

conditions $N \gg k$, $\lambda \ll 1$ and $\lambda N = \mu$ hold.

The mean is equals to the variance for a Poisson distribution. So the *Mandel-Q* factor is zero, $Q = 0$.

System in the Rydberg *blockade* regime

Let's consider again N atoms driven by a resonant laser to a Rydberg state. As shown in figure 1.7, when the light is resonant with the transition, if an atom is in the Rydberg state it will "block the excitation" of the atoms located within the *blockade radius* from it (see figure 1.11). Suppose now that at the time t of the evolution k atoms are in the Rydberg state. Because of the Rydberg blockade effect lots of atoms are blocked and the probability to excite further atoms is lower than at time $t = 0$.

$$p(k + 1, t + \Delta t | k, t) < p(1, \Delta t | 0, t = 0)$$

If the system evolves for enough time, the Rydberg excitations will saturate the volume (figure 1.11), and no atoms (or few) will be available for the excitation. I call this saturation threshold k_{th} .

$$p(k_{th} + 1, t + \Delta t | k_{th}, t) \simeq 0$$

From this qualitative approach one can see that if the evolution time is long enough and in each repetition of the experiment the threshold k_{th} is reached, and the fluctuations will be very low with respect to the sample mean of the detected excitations. The distribution in this regime will be sub-Poissonian. $s^2 < \bar{N} \Rightarrow Q < 0$.

System in the *facilitation* regime

Suppose to take the same system of N atoms. We now excite this sample off-resonantly with a detuning Delta. At $t = 0$ the atoms are all in the ground state and the rate which they are excited is given by expression 1.15,

$$\Gamma_{seed} = \frac{\Omega^2}{2\gamma} \frac{1}{1 + \frac{\Delta^2}{\gamma^2}}$$

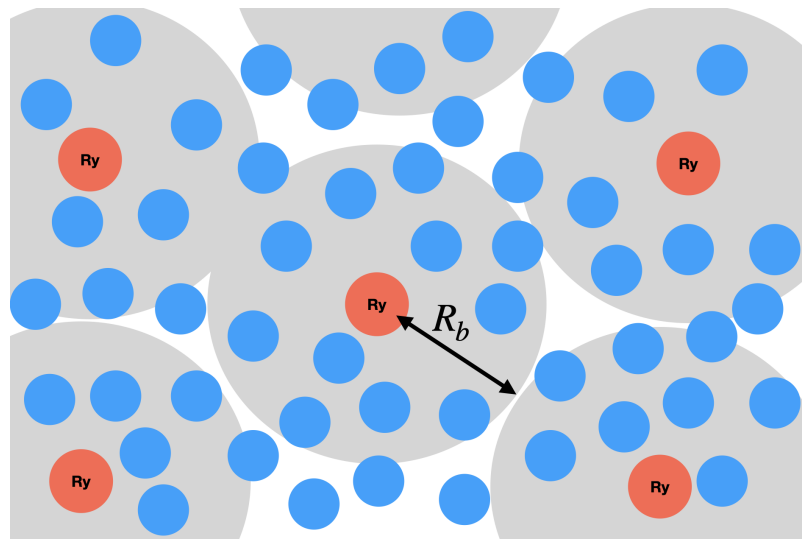


Figure 1.11: *Saturation of the Rydberg excitations because of the Blockade effect.*

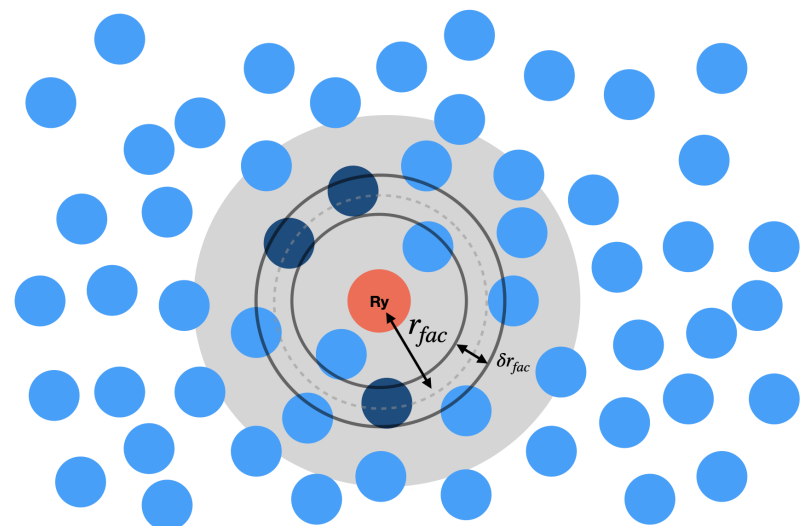


Figure 1.12: *The region between the two black circles is the facilitation shell. Dark blue points are the atoms that have a higher probability to be excited because of facilitation.*

Let's choose a detuning such that Γ_{seed} is much less than the resonant excitation rate $\Gamma_{seed} \ll \frac{\Omega^2}{2\gamma} \Rightarrow \Delta \gg \gamma$. The probability to excite an atom spontaneously is much less than the probability to excite it because of *facilitation*, if it is located in the *facilitation* shell of a Rydberg atom. We will call *seed* the spontaneous excitation.

If the system evolves for a time Δt , as soon as a *seed* is created, for some atoms (which are in the *facilitation* shell of the *seed*, see figure 1.12) this rate increase fast and an avalanche of excitation starts. But, if in the time Δt no *seeds* are created the avalanche can't begin and we will measure zero Rydberg excitations. Repeating the experiment, a large (super-Poissonian $\text{Var}(N) > \bar{N} \Rightarrow Q > 0$) distribution for the excited atoms will be observed. In ref. [11] a model for this process is proposed. This model consists in defining a bimodal distribution for the number of Rydberg atoms given by

$$p(N) = \alpha\delta(N - N_1) + (1 - \alpha)\delta(N - N_2)$$

where α is the probability to have no *seed*. $N_1 \simeq 0$ is the number of excitations when there are no seeds and $N_2 > 0$ is the number of final excitation when the avalanche is observed.

1.4.1 Mandel-Q with a noisy laser source.

To be able to discriminate whether a sub(super)-Poissonian behaviour is due to a physical reason (such as *facilitation*) or to noise in the experiment, I assume the presence of a Gaussian jitter in the excitation laser source. Let's consider the following scenario: I assume that the system is non-interacting. We repeat 100 times the experiment, and we compute the sample mean and the sample variance of the number of Rydberg atoms. The duration of a single evolution is a few μs , and the delay between one experiment and the next one is 1 ms . The laser frequency fluctuates faster than the cycles frequency, so we can assume that for each excitation pulse the frequency changes. I assume that this noise is Gaussian (figure 1.13)

$$P(f; f_0) = \alpha e^{-\frac{(f-f_0)^2}{2\sigma_f^2}}$$

where $P(f; f_0)$ is the probability that in one experiment the frequency of the laser is f given that it fluctuates around f_0 , $\alpha = 1/\sqrt{2\pi\sigma_f^2}$ is the normalization constant,

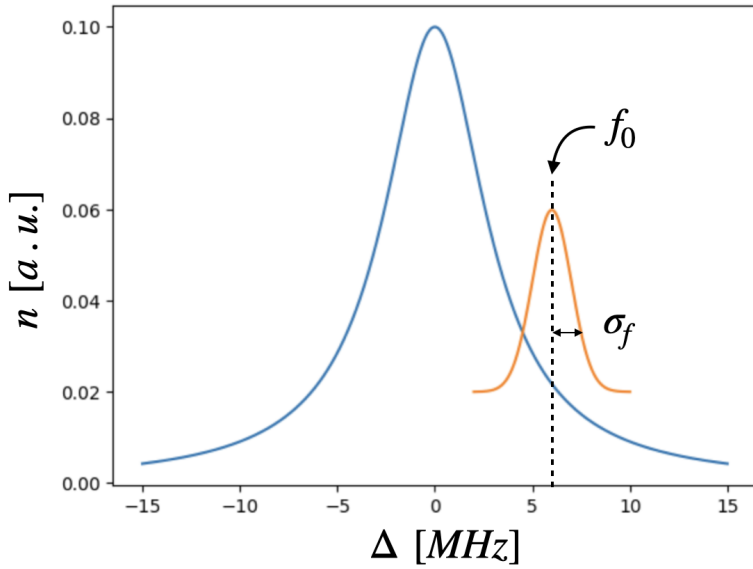


Figure 1.13: In blue the resonance profile of the atomic transition. In orange the Gaussian distribution of the laser frequency jitter.

f_0 is the frequency where the laser is locked, and σ_f is the width of the distribution.

Fixing a frequency, the number of Rydberg atoms measured in a single experiment is distributed as a Poisson distribution (as discussed in the previous section), since the system is non-interacting. The mean value of the Poisson distribution depends on the frequency as

$$P(n|f; f_0) = \frac{e^{-\mu(f)} \mu(f)^n}{n!}$$

with $\mu(f)$ the resonance profile, that can be a Lorentian or a Gaussian

$$\mu(f) = N_{max} \frac{\gamma^2}{(\gamma^2 + (f - f_r)^2)} \quad \text{or} \quad \mu(f) = N_{max} e^{-\frac{(f-f_r)^2}{2\gamma^2}}$$

where f_r is the frequency of the transition, N_{max} is the peak of the resonance and γ is the width to half height (FWHM) (for the Lorentian) or the standard deviation (for the Gaussian). Assuming that the resonance is in $f_r = 0$ we can write the joint distribution for n and f , given f_0 (the value we set when we lock the laser):

$$P(n, f; f_0) = P(n|f; f_0)P(f; f_0) = \frac{e^{-\mu(f)} \mu(f)^n}{n!} \alpha e^{-\frac{(f-f_0)^2}{2\sigma_f^2}}$$

Now, what we want is $P(n; f_0)$, because n and f_0 are the only two quantities that we can actually measure. We can compute it marginalizing over f :

$$P(n; f_0) = \int_0^\infty P(n, f; f_0) df = \int_0^\infty P(n|f; f_0) P(f; f_0) df$$

$$P(n; f_0) = \int_0^\infty \frac{e^{-\mu(f)} \mu(f)^n}{n!} \alpha e^{-\frac{(f-f_0)^2}{2\sigma_f^2}} df \quad (1.20)$$

To compute the *Mandel-Q* factor, we can use the following expressions to get the mean and the variance for n :

$$\langle n \rangle = \sum_0^\infty n P(n; f_0) ; \quad \langle n^2 \rangle = \sum_0^\infty n^2 P(n; f_0)$$

$$\sigma_n^2 = \langle n^2 \rangle - \langle n \rangle^2 ; \quad Q = \frac{\sigma_n^2}{\langle n \rangle} - 1$$

In figure 1.14 the mean and *Mandel-Q* are plotted for a Gaussian resonance with standard deviation 1.5 MHz and a Gaussian jitter with amplitude 0.7 MHz for the laser frequency.

$$\mu(f) = N_{max} e^{-\frac{(f-f_r)^2}{2\gamma^2}}$$

With $\Delta = f - f_r$ the detuning of the laser from the atomic transition. In the figure the curves are plotted together with the data points of an experiment, which consisted of computing the sample mean and the *Mandel-Q* with a sample of 100 repetitions. The laser frequency jitter we measure is usually $\sigma = 0.7$ MHz.

Closing remarks

In this chapter, I introduced the theoretical background necessary to understand the results of the thesis. I started deriving the trapping potential given by a dipole trap, then I introduced Rydberg atoms and their peculiar properties, discussing the differences between *facilitation* and *Rydberg blockade*. A derivation of the dynamics of many interacting atoms in an incoherent regime is given. I concluded by discussing how a noisy laser source can affect the experimental results, showing some experimental data and comparing them with a statistical model derived by myself. In the next chapter, I will introduce the experimental setup focusing on the set up of the infrared beam ($\lambda = 1013$), which was one target of my thesis,

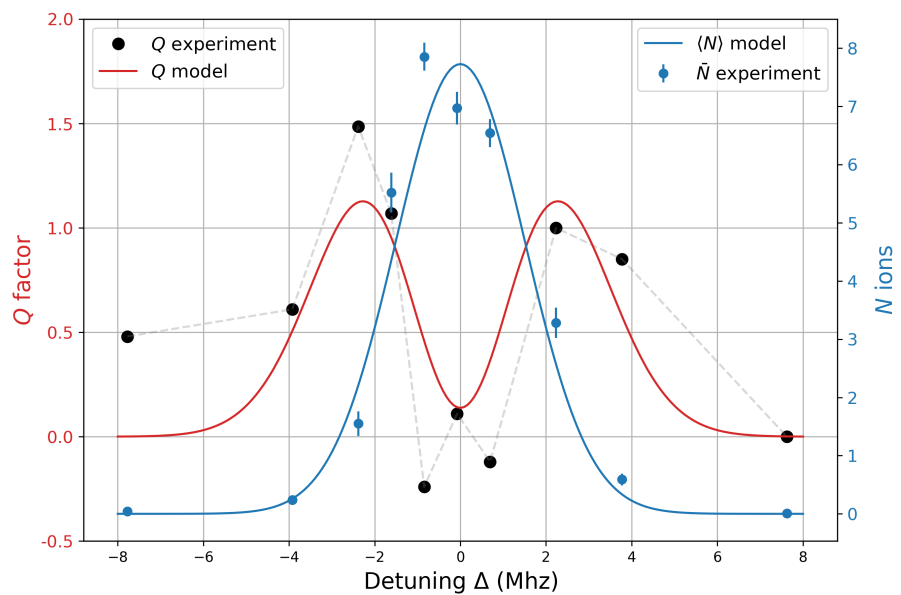


Figure 1.14: Mean value (blue curve) and Mandel-Q (red curve) computed from the distribution in expression 1.20, using a Gaussian profile for the resonance. Sample mean (blue points) and Mandel-Q (black points) from experimental data: typical resonance scan we observe for the Rydberg state $|70s_{1/2}\rangle$ using a two photon process described before in this chapter. Model parameters: Gaussian width = 1.5 MHz, jitter amplitude: $\sigma = 0.7$ MHz.

and on the detection limits: the *detection efficiency* and the *dead time*. These two quantities are introduced and experimentally estimated.

Chapter 2

Experimental set-up

The experimental set-up used in this work is located in the department of physics at the University of Pisa. It is composed of a Magneto-Optical Trap (MOT), a dipole trap (FORT), the lasers used for the control of the state of the system, and an ion detector (channeltron). In this chapter, they are described. Particularly, during my period in the lab, we built the setup of the dipole trap and the optical path of the infrared laser beam ($\lambda = 1013$ nm), so I will focus on them. In conclusion, I discuss the limits of our detector, defining and estimating the *detection efficiency* and the *dead time*. A scheme of all the setup is reported in figure 2.1.

2.1 Laser cooling

The MOT [17] consists in two laser sources (*trap* and *repump*) that couple respectively the transitions $|5s_{1/2}, F = 2\rangle \rightarrow |5p_{3/2}, F' = 3\rangle$ and $|5s_{1/2}, F = 1\rangle \rightarrow |5p_{3/2}, F' = 2\rangle$ (figure 2.2). Actually, to slow down the atoms only the *trap* transition is necessary. The *repump* is added to avoid the optical pumping of the atoms into a dark state. In fact, the *trap* laser can off-resonantly excite the atoms to the $|5p_{3/2}, F' = 2\rangle$ state that can decay both in the $F = 1$ and $F = 2$ sublevels of the $|5s_{1/2}\rangle$ state. Without a *repump* laser, the atoms will eventually end up in the $|5s_{1/2}, F = 1\rangle$ level and hence no longer be coupled to the cooling transition. Both *trap* and *repump* laser source in our set-up are in master-slave configuration (figure 2.1 table 2) and the lock of the frequency on the atomic transition is done using the doppler-free laser spectroscopy [17] applied to a cell which contains rubidium vapour at room temperature. The output signal of the doppler-free spectroscopy

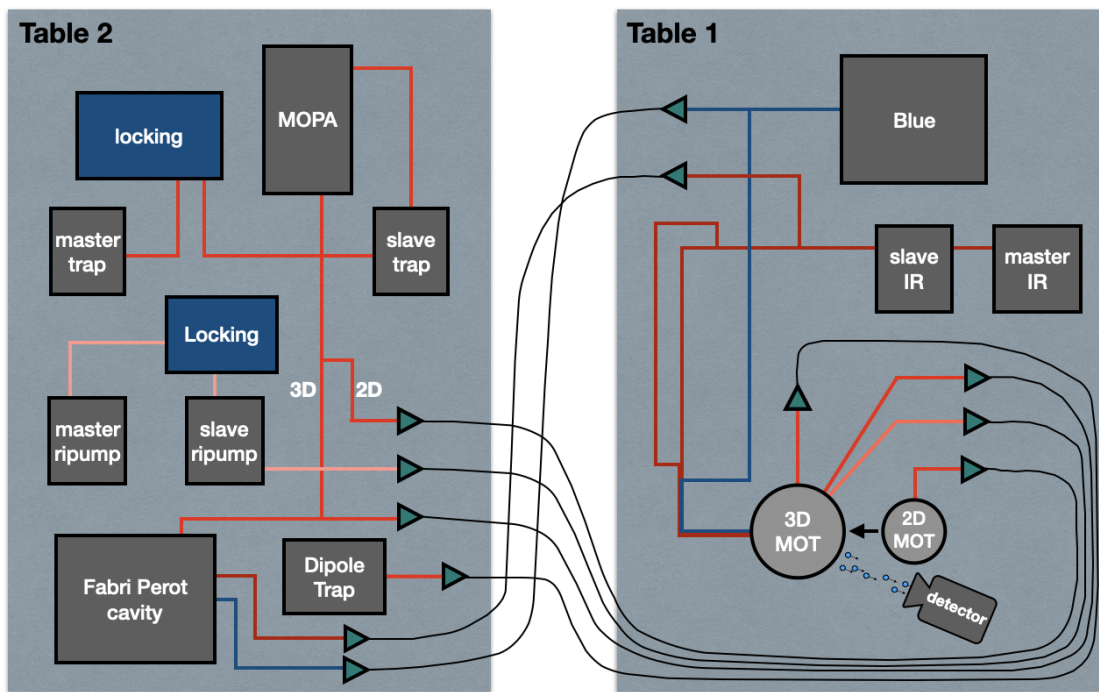


Figure 2.1: Scheme of the two optical tables. On the table 2 the laser for MOT and dipole trap are prepared. On the table 1 the excitation beam are prepared.

Rb87

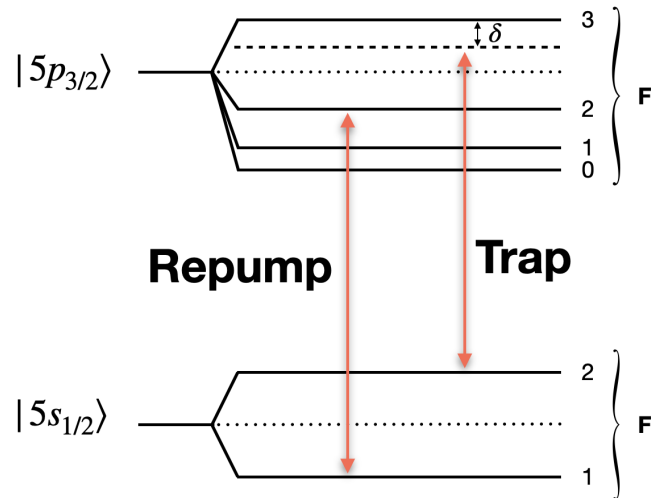


Figure 2.2: Trap and repump beams for a MOT with ^{87}Rb .

is sent to a lock-in amplifier that returns the derivative of the resonance. We set the laser frequency to the point where the derivative is zero (that is the peak of the resonance) and use the output signal of the lock-in as feedback for the piezo-electric actuator inside the current control of the master laser.

To load atoms in the MOT, we have a 2D MOT that slows down the atoms only in two spatial directions and accelerates them (with a *push beam*) in the third direction, toward the 3D MOT (fig. 2.1). The quadrupolar magnetic field gradients for the 2D and 3D MOTs are respectively $\simeq 22 \text{ G/cm}$ and $\simeq 12 \text{ G/cm}$. The pressure that we typically have in the vacuum chamber is 10^{-8} to 10^{-10} mbar . The number of atoms that we can trap in the MOT goes from a few thousand to millions, and the radius of the MOT can be between tens and hundreds of microns. So we have a typical density of 10^9 to 10^{11} cm^{-3} .

All the experiments we do with dipole traps require that we first create the MOT. After that, we switch on the laser beam of the FORT and load it. Then one can perform the evolution of the system and measure the outcome. The entire cycle usually takes a few seconds. The faster the MOT loads, the faster the experiments can be done. In the next section, the second step of this sequence of operations is described: the dipole trap.

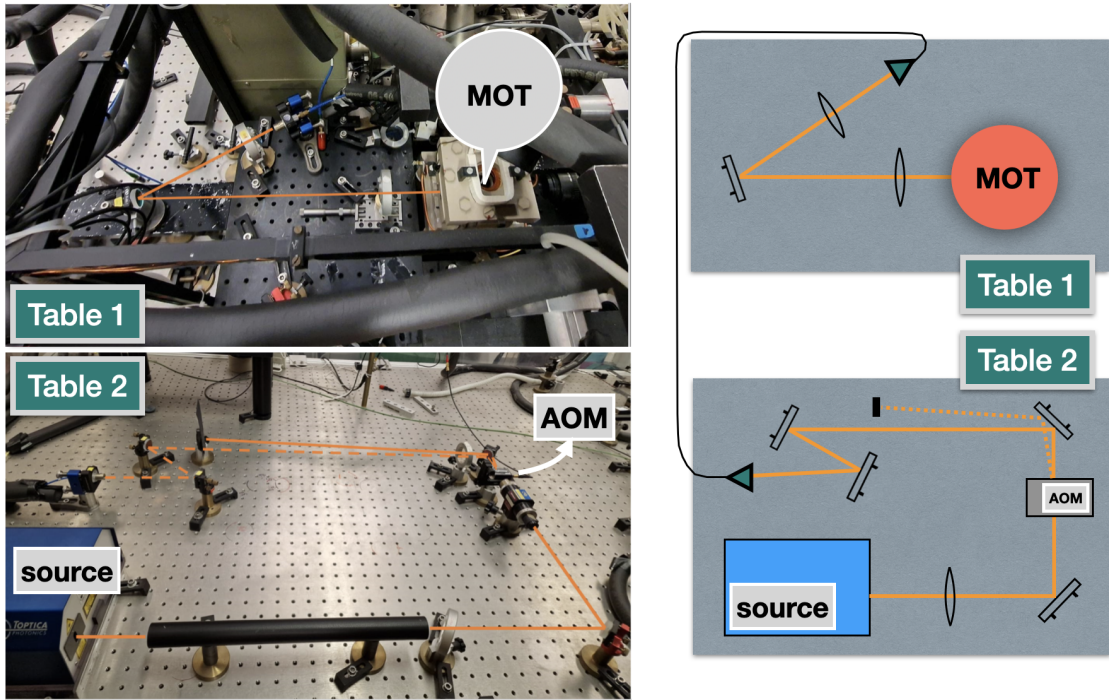


Figure 2.3: Photos and schemes of the dipole trap setup.

2.2 Dipole trap

Trapping atoms is the basis step for *Rydberg Atomtronics*. In our set-up we have a red detuned dipole trap made with a 840 nm laser source, that couple the $|5s\rangle \rightarrow |5p\rangle$ states with a red detuning $\Delta \simeq 25$ THz. Figure 2.3 shows a scheme of the dipole trap optical path with relative photos. On table 2 the source beam pass through an AOM, that permits fast control (rise time ~ 20 ns) of the power in the diffracted order, which is than injected in an optical fiber to bring it on the table 1. On table 1 (figure 2.1), the beam is focalized on the center of MOT. The power of the beam just before the focal point of the dipole trap is up to 150 mW. The waist of the trap is estimated to be $5 \mu\text{m}$ and the depth is up to $1 - 2$ mK. A description of the typical temperature and the lifetime of the FORT was the topic of the thesis of F. Bensch [36]. He estimated the temperature to be in the order of magnitude of tens of μK , and the lifetime to be $\sim 1\text{s}$, for a trap 1.6mK deep.

To excite the atoms either to a Rydberg or an intermediate state, an excitation laser system is necessary. In the next section, it is introduced.

2.3 Lasers for internal state control

Our method of communicating with atoms is through atom-light interactions. Having a well-prepared excitation setup is primary for any experiment we do. As discussed in the introduction, our aim is to be able to control simultaneously a resonant laser beam (*excitation channel* for *seed* excitation), an off-resonant one (*facilitation channel*), and one for engineered dissipation (*dissipation channel*). In this section, I will explain how we built the setup.

First of all it is important to know how many laser source we need. In the experiments of this thesis we always use three internal states of the ^{87}Rb : the $|g\rangle = |5s_{1/2}\rangle$, the $|i\rangle = |6p_{3/2}\rangle$ and the $|r\rangle = |70s_{1/2}\rangle$ (Rydberg). To reach the state $|i\rangle$ from the ground, we need a **blue** photon ($\lambda = 420\text{nm}$), while to reach the Rydberg $|r\rangle$, a two-photon process is used: **blue + infrared**. ($\lambda_{blue} = 420\text{ nm}$; $\lambda_{IR} = 1013\text{ nm}$). To artificially control the dissipation only the **infrared** is necessary. At the end, with two sources (a **blue** laser and an **infrared** laser) We can achieve our goal. Next, I will briefly describe the setup of these two laser sources.

2.3.1 Blue laser

The source of the blue light is a TOPTICA TA-SHG Pro, which consists in a 840 nm external cavity diode laser and a tapered amplifier before an integrated frequency duplicator that transmits in output the 420 nm . The output blue beam is directed toward the MOT, passing by a dichroic mirror (figure 2.4 left) that superimposes it on the IR beam. A bit of the output of the 840 nm diode laser is sent to the Fabry-Perot cavity (figure 2.1) in order to be able to fine tune the frequency and stabilize it. The output signal of the Fabry-Perot is sent to a computer that through a *LabWiev* program sends a feedback to the laser. The power just before the vacuum chamber of the blue laser is up to 2 mW and its waist in the MOT position is $40 - 90\mu\text{m}$.

2.3.2 Infrared laser

For the infrared beam ($\lambda = 1013\text{ nm}$) a master-slave configuration is prepared (figure 2.1), where the master laser is a Toptica DL 100 and the slave is a Sacher

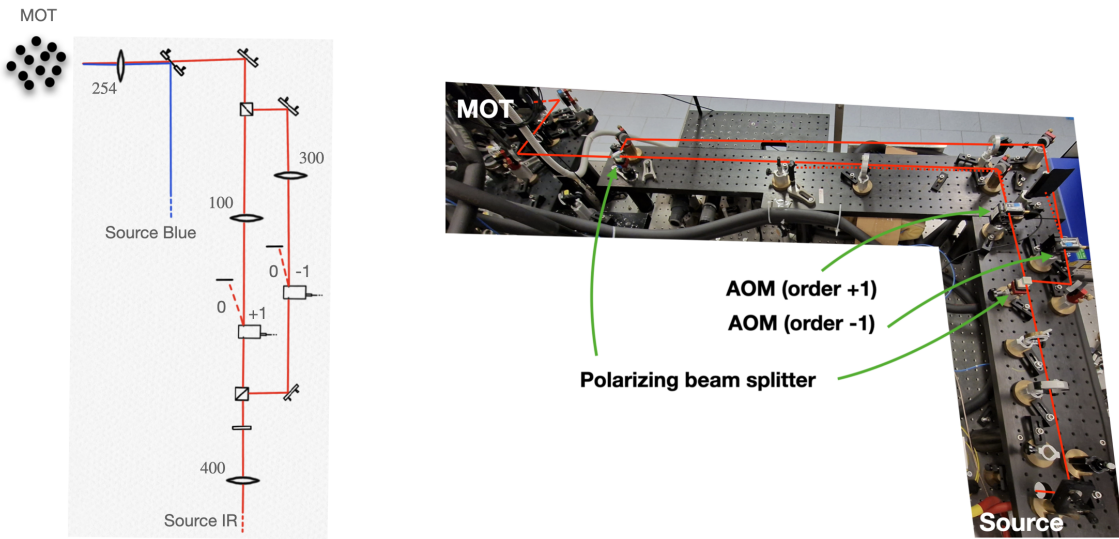


Figure 2.4: *Experimental setup for the excitation beams. The numbers near the lenses are the focal lengths in mm.*

Lasertechnik TIGER. The frequency lock and stabilization techniques are the same as those used for the 420 nm laser. I will first introduce the *facilitation* and *dissipation* channels and after the *excitation* channel.

The *facilitation* and *dissipation* channels

In order to have an *excitation* and a *dissipation* channels simultaneously (figure 2.5) we split the 1013 nm beam into two branches (figure 2.4) with a polarizing beam splitter. The goal is to have one branch off-resonant (by a detuning $\Delta_{blue} + \Delta_{IR}$) from the transition $|6p_{3/2}, F = 3\rangle \leftrightarrow |70s_{1/2}\rangle$ and the second branch resonant with the transition $|6p_{3/2}, F = 2\rangle \leftrightarrow |70s_{1/2}\rangle$ used for the engineered dissipation. To do that, we used two Acusto-Optic Modulators¹ (AOM. model: crystal technology 3080-122) (figure 2.4) using the order +1 for the *excitation* branch and the order -1 for the *dissipation* branch. I will call f^+ and f^- the radiofrequencies sent to the AOMs. Since the source ω is the same for the two beams the following

¹An AOM, or acousto-optic modulator, is an optical device that can modify the frequency of a laser beam by using an applied radiofrequency signal.

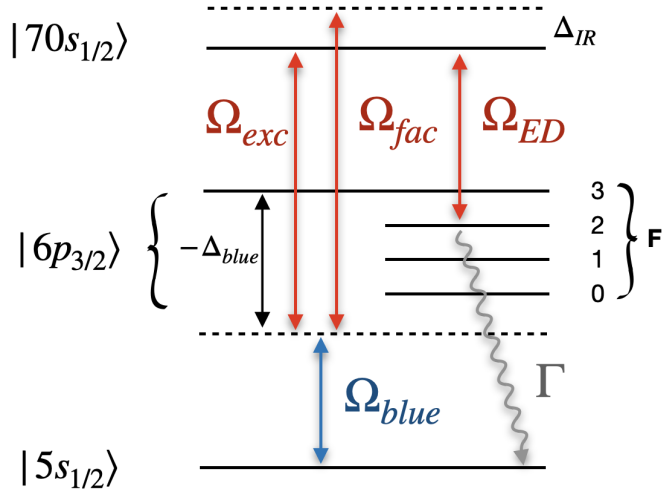


Figure 2.5: Levels scheme for blue ($\lambda = 420 \text{ nm}$) and infrared ($\lambda = 1013 \text{ nm}$) beams. The infrared is used in three different ways simultaneously: for excitation of seeds (most left), for facilitation (middle) and for dissipation (most right). They are, respectively, the excitation, facilitation, and dissipation channels. The energy gaps of the hyperfine states are reported in table 2.1.

equations must hold

$$\begin{cases} \omega + f^+ = (E_{70s} - E_{6pF3}) - \Delta_{blue} + \Delta_{IR} \\ \omega - f^- = (E_{70s} - E_{6pF2}) \end{cases}$$

where on the left the frequency of the two branches is reported and on the right the energy gap they must match. Computing the difference between the two expressions, we get

$$f^+ + f^- = \Delta_{IR} - \Delta_{blue} - \Delta_{23}$$

where $\hbar\Delta_{23} = E_{6pF3} - E_{6pF2}$ is the energy gap between the hyperfine states $F = 3$ and $F = 2$ of the $|6p_{3/2}\rangle$. Since the central frequency of both the AOMs is $f_0 = 80 \text{ MHz}$ to optimize the diffraction efficiency we fix $f^+ = f^- = f_0$. Finally the equation 2.1 must hold.

$$\Delta_{blue} = \Delta_{IR} - 2f_0 - \Delta_{23} = \Delta_{IR} - 247 \text{ (MHz)} \quad (2.1)$$

So, if for example we want $\Delta_{IR} = 20 \text{ MHz}$ than Δ_{blue} must be equal to -227 MHz . Δ_{blue} is referred to the $F = 3$, if we want to refer it to an other F in table 2.1 I

$F \leftrightarrow F'$	$0 \leftrightarrow 1$	$1 \leftrightarrow 2$	$2 \leftrightarrow 3$
Energy gap in MHz	23.74	51.44	87.05

Table 2.1: Energy gaps of the hyperfine structure of the $|6p_{3/2}\rangle$.

report the energy gaps of the hyperfine states of the $|6p_{3/2}\rangle$. If for example we want to refer Δ_{blue} to the $F = 0$

$$\Delta_{blue}^{F=0} = \Delta_{blue} + 162.23 \text{ (MHz)}$$

We have seen how we have built the setup for the *facilitation* and *dissipation* channels so far.

The excitation channel

In our setup we would like to be able to resonantly create a small number of Rydberg excitations (*seeds*) before to switch on the *facilitation* beam. To do that we can just decrease the radiofrequency of the AOM order +1, f^+ , by Δ_{IR} . For example, if $\Delta_{IR} = 20$ MHz we can send the radiofrequency $f^+ = 60$ MHz (to resonantly create the seeds) and then switch the frequency to $f^+ = 80$ MHz to start the *facilitation* excitations. With this setup the *facilitation* channel has always the maximum diffraction efficiency (since the radiofrequency of the AOM is the central one) and one can fine tune the Rabi frequency just changing the radiofrequency amplitude. To excite a small amount of seeds a smaller amount of power is necessary (typically $100 \mu\text{W}$ for $1 \mu\text{s}$), so even a lower diffraction efficiency doesn't affect the experiment. In figure 2.6 is reported the relative diffraction efficiency versus the radiofrequency sent to the AOM.

Anyway, with this configuration of the setup, it is possible to choose a Δ_{IR} up to about $25 - 30$ MHz because the diffraction efficiency limits us in the creation of *seeds* and because the excitation on the intermediate state becomes more likely; in fact, a higher Δ_{IR} corresponds to a lower Δ_{blue} (equation 2.1 must hold), which can cause a loss of atoms due to the two-photon ionization by two resonant blue photons. In figure 2.7 the number of ions created by two-photon ionization (with the 420 nm laser) are plotted versus the pulse duration for different detunings. If the ions don't repel each other, they may become stuck in the region, leading to a plateau in figure 2.7 rather than a decrease. For the negative detuning -100 MHz,

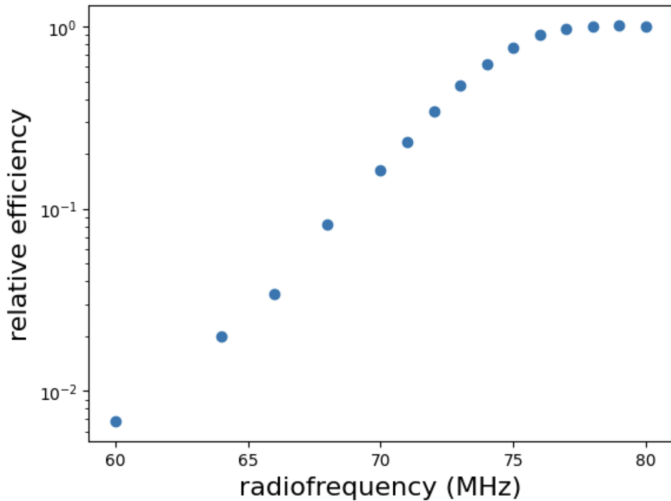


Figure 2.6: Relative diffraction efficiency of the AOMs versus the radiofrequency.

the behaviour is similar to the resonant case. This is because of the presence of the other hyperfine states $F = 1$ and $F = 2$ (table 2.1).

2.4 Detection

In our setup, an ion detector is employed to quantify the population of Rydberg excitations or ions generated by photoionization. Our experimental protocol consists of creating ions either by field-ionization of Rydberg atoms or by photoionization and activate an electric field ($E \sim 100$ mV/cm) that impels the resulting ions towards a charge multiplier (channeltron, see figure 2.9 for a scheme). Then, The channeltron sends a voltage pulse to the oscilloscope, for each arriving ion. The oscilloscope (figure 2.8) captures the input signal and sends it to a computer, figure 2.8 reports an example. A *LabWIEV* program, counts the peaks in that signal which corresponds to the number of arrived ions.

2.4.1 Detector limits

The detection system, like every measurement device, makes errors. It is important to keep in mind which errors can happen to be able to discriminate whether a result is corrupted by any systematic measurement error or not. Here we discuss two such detection errors. The *detection efficiency* is the probability of detecting an atom knowing that it has been ionized. This affects the measurement of each

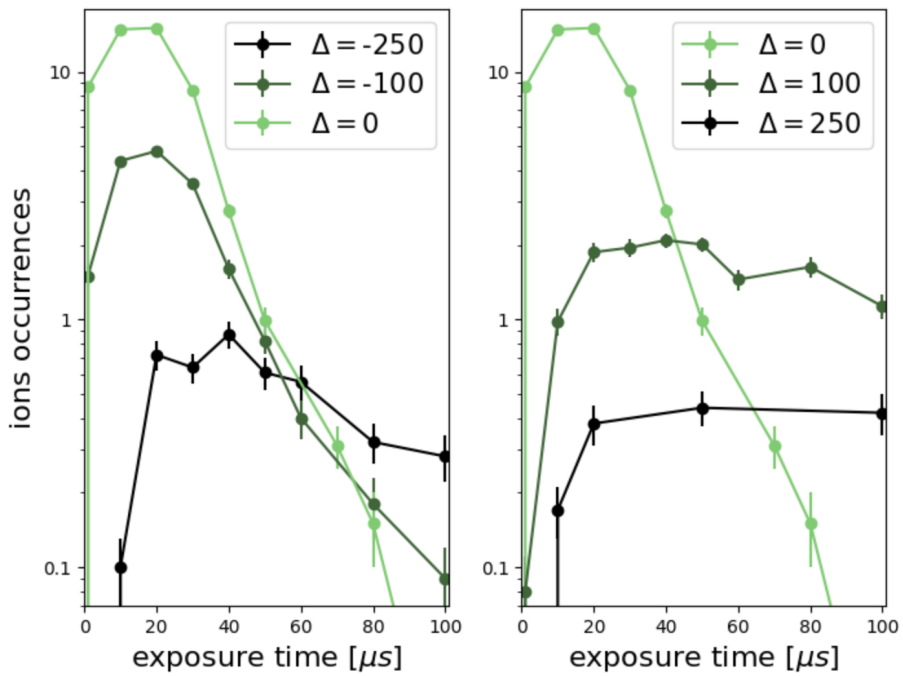


Figure 2.7: The number of ions obtained by two-photon ionization with the 420 nm blue laser, for different detunings from the $|6p_{3/2}, F = 3\rangle$. Red detunings (left), blue detunings (right). The curves are obtained varying the duration of the 420 nm laser pulse. It can be see that after about $\sim 30 \mu\text{s}$ the observed signal decreases. This is due to the strong repulsion between positive ions that are ejected from the interaction region. Moreover, the interaction region gradually empties, no longer leaving any available atoms for photoionization.



Figure 2.8: Typical signal observed on the oscilloscope during the detection. Each peak corresponds to an arrived ion.

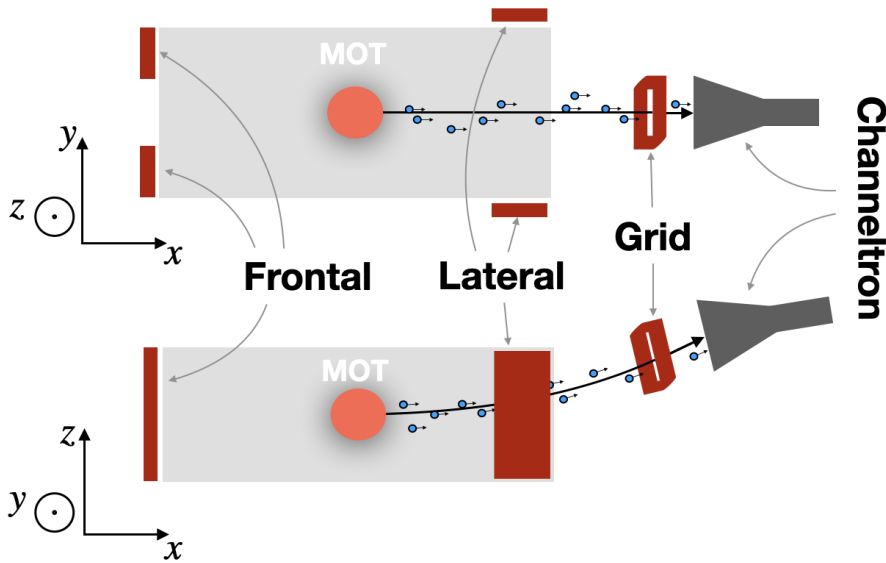


Figure 2.9: Scheme of the detection system, projection on $x - y$ plane (top) and on $x - z$ plane (bottom). The Frontal, Lateral and Grid plates are used to field-ionize the Rydberg atoms and/or adjust their trajectory toward the channeltron (the blue points represents the ions). The channeltron and the Grid are located inside the vacuum system that is not completely represented in this scheme.

ion independently of the number of ions. The second error is due to the *dead time* of the detector, which depends on the number of detected atoms, and hence becomes relevant for large numbers of detected ions.

Detection efficiency

Assuming that the detection setup does not change in time and that the detection of one ion does not affect the detection of another, in the first approximation, we assume that the detector commits a constant error independently for each ion. Let's suppose we have an ion in the interaction volume. I define the *detection efficiency* α as the probability of detecting that ion with the channeltron. Next the method we used to estimate α is presented.

The *detection efficiency* is defined as the probability to measure an atom knowing that it has already been ionized.

$$\alpha = p(\text{"detect"} | \text{"ionized"})$$

Following a frequentist approach I write it as the ratio between the number of

detected ions N_{det} and the number of ionized atoms N_{ion} .

$$\alpha = \frac{N_{det}}{N_{ion}} \leq 1$$

We already have N_{det} . What we need is N_{ion} . To measure it we use a CCD, with the following procedure.

- we create the MOT, and wait for it to stabilize (i.e., reach a steady state).
- at time $t = 0$ we block the flux of atoms from 2D MOT to 3D MOT (blocking the *push beam*) and start the excitation and detection cycles.
- Each cycle consists in sending a pulse of the blue beam of duration Δt and then measure the ions with the channeltron. The duration of one cycle is 1 ms.
- while the cycles run we take several measurements of the number of atoms with the CCD. We repeat the same experiment twice: with the photoionization ON or OFF. Results are plotted in figure 2.10.
- The loss is exponential in the first 40 s, so we fit it with a line (in semi-log scale), and then we estimate the rate for both curves.
- We estimate the loss rate due to photoionization computing the difference between the two rates. This difference is equal to $\frac{d}{dt} N_{ion}$.

In figure 2.10 the results are reported. The blue points are the natural loss of the MOT when the flux of atoms from the 2D MOT is blocked. The orange points are obtained adding a loss using the photoionization. When an atom is photoionized, it will not be able to be excited with the MOT beams and is quickly lost through acceleration by background electric fields. In the first 40 s we measured with the channeltron a mean value of ions $\bar{N} = 2.0 \pm 0.2$ atoms/cycle. So for unit of time

$$\frac{d}{dt} N_{det} = (2.0 \pm 0.2) \times 10^3 \text{ s}^{-1}$$

The rates given by the linear fits in figure 2.10 are

$$m_1 = (1.84 \pm 0.06) \times 10^3 ; \quad m_2 = (6.4 \pm 0.4) \times 10^3$$

$$\frac{d}{dt} N_{ion} = m_2 - m_1 = (4.6 \pm 0.4) \times 10^3$$

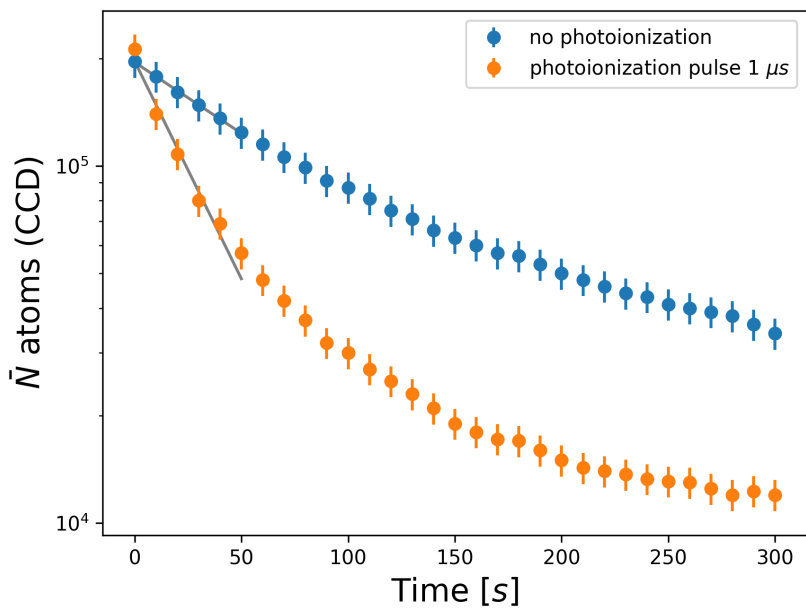


Figure 2.10: Number of atoms detected with CCD versus release time, in semilogarithmic scale. In $t = 0$ we block the flux of atoms from 2D MOT to 3D MOT. Cycle period $T = 1 \text{ ms}$. blue points: photoionization beam off. orange points: photoionization pulse $\Delta t = 1 \mu\text{s}$ for each cycle. Initially the loss is exponential (line in semi-log), and we fit it with a line.

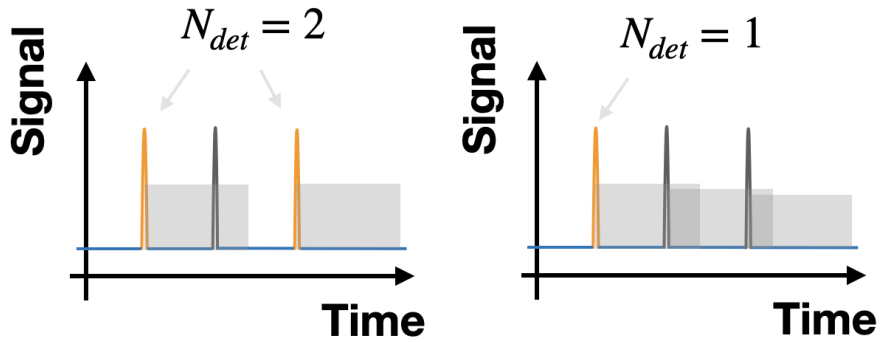


Figure 2.11: *Left: non-paralyzable dead time, if an ion arrives during the non-sensitive period (because of an other ion) does not increase the non-sensitive period itself. Right: paralyzable dead time, the arriving ion increase the non-sensitive period.*

so, the detection efficiency is given

$$\alpha = \frac{2.0 \pm 0.2}{4.6 \pm 0.4} \simeq 0.43 \pm 0.08$$

In the next two chapters I will use the *detection efficiency* as the calibration of the detector. When I rescale the data points, I note it in the captions.

Dead time

When an ion arrives at the channeltron, an electric pulse is sent to the oscilloscope. The temporal width of this pulse is non zero and can affect the measurement. Particularly, if two ions arrive with a temporal delay that is less than the width of the pulse, the oscilloscope will receive only one peak and the computer will count one ion only (figure 2.12). The *dead time*, τ , of a detector is defined as the minimum time interval that two consecutive counts must be separated in order to be recorded as two different events [29] [30]. Actually, there are two kind of *dead time* (figure 2.11): *paralyzable* and *non-paralyzable*. In the *paralyzable* case when an ion arrives it paralyzes the detector for a time τ even if the detector is already paralyzed by another ion. We assume to have a *non-paralyzable death time*.

Let's assume a *detection efficiency* equal to one, $\alpha = 1$. Suppose to detect ions for a time T in which the probability that an ion arrives at the detector is described by a uniform distribution. The number of ions that arrive at the detector will be

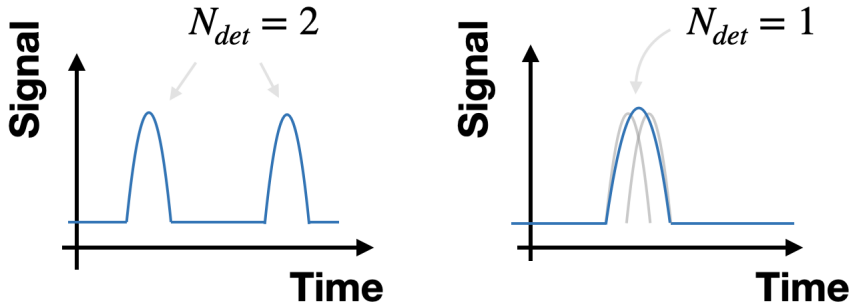


Figure 2.12: Left: the arriving delay is enough to well distinguish two ions. Right: the arriving delay is comparable with the width of a single pulse, the computer counts only one ion.

distributed as a Poissonian. We measure a rate m of ions and are interested in finding the true value of the rate n . If we know the value of the *dead time* τ we can say that the fraction of time in which the detector was not able to detect is $m\tau$. So the undetected ions will be $nm\tau$. The undetected ions are also given by the difference of the two rates

$$n - m = nm\tau$$

So, knowing τ we have an expression for n

$$n = \frac{m}{1 - m\tau} \quad (2.2)$$

This expression holds only for Poissonian distributed arriving atoms, so for the non-interacting case (see first chapter).

Estimation of the *dead time*

The *dead time* can be estimated from the distribution of time intervals between consecutive counts. In [30] an explicit expression for the distribution of time intervals between consecutive counts is given.

$$p(\Delta t | n, \tau) = ne^{-n(\Delta t - \tau)} \quad (\Delta t > \tau)$$

Where n is the rate of the arriving ions. If we approximate the distribution of the arriving time of one ion to a uniform distribution with width equal to the width of

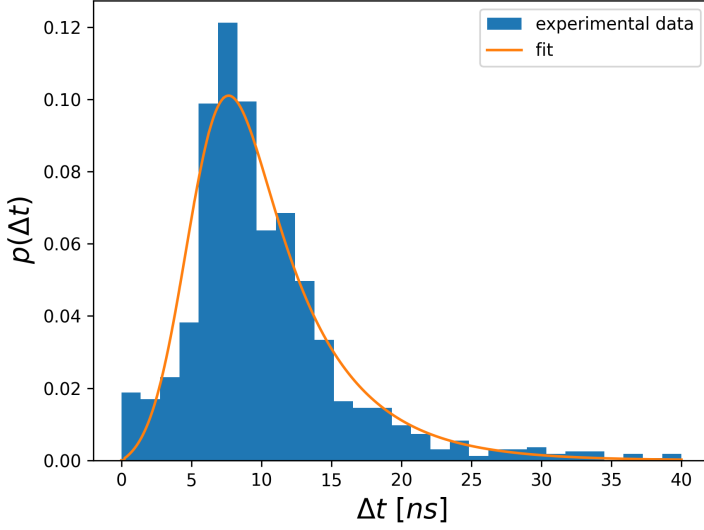


Figure 2.13: Histogram fit of the experimental data with the fit function of equation 2.4.

the observed distribution σ_0 , then n can be written in terms of the mean number of arriving ions per experiment \bar{N} .

$$n = \frac{\bar{N}}{\sigma_0}$$

Observing in figure 2.8 that the peaks on the oscilloscope have different sizes, I assume that the *dead time* is affected by a Gaussian jitter (i.e. the width of one peak is distributed with a Gaussian). The distribution is

$$p(\Delta t|n, \hat{\tau}, \sigma_\tau) = \int_0^\infty p(\Delta t|n, \tau)p(\tau|\hat{\tau}, \sigma_\tau)d\tau \quad (2.3)$$

$$p(\Delta t|n, \hat{\tau}, \sigma_\tau) = \int_0^\infty n e^{-n(\Delta t - \tau)} \frac{1}{\sqrt{2\pi\sigma_\tau^2}} e^{-\frac{(\tau - \hat{\tau})^2}{2\sigma_\tau^2}} d\tau \quad (2.4)$$

Where $p(\Delta t|n, \hat{\tau}, \sigma_\tau)$ is the probability to observe to consecutive arriving with a temporal delay of Δt . σ_τ is the width of the Gaussian noise. Using this function as fit function (with parameters n , $\hat{\tau}$ and σ_τ), we performed an histogram-likelihood fit on the histogram of the time interval between consecutive counts. To build the histogram we repeat 100 times an experiment which consists in exciting few atoms (up to 5, in order to have no interactions) to the Rydberg state and than

detect them. We got the result in figure 2.13, with estimated parameters:

$$\begin{cases} n = 0.21 \pm 0.07 [ns^{-1}] \\ \hat{\tau} = 5.3 \pm 0.6 \text{ [ns]} \\ \sigma_{\tau} = 2.3 \pm 0.5 \text{ [ns]} \end{cases}$$

Where the errors are computed with a bootstrap; the fit is repeated 10 times with 100 random points from a total sample size of 2000 points.

We typically measure a width for the absolute arrival time distribution between tens and hundreds of ns. So, for example, if the width is 200 ns, we expect saturation due to the *dead time* when there are about ~ 40 arriving ions.

Closing remarks

In this chapter the experimental setup was described. Particularly focusing on the excitation lasers setup. In conclusion an estimation of the *detection efficiency* and the *dead time* is given. In the last two chapters the *detection efficiency* will be used to correct the data points. I will indicate it in the captions. In the next chapter I will show the results about the characterization of the dipole trap, which is a target of this thesis. I will provide a method to estimate the number of atoms trapped in a dipole trap, followed by a characterization of the loading process of a dipole trap.

Chapter 3

Characterization of the FORT

As discussed in the introduction, dipole traps are the building block for any Rydberg Atomtronics device. During my work we setup and characterized such a dipole trap. The technical details are reported in chapter two, and the methods used for setting up have been covered in [36].

In this chapter I will show the experiments we did in order to characterize the dipole trap. Particularly, I will answer the question "how many atoms are we trapping?" providing a simple model to interpret the experimental data. Furthermore, I will show a method to experimentally estimate the photoionization rate (section 1.3.5). In the last section I will introduce a model for the loading of the FORT, showing an experimental result in order to characterize the order of magnitude of loading time of our FORT. In conclusion I will discuss some methods that could be used for trapping a single atom, since the long-term project aims to that. I begin by giving a detailed description of the experimental protocol.

3.1 Experiment description

Figure 3.1 shows the pulses diagram we typically use in the experiments, and figure 3.2 shows a graphic representation of the experiment steps. We start cooling the atoms with the MOT for few seconds, then we switch on the FORT in point C. The FORT starts to fill until point t_0 , where the MOT beams are switched off. In the interval from t_0 to A, only the FORT is kept on. During this interval ($\sim 100 \text{ ms}$)

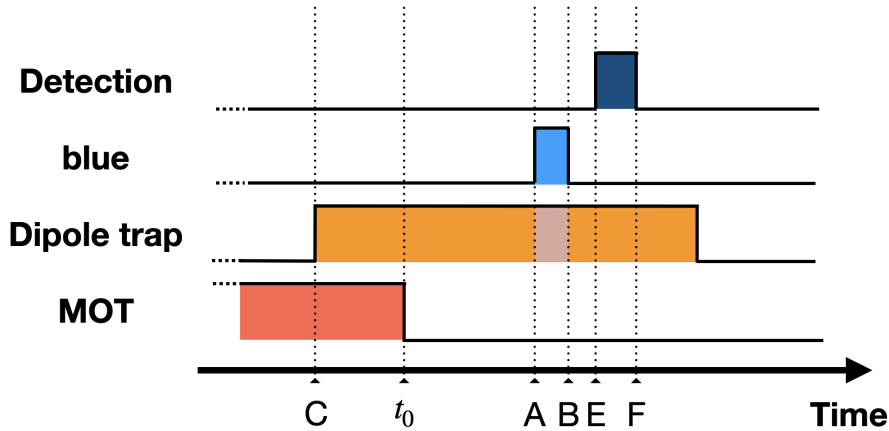


Figure 3.1: *Typical pulses diagram used in the experiments. The typical timescales used for these intervals are: loading MOT \sim s, C- t_0 \sim ms – s, t_0 -A \sim 100 ms, A-B \sim μ s, B-E \sim μ s, E-F = 30 μ s.*

the residual atoms (i.e. the atoms that are not in the trapping region of the FORT) move away from the interaction region due to thermal motion and acceleration under gravity. In the interval from **A** to **B** the 420nm laser is switched on and the atoms can be photoionized with a two-photon ionization process (both with 420nm+420nm or 420nm+840nm)¹. The intensity of the FORT beam during this interval is different than during the loading stage, in figure 3.1, the different color of the dipole trap orange pulse emphasizes it. This is done to keep always the same intensity of the two beams during the photoionization, to have always the same photoionization rate. The 420nm beam has a power of 1.5mW and a waist 40 μ m, which implies an intensity $I_{420} = 29\text{W/cm}^2$. The 840nm has 135mW of power and a waist of 5 μ m which implies $I_{840} = 170\text{kW/cm}^2$. The interval **B** to **E** is fixed to 0.7 μ s, which is empirically chosen during the calibration to optimize the detection. Between **E** and **F** (30 μ s for all the experiments) the electric field, which accelerates the atoms to the *channeltron*, is switched on.

Since the lifetime of the FORT ($\sim 1\text{s}$) is much longer than the time necessary for the residual atoms to move away from the interaction region (from t_0 to **A**), I divide the experiment in the following three consecutive processes: Loading (from **C** to t_0), Photoionization (from **A** to **B**) and Detection (from **E** to **F**). For these three consecutive processes we can observe the following properties.

¹Actually, when we tried to photoionize the atoms only with two 420nm photons we measured no ions. The main process is 420nm + 840nm.

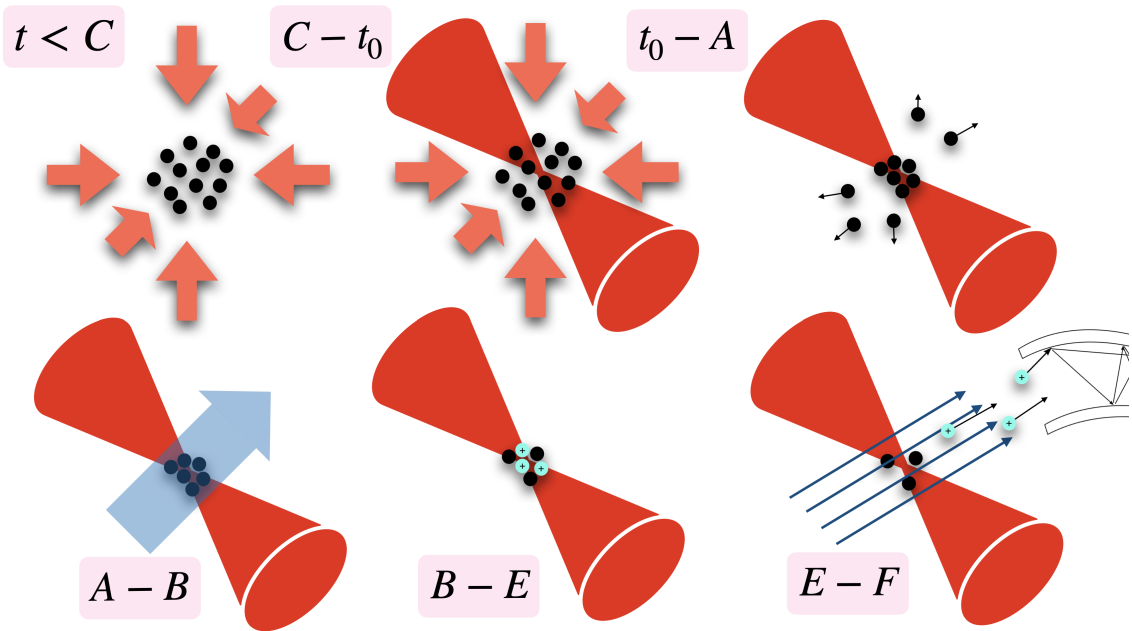


Figure 3.2: A graphic representation of the phases of the experiment. The labels correspond to the times of figure 3.1.

- **Loading (from C to t_0)**

I call $p_L(N; \bar{q})$ the distribution of the number of atoms in the dipole trap.

$$N \sim p_L(N; \bar{q})$$

where \bar{q} is a set of parameters of the distribution. A model to find this distribution is treated later in this chapter.

- **Photoionization (from A to B)**

I define λ the probability to photoionize an atom with a photoionization pulse of duration Δt as

$$\lambda = p(\Delta t) = 1 - e^{-\Gamma_{ph}\Delta t} \quad (3.1)$$

Where Γ_{ph} is the photoionization rate. Since the excitation of different atoms are independent events, the probability to photoionize k atoms given N

atoms in the dipole trap is a binomial with probability of an event equals to λ .

• Detection (from E to F)

As discussed in section 2.4.1 our detector is affected by two type of errors. If, in first approximation, we neglect the effect of the *dead time* ($m\tau \ll \sigma_0$, using the notation introduced in section 2.4.1), the probability to detect M ions given k photoionized atoms in the trapping region is a binomial, where α is the probability to detect an atom knowing that it has been photoionized, or in other words the *detection efficiency*.

Under these assumptions one can see that the process **Photoionization + Detection** is also a binomial, with probability of a single event equal to $\lambda\alpha$:

$$p(M|N) = \binom{N}{M} (\lambda\alpha)^M (1 - \lambda\alpha)^{N-M}$$

where N is the number of atoms in the dipole trap, and M are the detected ions. Marginalizing over N the distribution for M is finally given.

$$p(M; \bar{q}) = \sum_{N=M}^{\infty} p(M|N)p_L(N; \bar{q}) = \sum_{N=M}^{\infty} \binom{N}{M} (\lambda\alpha)^M (1 - \lambda\alpha)^{N-M} p_L(N; \bar{q}) \quad (3.2)$$

It is reasonable to assume that $p_L(N; \bar{q})$ is a monomodal distribution. If we assume that it is also sub-Poissonian we approximate it to a delta centered in \hat{N} , $p_L(N; \bar{q}) = \delta(N - \hat{N})$. Where \hat{N} is the fixed number of atoms. Under this assumption the probability distribution for M becomes:

$$p(M; \hat{N}) = \binom{\hat{N}}{M} (\lambda\alpha)^M (1 - \lambda\alpha)^{\hat{N}-M}$$

If one knows λ and α it would be possible to estimate the number of atoms \hat{N} using that the mean of the binomial distribution is $\lambda\alpha\hat{N}$ and that the sample mean is an unbiased estimator for it:

$$\langle \bar{N} \rangle = \lambda\alpha\hat{N} ; \quad \bar{N} = \frac{1}{n} \sum_i^n k_i$$

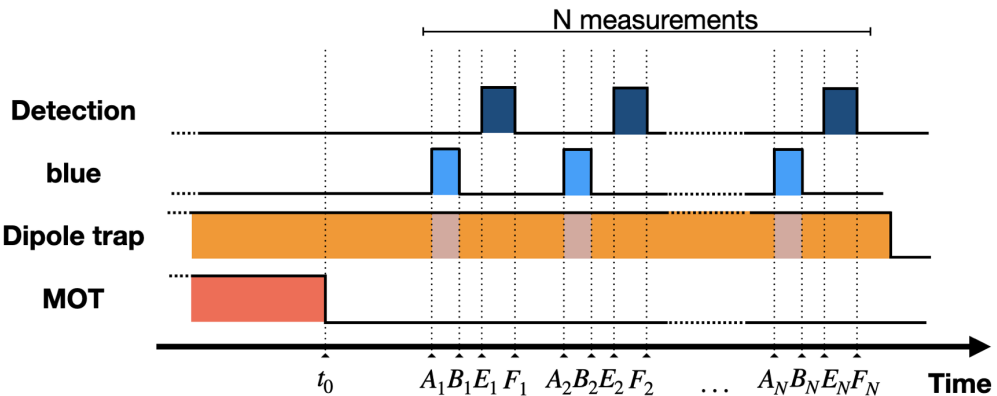


Figure 3.3: *Multiple measurements experiment pulses diagram.* The darker regions in the "Dipole trap" line correspond to changes of power. To be able to measure always with the same photoionization rate, when we change the dipole trap depth, during the photoionization, we came back to the same power.

with \bar{N} the sample mean, n the number of experiments and k_i the outcome of the i^{th} experiment. Next in this chapter, I will rescale some plots with $1/\lambda\alpha$. I will indicate it in the captions.

3.2 How many atoms?

Our aim is to estimate the number of atoms N trapped in the FORT. To avoid having to deal with numerical estimation of λ one could think to choose a photoionization pulse long enough so that $\lambda \simeq 1$, which is true when $\Delta t \gg \frac{1}{\Gamma_{ph}}$. In this limit, one needs only to estimate α and not λ to rescale the data points. Increasing the pulse duration actually imposes some limits. With longer exposure times the detection is delayed, and the ions have more time for to interact and repel with each other (because of the Coulomb force), which can lead to them not arriving at the channeltron. Moreover, with a longer pulse the number of arriving ions will be much larger, and this could saturate the detector (because of the *dead time*), affecting the measurements. The solution I propose to solve this problem goes in the opposite direction: $\Delta t \ll \frac{1}{\Gamma_{ph}}$. The idea is to perform multiple measurements with a shorter photoionization pulse (such that $\lambda \simeq 0$) each, in order to empty the FORT piecemeal. Summing all the consecutive experiments, one gets an estimation of the FORT occupation. Figure 3.3 shows the pulses diagram of the *multi-measurement* experiment. With this method we are stretching the ph-

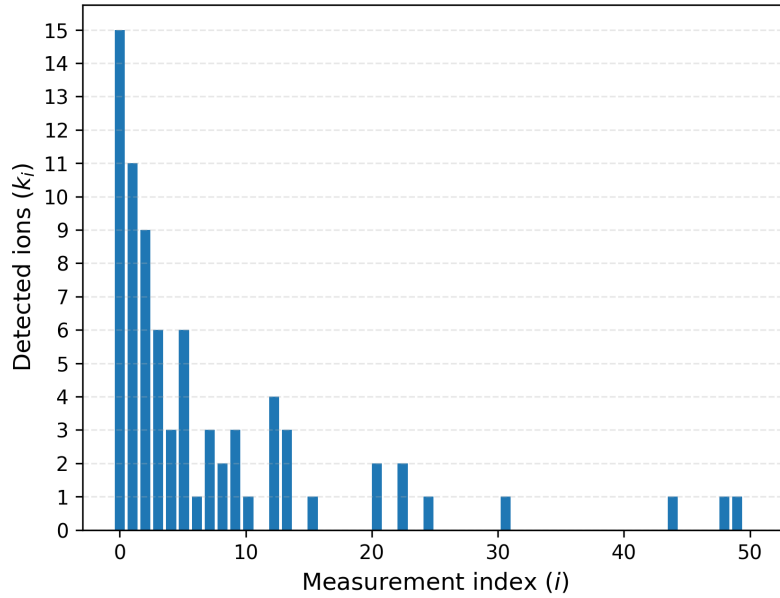


Figure 3.4: Example of one experiment result. Obtained executing once the pulses diagram in figure 3.3. k_i is the number of ions detected in the i^{th} measurement. Not rescaled data.

toionization pulse duration dividing it into several shorter pieces. To be sure that the natural atoms losses of the dipole trap do not affect the experiment, the dipole trap lifetime must be much longer than the overall *multi-measurement* duration. In the experiment described in this section the overall time for each experiment is 50ms (50 measurements of 1ms duration), and the lifetime is ~ 1 s, so that the above condition is fulfilled.

Running the experiment once (diagram in fig. 3.3) we obtain the raw data reported in figure 3.4. Repeating the same experiment 10 times and keeping the mean and standard deviation for each measurement we obtain the plot in figure 3.5.

Summing all the consecutive measurements for each of the 10 experiments, and computing sample mean and standard deviation, we finally get an estimate of the number of atoms versus the trapping depth, figure 3.6.

Actually, as introduced at the beginning of the present chapter, the *detection efficiency* defines a calibration for the detection, so I rescaled the points in figure 3.6 by α . The *detection efficiency*, α , can be estimated using as reference the measurement of the number of atoms done with a CCD. I've reported the complete

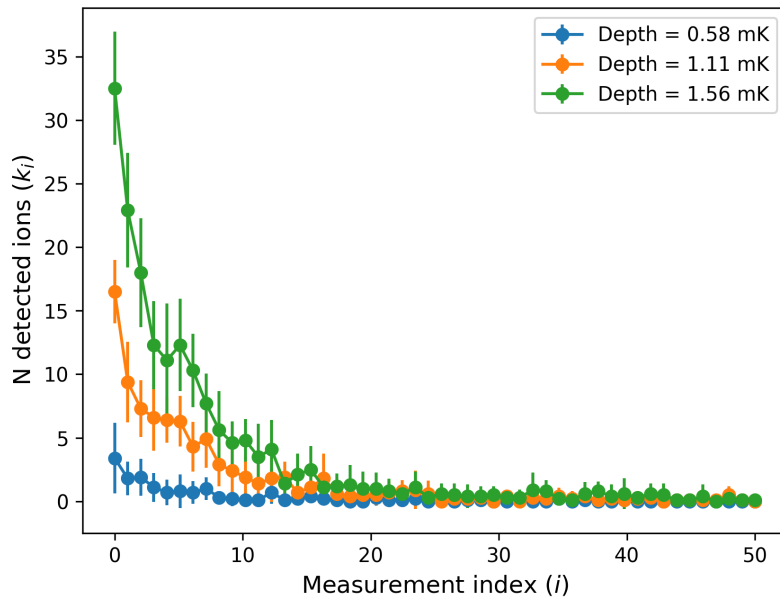


Figure 3.5: *Multi-measurement experiment. Each line is obtained repeating the experiment (of figure 3.4) 10 times and taking the mean and standard deviation for each measurement. Distance between the beginning of two consecutive measurements is 1 ms. Photoionization pulse duration (for each measurement) is 1 μ s. Not rescaled data.*

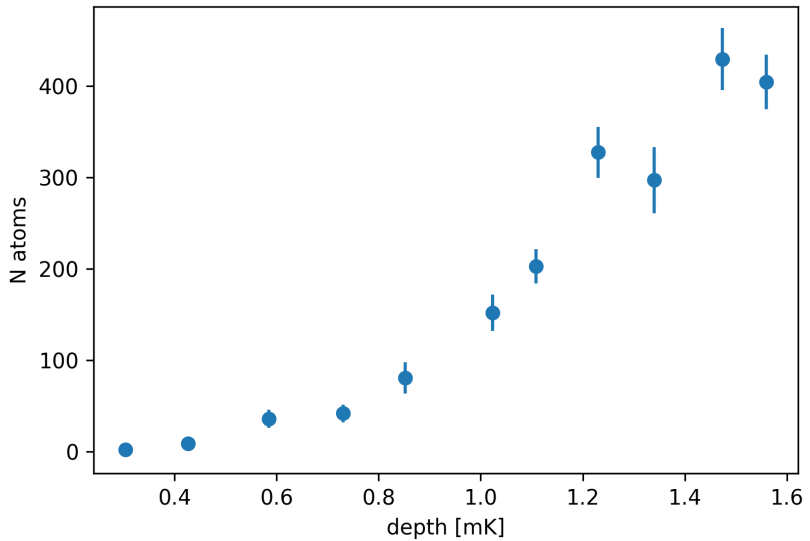


Figure 3.6: *Measured number of atoms vs. FORT depth. Data points are rescaled by $1/\alpha$.*

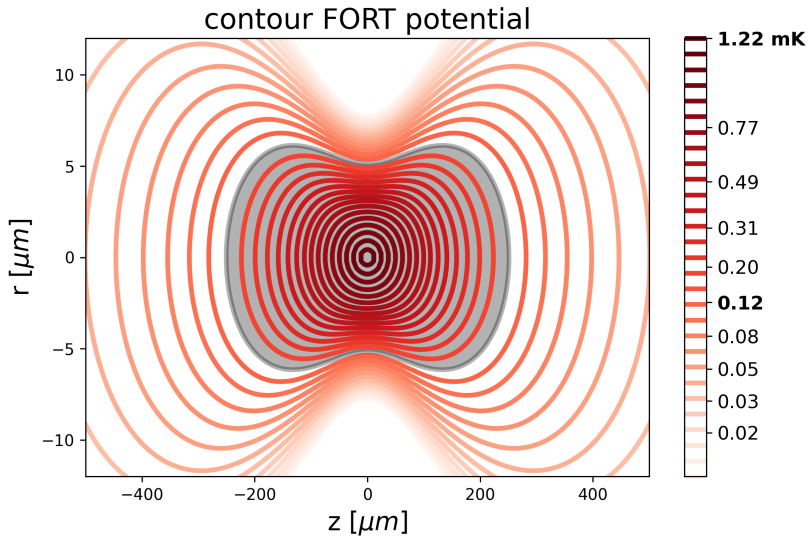


Figure 3.7: Fixed-potential curves from expression 3.3, with $P = 100 \text{ mW}$, $\lambda = 840 \text{ nm}$, $w_0 = 5 \mu\text{m}$, $\Delta \simeq 30 \text{ THz}$. x and y axes are longitudinal and radial axis of the dipole trap. The maximum depth is bold in the top of the colorbar $U_{max} = 1.22 \text{ mK}$. The grey shadow region indicates the trapping volume if the temperature of the system is $T = 120 \mu\text{K}$.

procedure in section 2.4.1 of this work.

3.2.1 A model for the number of atoms in the FORT

To describe the data obtained in figure 3.6 we made a model that consists in estimating the number of atoms in the MOT within a certain trapping volume and with a certain density. The trapping volume can be estimated by integrating the grey region in figure 3.7 (from chapter one. I report the figure here for the convenience of the reader). The potential given by the dipole trap is (from chapter one):

$$U_{dip}(z, r) = \frac{3c^2 P}{\omega_0^3 w(z)^2 \Delta} e^{-\frac{2r^2}{w(z)^2}} \quad (3.3)$$

where $w(z)$ is the waist in z (longitudinal axis), P is the power of the dipole trap laser beam, Δ is the detuning from the atomic resonance of the dipole trap laser beam, ω_0 is the frequency of the atomic transition, and r is the radial coordinate. The trapping volume is defined as all the points (r, z) in which the optical potential energy $U_{dip}(r, z)$ is higher than the mean kinetic energy of the atoms in the MOT

$k_b T$,

$$|U_{dip}(r, z)| > k_b T$$

in our MOT the temperature is about $T = 120 \mu K$. Taking equation 3.3 and solving for r , and fixing the energy to $k_b T$, one obtains

$$r(z) = w(z) \sqrt{\frac{1}{2} \ln \left(\frac{3c^2 P \Gamma}{\omega_0^3 w(z)^2 \Delta} \frac{1}{k_b T} \right)} \quad (3.4)$$

The longitudinal width of the trapping volume is defined by,

$$r(z) = 0 \Rightarrow z_0 = z_r \sqrt{\frac{U_0}{k_b T} - 1}$$

where z_r is the Rayleigh length and $U_0 = U_{dip}(0, 0)$ is the deepest point of the optical potential. The trapping volume can be estimated by the following integral,

$$V = 2 \int_0^{z_0} \pi r(z)^2 dz \quad (3.5)$$

The surface area of this volume is given by,

$$A = 2 \int_0^{z_0} 2\pi r(z) dz. \quad (3.6)$$

To estimate the order of magnitude of the number of atoms trapped in the dipole trap we assume that the density in the dipole trap has the same order of magnitude than the density in the MOT. This assumption is supported by the fact that the MOT density is mainly limited by the collisions between atoms. Particularly, collisions are induced by MOT beams [28]: Assume that a pair of atoms in the ground state are dressed by a near-resonant laser to an excited P state. When one of the two is excited, the two atoms start to interact through the long-range dipole-dipole potential $V(d) \propto -\frac{1}{d^3}$, where d is the inter-atomic distance. If the depth of the dipole trap U_0 is exceeded by the kinetic energy the atoms acquire before the excited one radiates back to the ground state, both (or only one) escape the trap. The MOT beams are kept on during the loading of the dipole trap, and are switched off when the loading ends. So, the flux of atoms toward the FORT is interrupted. By these considerations we expect that the FORT loading is limited by the same process as the MOT. In other words we expect that the density of atoms

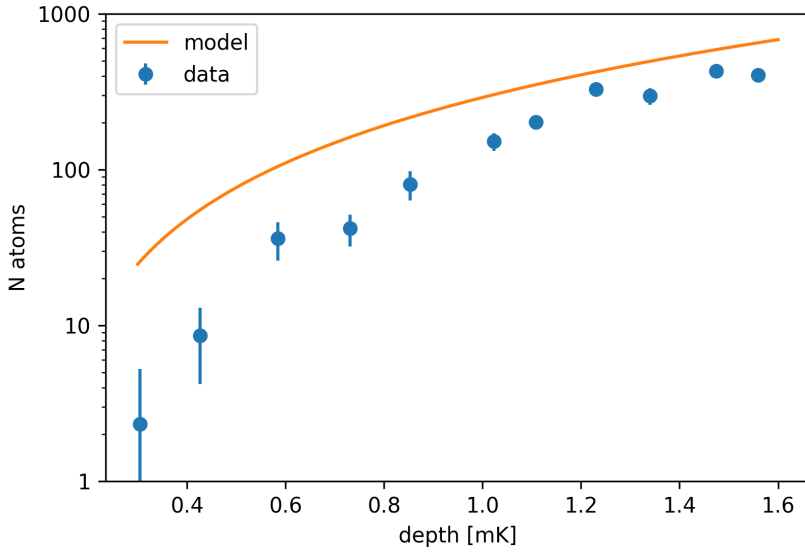


Figure 3.8: Number of atoms trapped in the dipole trap in semi-log scale. Blue points are obtained experimentally, orange curve is obtained by the model discussed in the text. Parameters used for the model: $d_{\text{MOT}} = 10^9 \text{ cm}^{-3}$, $w_0 = 5 \mu\text{m}$, $T = 120 \mu\text{K}$. Data points are rescaled by $1/\alpha$.

in the MOT and in the FORT is the same. The typical mean density we measure with the CCD in the MOT is in the order of magnitude of $d_{\text{MOT}} = 10^9 \text{ cm}^{-3}$. Using this value we just multiply it by the volume computed numerically by expression 3.5, obtaining

$$N = V d_{\text{MOT}}$$

We repeated the same calculation for different depths. In figure 3.8 the experimental data and the model are shown together in semi-log scale, to emphasize differences of the orders of magnitude. For deeper FORTs model and data points differ by a factor 2. While for a shallow trap there is an order of magnitude of difference. This could be explained by the following reasoning: In the experiment we wait 100ms from point t_0 to point A_1 (figure 3.3) assuming that this time is much shorter than the FORT lifetime. Actually this is true only for deeper traps. We observed that the lifetime for a trap with a depth of 0.6mK is $\sim 100\text{ms}$. This is comparable with the waiting time, so the losses in the first 100 ms are not negligible.

3.3 Estimation of the Photoionization rate

One way to detect the atoms with our apparatus is by photoionization. So, for many applications (such as the correction of the data, as I've shown before in this chapter) can be useful to have a quick way to estimate the photoionization rate. From the data of the experiment shown in figure 3.5 is also possible to estimate the ionization rate Γ_{ph} of the two-photon process 420nm+840nm. Let me write again the probability of an atom to be photoionized with a beam pulse of duration Δt :

$$p(\Delta t) = 1 - e^{-\Gamma_{ph}\Delta t}$$

If we repeat n_c consecutive measurement (as in fig. 3.3, label with N), with a photoionization pulse duration Δt , then the probability that an atom is photoionized in the i^{th} measurement is equal to the product of the probability that this atom is not photoionized in the previous $i - 1$ measurements times the probability to photoionize it in the i^{th} . I will call it P_i .

$$P_i = (1 - p(\Delta t))^i p(\Delta t)$$

Given the results of one experiment (example in fig. 3.4) and assuming that the number of consecutive experiments n_c is big enough such that $P_{n_c} \simeq 0$, I assume that, at the end of the *multi-measurement* experiment, all the atoms in the dipole trap have been photoionized and so that $N = \sum_i^n k_i$. As we can see, in figure 3.5, after 20 measurements the number of detected ions is $\simeq 0$, which means that most of the atoms have been ionized. The likelihood $L(\Gamma_{ph})$ is a multinomial function given by the following expression

$$L_{k_0, \dots, k_{n-1}}(\Gamma_{ph}) = p(\{k_i\}_{0, \dots, n-1} | \Gamma_{ph}) = N! \prod_i \frac{P_i^{k_i}}{k_i!}$$

where k_i are the ions detected in the i^{th} measurement, with $i \in \{0, \dots, n\}$. Imposing that

$$\frac{d}{d\Gamma_{ph}} \log L = 0$$

One finds the maximum likelihood estimator (MLE) reported in expression 3.7.

$$\hat{\Gamma}_{ph} = \frac{1}{\Delta t} \log \left(\frac{N}{\sum_i i k_i} + 1 \right) \quad (3.7)$$

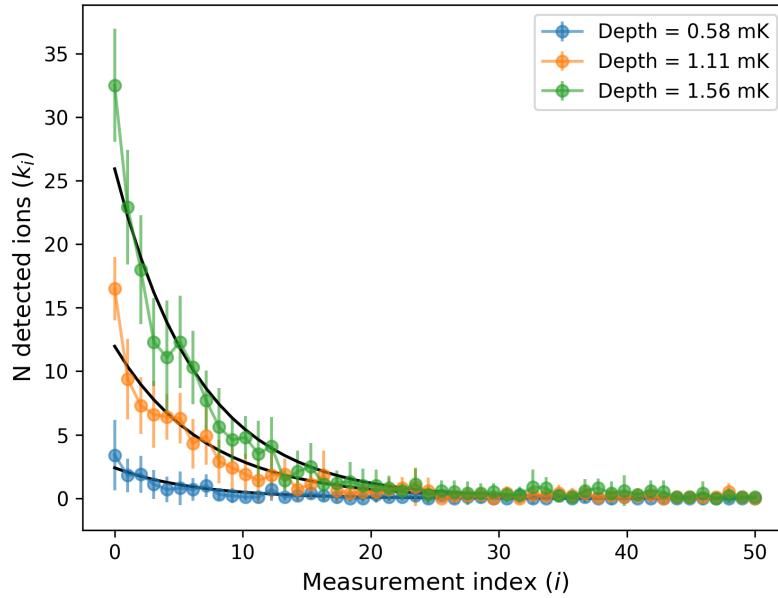


Figure 3.9: *Histogram likelihood fit.*

Where $N = \sum_i^n k_i$. If we correct the data $\{k_i\}$ dividing them by the *detection efficiency* α . Since N is the sum of these bins, it is corrected in the same way.

$$k_i \rightarrow \frac{k_i}{\alpha} ; N \rightarrow \frac{N}{\alpha}$$

If one substitutes them in the expression 3.7 one sees that α cancels out, so even if $\alpha < 1$ the expression of the MLE of the rate remains the same.

Fitting 10 experiments with the MLE, and taking the mean and the standard deviation of the results, figure 3.10 reports the estimated rates versus the dipole trap depth. The obtained points agree each other since we used the same intensities of the two laser beams (840 nm and 420 nm) in all the experiments. Figure 3.9 shows three of these fits explicitly.

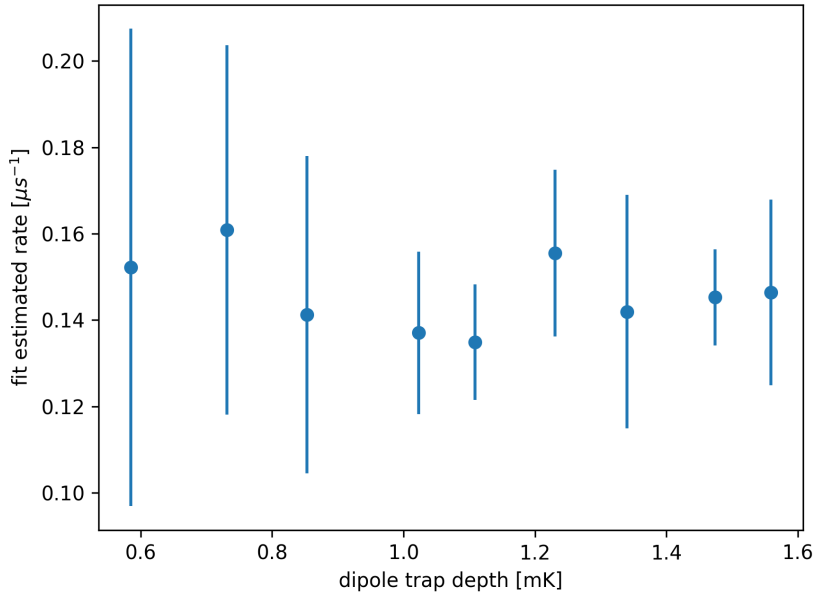


Figure 3.10: *Estimated photoionization rate obtained by maximum likelihood estimator.* We repeated the experiment 10 times, the points and errorbars are the mean and standard deviation of the estimated rate of each repetition of the experiment. Computing mean and standard deviation of the means we get the rate $\Gamma_{ph} = 0.15 \pm 0.01 \mu\text{s}^{-1}$.

Computing mean and standard deviation of the points in figure 3.10 I obtain the rate $\Gamma_{ph} = 0.15 \pm 0.01 \mu\text{s}^{-1}$. I will use this number to correct the data points in the next section.

3.4 Loading of the FORT

The understanding of the loading statistics of a dipole trap is interesting mainly for practical reasons. First of all, knowing the time scale of loading (i.e. the order of magnitude of the time necessary to reach the steady state) would permit us to adapt the experiment duration, and optimize it. Second, with the goal of trapping a single atom, it is important to understand how to artificially control the number of atoms occupying the trap. In this section I will show the experimental results for the loading of the FORT and discuss how a single atom can be trapped.

3.4.1 Loading time experiment

To measure the order of magnitude of the loading time we did an experiment which consists in the same pulses diagram reported in figure 3.1. We define the loading time as the time interval from point **C** to point t_0 in the figure. Figure 3.11 (top) shows the experimental result. The stationary state is reached after about 10 ms. Figure 3.11 (bottom) shows the number of ions detected with a negative loading time, i.e. the FORT is switched on after that the MOT is switched off. In the first 2 ms after switching off the MOT beams some atoms remain in the trapping region, and they may still be trapped.

3.4.2 A model for FORT loading

We can imagine that when the FORT is switched on, and it is focused in the middle of a MOT, the atoms located in the trapping volume will feel a force toward the maximum intensity point of the FORT beam. The atoms will accumulate in the FORT until collisions start to limit the loading process [28] [2]. Following ref. [28] we can define the rates of the possible processes that can happen. One atom can either enter in the dipole trap or be lost. We define R the rate of loading, which doesn't depend on the number of atoms contained in the FORT. The losses, instead, can be of two types. The lost atom could have hit either a background atom (i.e. an atom that is in the vacuum chamber and hasn't been cooled), which was not trapped, or one that was trapped in the FORT. In the first case we define γ the rate of one-body collisions of one atom. If the FORT contains N atoms, the atoms loss rate due to one-body collisions is γN . In the second case both colliding atoms belong to the trap. The number of possible collisions, if in the FORT there are N atoms, is equal to $N(N-1)/2$ and the loss rate is $\beta N(N-1)/2$. Where β is the rate of two-body collisions if only two atoms fill the FORT. I have modelled this system with a *birth death* model that corresponds to the *continuous-time markov chain* shown in figure 3.12, where $r_N = \gamma N + \beta N(N-1)/2$ is the overall loss rate. When a two-body collision occurs, we have to distinguish two cases: one or both of the atoms may be lost. The figure shows the model in which only one atom is lost after a collision. The *transition rate matrix* of the chain is the following

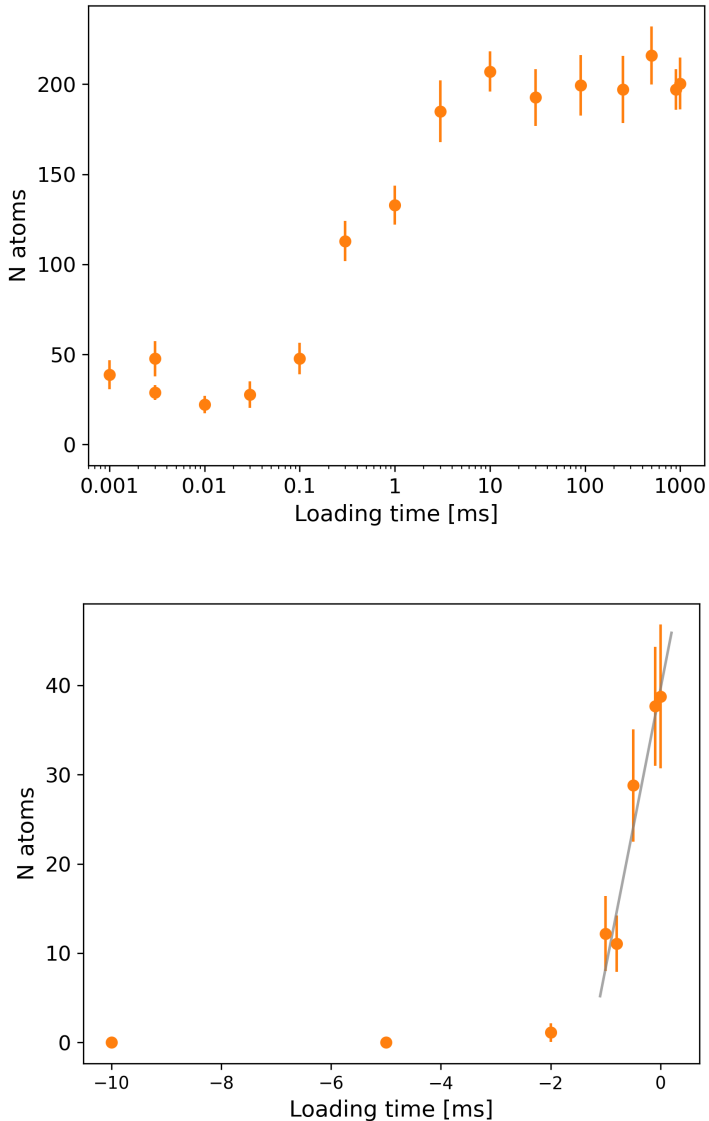


Figure 3.11: The number of trapped atoms versus the loading time. Referring to the diagram in figure 3.1 the loading time corresponds to the interval $C-t_0$. The other intervals are fixed to: $t_0-A=100$ ms, $A-B=1.6$ μ s. The cycles period is 4s and so the loading time of the MOT is 4s too. The upper graph shows, in semi-logarithmic scale, the results for positive loading times, the lower graph, in linear scale, negative loading times (i.e. the dipole trap switches on after that the MOT switches off). The mean density of atoms in the MOT is $6 \cdot 10^9$ cm $^{-3}$. Depth of the dipole trap is $U_0 = 1.6$ mK. Points are rescaled by $1/\alpha\lambda$, with $\lambda \simeq 0.21$ computed using expression 3.1, and the photoionization rate estimated in the previous section $\Gamma_{ph} = 0.15\mu\text{s}^{-1}$.

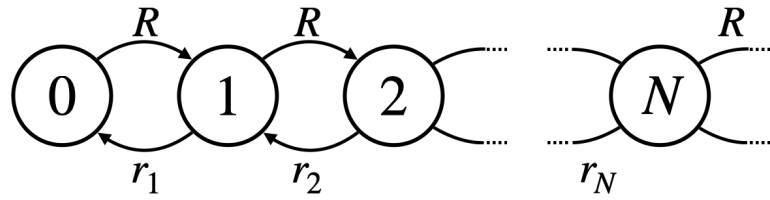


Figure 3.12: Here a diagram of the continuous-time Markov Chain model. $r_N = \gamma N + \beta N(N - 1)/2$ is the loss rate.

tridiagonal matrix,

$$P = \begin{pmatrix} -R & R & 0 & 0 & \dots & 0 & \dots \\ r_1 & q_1 & R & 0 & \dots & 0 & \dots \\ 0 & r_2 & q_2 & R & \dots & 0 & \dots \\ \vdots & \vdots & \vdots & \vdots & \ddots & R & \dots \\ 0 & 0 & 0 & 0 & r_N & q_N & \dots \\ \vdots & \vdots & \vdots & \vdots & \vdots & \vdots & \ddots \end{pmatrix}$$

where $q_N = -r_N - R$. The evolution of the system is given by

$$\frac{d\bar{p}}{dt} = \bar{p}P$$

where \bar{p} is the probability vector associated to the state of the system (i.e. the i^{th} component of the vector is the probability to find i atoms in the trap). To trap a single atom we would like to know the stationary state of the system, and how it changes with the parameters R , γ and β . The stationary state of the chain can be computed solving the equation,

$$\frac{d\bar{p}}{dt} = 0 \Rightarrow \bar{p}P = 0$$

that corresponds to the following linear system,

$$\begin{cases} -Rp_0 + r_1 p_1 = 0 \\ Rp_0 - (r_1 + R)p_1 + r_2 p_2 = 0 \\ \vdots \\ Rp_{i-1} - (r_i + R)p_i + r_{i+1} p_{i+1} = 0 \end{cases} \quad (3.8)$$

which has solution

$$p_i = \frac{R}{r_i} p_{i-1} \Rightarrow p_i = \frac{R^i}{\prod_{j=1}^i r_j} p_0$$

imposing the normalization the stationary state distribution is found,

$$\sum_{i=0}^{\infty} p_i = 1 \Rightarrow \frac{1}{p_0} = \sum_{i=1}^{\infty} \frac{R^i / i!}{\prod_{j=1}^i (\gamma + \beta(j-1))}$$

$$p_i = \frac{R^i}{\prod_{j=1}^i (\gamma j + \beta j(j-1)/2)} p_0 \quad i \geq 1$$

Using *Wolfram Alpha* I rewrite this expression in a closed form (i.e. without an infinite series) as

$$p_i = \frac{\left(\frac{R}{\beta}\right)^i}{i! \Gamma\left(\frac{\gamma}{\beta} + i\right)} p_0 ; \quad p_0 = \frac{\left(\frac{R}{\beta}\right)^{\frac{\gamma/\beta-1}{2}}}{I_{\frac{\gamma}{\beta}-1}\left(2\sqrt{\frac{R}{\beta}}\right)}$$

(3.9)

where $\Gamma(\cdot)$ is the *gamma* function and $I_\nu(\cdot)$ is a modified Bessel function of the first kind of order ν . Once we have computed the stationary state $\{p_i\}$, the mean value and the variance are given by,

$$\langle N \rangle = \sum_{i=0}^{\infty} i p_i ; \quad \langle N^2 \rangle = \sum_{i=0}^{\infty} i^2 p_i$$

$$\text{Var}(N) = \langle N^2 \rangle - \langle N \rangle^2$$

Figure 3.15 shows the mean value of N and the *Mandel-Q* parameter in the stationary state versus the ratio R/γ . The different red curves are obtained changing the ratio β/γ in the range 10^{-1} to 10^5 . It is interesting to notice that, for $\beta/\gamma \gtrsim 10^2$, there is a "flat" region for $R \gtrsim 2\gamma$. In this region the mean number of trapped atoms is ~ 1 and the statistics is strongly sub-Poissonian ($Q < 0$). This means that with a good set of parameters would be possible to trap a single atom. To give an order of magnitude to these parameters I followed the models realized by Kuppens *et al.* in [28].

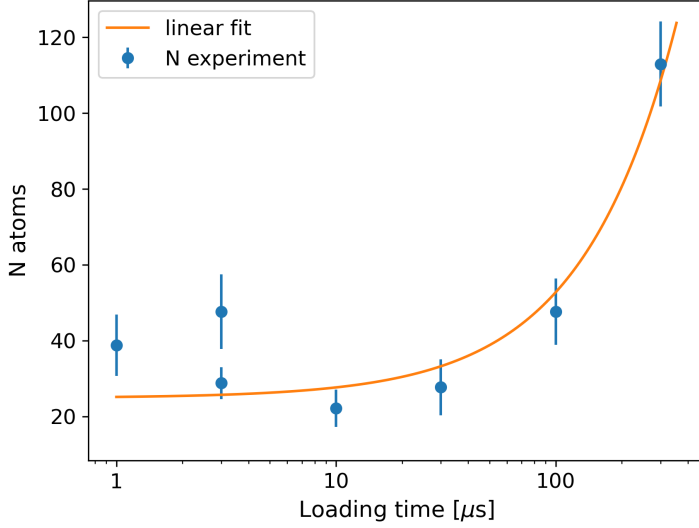


Figure 3.13: Linear fit of the data in figure 3.11, in the first $300\mu\text{s}$, in semi-log scale.

The loading rate: R

Ref. [28] defines the rate R as the flux of atoms crossing the surface of the trap region multiplied by the probability of trapping,

$$R = \frac{1}{4}d_{\text{MOT}}\bar{v}AP_{\text{trap}} \quad (3.10)$$

where d_{MOT} is the density of the MOT, $\bar{v} = \sqrt{K_b T/m}$ is the root mean square velocity of the atoms in the MOT, A is the surface of the trapping volume (given by expression 3.6) and P_{trap} is the probability that an entering atom remains in the FORT. We measure a MOT mean density of $d_{\text{MOT}} \simeq 10^9 \text{ cm}^{-3}$. The mean velocity, with a temperature of $120 \mu\text{K}$, is $\bar{v} \simeq 0.1 \text{ m/s}$. The trapping region surface, computed with equation 3.6 is $A = 4 \cdot 10^{-8} \text{ m}^2$. To estimate R I performed a linear fit in the first $300 \mu\text{s}$ (figure 3.13). In fact, when the FORT contains few atoms the loading rate R is much greater than the two loss rates (γ and β). Seeing the plot 3.11 (up) we assume that until $300 \mu\text{s}$ we are in a linear regime.

$$\langle N \rangle(t) = Rt$$

Fitting with this linear model I obtain $R = (2.7 \pm 0.5) \times 10^5 \text{ s}^{-1}$ which implies a trapping probability $P_{\text{trap}} = 0.3$.

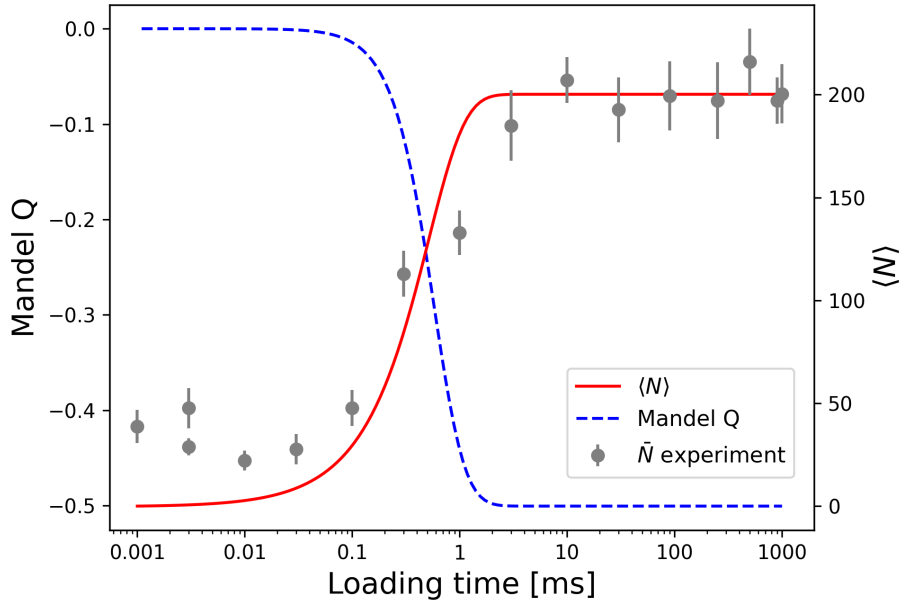


Figure 3.14: Evolution over time of mean value and Mandel-Q of the Markov chain model. Parameters used: $R = 2.7 \cdot 10^5 \text{ s}^{-1}$, $\beta = 6.7 \text{ s}^{-1}$, and $\gamma = 1 \text{ s}^{-1}$.

The one-body collisions rate: γ

The one-body losses are due to collisions between trapped atoms and background atoms at vapour temperature. So, stronger vacuum regimes permit to reach lower one-body collision rates. To give an order of magnitude to this quantity we can observe that two-body collisions, which are induced by the MOT beams, are the most relevant process while the FORT is filling. Instead, while the FORT is emptying, the MOT beams are off, and the one-body collisions are the most relevant process. By this consideration we can assume that the order of magnitude of $1/\gamma$ is equal to the order of magnitude of the FORT lifetime. We measured a lifetime of about 1 s, so, $\gamma \simeq 1 \text{ s}^{-1}$, for a FORT depth of 1.6 mK.

The two-body collisions rate: β

The two-body collisions depend mainly on the trapping volume size, particularly in the model proposed by [28], β is inversely proportional to the volume. Since the volume is proportional to the waist to the four², $V \propto w_0^4$, the parameter $\beta \propto w_0^{-4}$.

²One can approximate the volume with a cylinder. It will be proportional to $z_r w_0^2$. Since $z_r \propto w_0^2$ we finally get $V \propto w_0^4$.

That means that with a smaller FORT (i.e. smaller waist) the two-body collisions become more relevant. To estimate an order of magnitude for β we can observe the steady state of the data shown figure 3.11. Neglecting the one-body collisions, in the stationary state the loss and the loading must be equal,

$$R = \beta \frac{N(N - 1)}{2}$$

Knowing R we can calculate β using,

$$\beta = \frac{2R}{N^2}$$

We estimated $R = 2.7 \cdot 10^5 \text{ s}^{-1}$, so $\beta = 6.7 \text{ s}^{-1}$.

Figure 3.14 shows the evolution of the model using the estimated parameters $R = 2.7 \cdot 10^5 \text{ s}^{-1}$, $\gamma = 1 \text{ s}^{-1}$, and $\beta = 6.7 \text{ s}^{-1}$. The figure reports also the *Mandel-Q* parameter of the distribution of the model. In the stationary state of the model the statistics of the number of atoms in the FORT is sub-Poissonian. In the next section, I will show that thanks to this sub-Poissonian trend, it is possible to trap a single atom. Figure 3.16 (a) shows the histogram of the stationary state distribution.

3.4.3 How to trap a single atom

Based on the results obtained in this chapter so far, and using some results from literature, I would like to show how it would be possible to trap a single atom. To reach the goal of building a simple Rydberg Atomtronics device this is primary. Using the expression 3.9 for the steady state distribution of the Markov chain (figure 3.12) I plotted, in figure 3.15, the mean value and the *Mandel-Q* factor of the steady state distribution. Figure 3.16 shows the stationary state distribution for four points in the parameters space pointed out in grey. There is a region in the parameters space where the mean value of the number of atoms presents a plateau with $\langle N \rangle_p = 1$. In this region to capture a single atom is possible. This region exists only if β is big enough $\beta \gtrsim 10^2$. Since $\beta \propto w_0^{-4}$, to have higher β means to have a smaller waist of the FORT beam. In our experiment, for example,

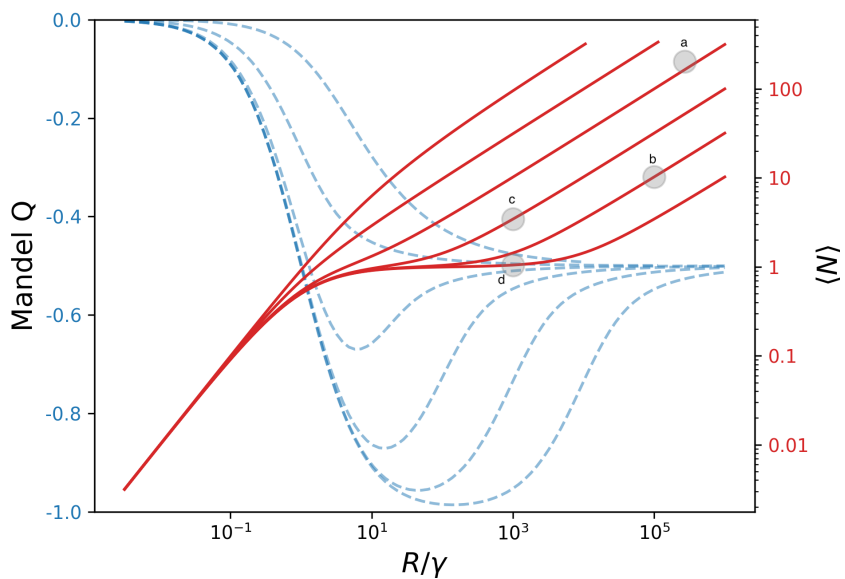


Figure 3.15: The mean value of N and the Mandel- Q are of the stationary distribution are shown for β/γ in the range $(0.1, \dots, 10^5)$ respectively for the red curves from top to bottom. In the x-axis the value of R/γ . The grey circles are drawn in the parameters values used in the histograms of figure 3.16. The point (a) is obtained using the same parameters used for the model in figure 3.14.

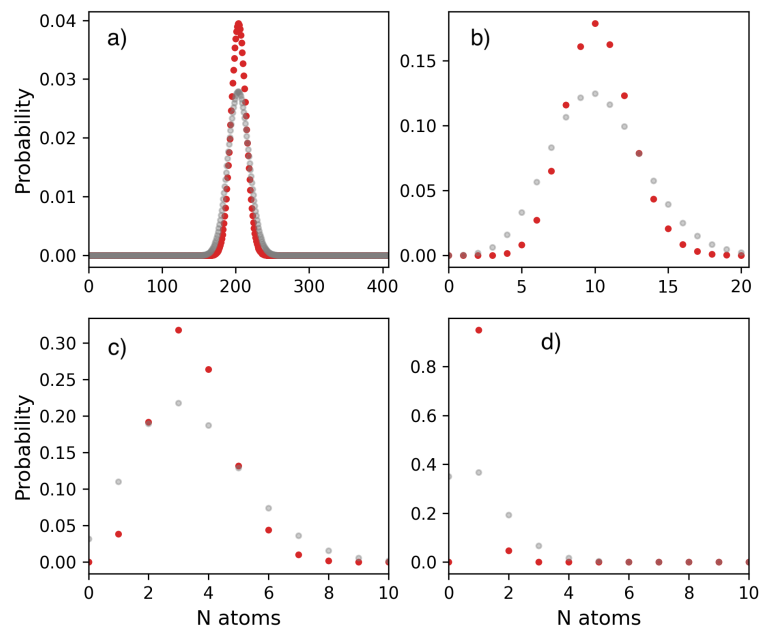


Figure 3.16: Histograms of the steady state distribution of the Markov chain for four sets of parameters. a) $R = 2.7 \cdot 10^5$, $\beta = 6.7$. b) $R = 10^5$, $\beta = 10^3$. c) $R = 10^3$, $\beta = 100$. d) $R = 10^3$, $\beta = 1000$. $\gamma = 1$ for all. All the rates are in s^{-1} . The red points are the stationary state distributions. The grey points are Poisson distributions with the same mean value as the red ones.

to have $\beta = 1000$ we need a waist³ $w_0 = 1.4 \mu\text{m}$. In [2] a similar result is shown. To trap a single atom one needs a waist $w_0 \lesssim 1 \mu\text{m}$. A similar result of what figure 3.15 shows is reported in [2] where N. Schlosser *et. al* studied with a monte-carlo approach the same model. Particularly, they studied the case in which a two-body collision involves the loss of both the colliding atoms (In my case only one atom is lost). They show a similar behaviour, with the difference that the plateau is less than one, $0.5 < \langle N \rangle_p < 1$. Moreover they experimentally observe the sub-Poissonian behaviour of the distribution of the number of atoms, shown in figure 3.16. Y. R. P. Sortais *et. al* [3] also show some experimental data that confirm the sub-Poissonian behaviour and propose a stochastic model, which match with my approach. A protocol to trap a single atom in a FORT, using *light-assisted-collisions*, is proposed by Yin Hsien Fung *et. al* in [1]. They show that the two-body collisions induced by light (a laser resonant with the *trap* transition can be used) can result in the loss of either one or both of the colliding atoms. Depending on the detuning of the used light. Blue detunings corresponds to single atom losses, while red detunings corresponds to double atom losses.

Closing remarks

In the last chapter I presented a characterization of the dipole trap that we set up during my period in the laboratory. I provided a method to estimate the number of atoms in the FORT and the photoionization rate. I concluded discussing the statistics of the loading process and how a single atom can be trap, providing some example from the literature. In the next chapter I will focus on the study of dissipation and interactions of Rydberg atoms.

³I used the relation $\beta = (\beta_m w_{0m}^4)/w_0^4$, where β_m and w_{0m} are the values estimated above in this chapter.

Chapter 4

Facilitation and dissipation for Rydberg Atomtronics

Figure 4.2(a) shows the simplest *Rydberg Atomtronics* circuit one can build: a 1D chain of single atoms in the ground state (blue circles), trapped in an optical tweezers array. We need three essential tools for controlling a Rydberg current flow through the array. In this chapter, these three channels are experimentally tested in two experiments after an introduction of the background. They are schematically shown in figure 4.1 and introduced here.

The *excitation channel*

The first tool we need, in order to control the excitation flux on the chain¹, is an *excitation channel* for the first atom. As shown in section 1.3 an atom can be driven to a Rydberg state by a two-photon process. We use an infrared laser beam $\lambda = 1013 \text{ nm}$ and a blue one $\lambda = 420 \text{ nm}$ to achieve our goal.

The *facilitation channel*

Once we excite the first atom of the chain with this process (figure 4.2(b)) we want the second atom to be excited conditioned on the state of the previous one. Thanks to *facilitation* (introduced in the first chapter) we can excite a ground state atom with an off-resonant laser driving only if another atom in the Rydberg state

¹The simplest Rydbergtronics circuit one could realize in a simple chain, where the transport of Rydberg excitation can be studied.

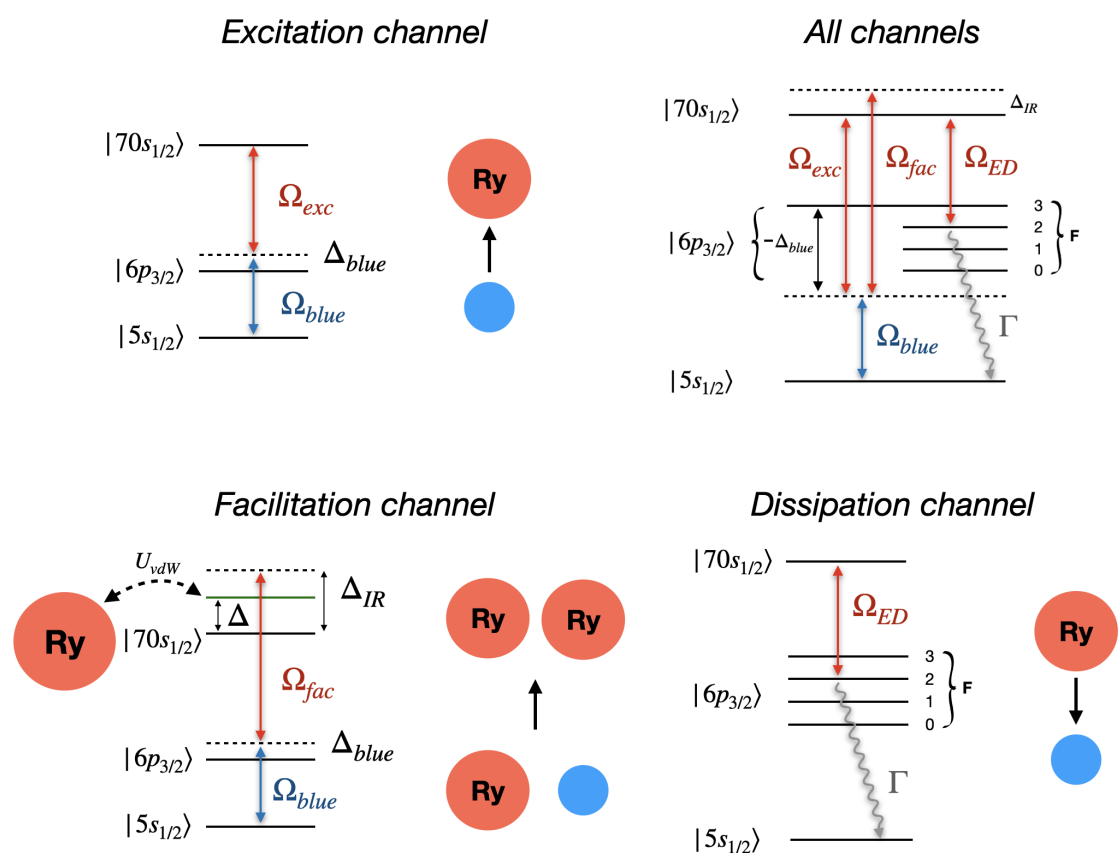


Figure 4.1: The three channels. The top right figure reports a more detailed scheme of the three channels together.

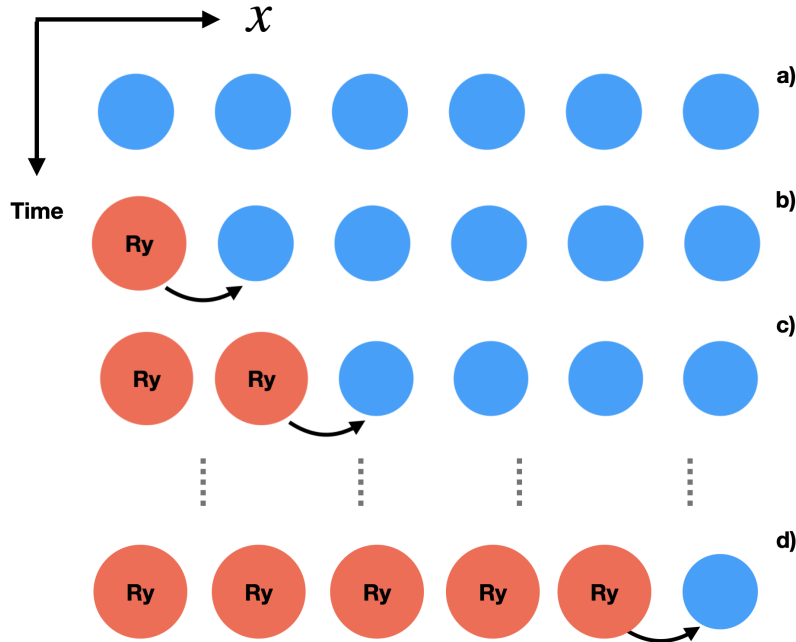


Figure 4.2: *Rydberg current flow in a Rydbergtronics circuit.*

is close enough². In fact, the van der Waals interaction shifts the energy level of the Rydberg state, resulting in two processes: *facilitation* and *Rydberg blockade*. If the energy shift, due to the interaction, matches the detuning of the driving laser, *facilitation* can occur. By this considerations, the second tool we need is an off-resonant excitation channel, I call it the *facilitation channel*. As figure 4.1 (top right) shows, the same laser sources can be used for both³ the *excitation* and *facilitation* channels. Thanks to the fine control we have on the frequency of the laser we can perform frequency shifts of tens of MHz in timescales⁴ of 10ns. The evolution timescales in our experiments are usually in the order of magnitude of few to hundreds of μ s, so we can consider any frequency shift to be instantaneous. Going on by following figure 4.2, using the *facilitation channel*, one could induce a current of Rydberg excitations through the atom array, (c) to (d) in the figure.

Problems from the environment: black-body transitions

The interaction with the environment is not always negligible. When an atom is excited to Rydberg states, the density of states rapidly increases with the prin-

²As shown in the introduction the typical distances to have a significative interaction are few μ m for ^{87}Rb and target Rydberg state $|70s_{1/2}\rangle$.

³See also figure 2.4 for technical details.

⁴This time is mainly due to the rise time of the AOMs.

cipal quantum number, and so the energy difference between consecutive states decreases ($E_n - E_{n+1} \sim n^{-3}$). The black-body radiation from the environment, at room temperature, can induce dipole transitions (either with absorption or stimulated emission) between neighbouring Rydberg states. These processes affect our experiments imposing some limits in the timescales of the system evolution. When many atoms have black-body transitions they drastically change the physics of the studied system. Recently, in the same lab where I conducted this work, [32] studied and characterized the timescales of such transitions, showing that for the state $|70s_{1/2}\rangle$ the black-body radiation limited lifetime is $\sim 100 \mu\text{s}$. The time scales of the system dynamics are governed by the Rydberg atom lifetime, which rapidly grows with n ($\tau \propto n^3$).

The *dissipation channel*

In order to make the black-body transitions negligible we need to speed up the dynamics, in other words we need a faster *dissipation channel*. The engineered dissipation consists in the use of a laser beam that resonantly drives the Rydberg atoms to an intermediate state, which spontaneously decays⁵ to the ground state. As second chapter shows (section 2.3.2), the same laser source used for both the *excitation* and *facilitation* channels can be used also for the *dissipation channel*. The source light is split into two branches, which can be used for both the processes.

As can be seen from the first part of the thesis, we have not an array of atoms yet. We can study the interactions in a many-body disordered system⁶ seeing the emergent behaviours when many atoms interact with each other. Moreover, we can test on it the three channels described above, which have been set up during this work.

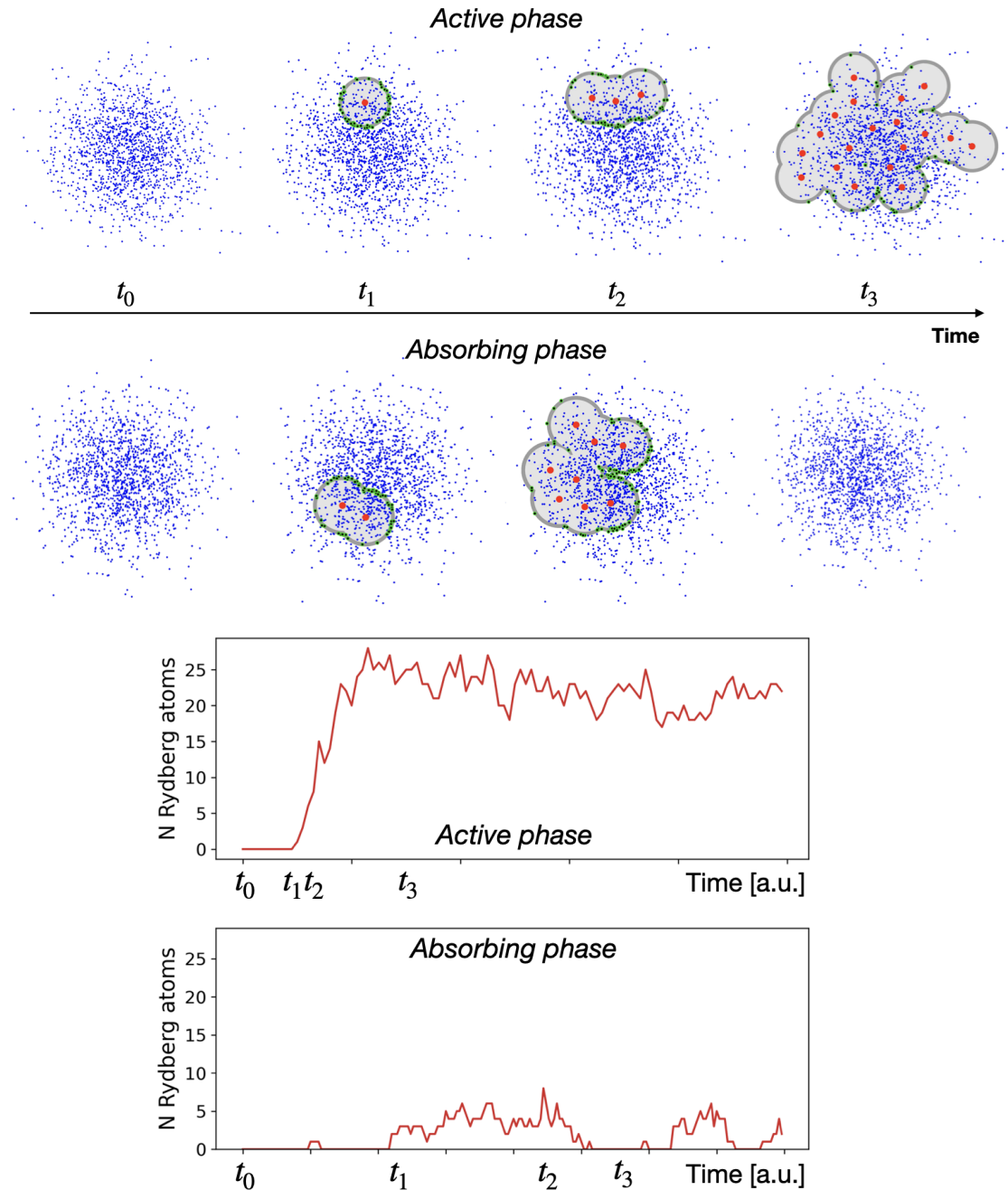


Figure 4.3: Example of evolution of either the active and absorbing phases. (top) shows four screenshot of the evolution in both the phases. The times of the screenshots are marked with t_i . (bottom) the number of Rydberg atoms versus the evolution time. t_i points out the corresponding screenshot. These simulations have the aim of intuitively introduce the two phases.

4.1 Facilitation on a many-body disordered system

Figure 4.3 (t_0) shows a cloud of cold atoms (blue pixels) distributed with a Gaussian distribution in a 2D space⁷. When the *facilitation channel* is switched on, the probability that an atom is excited, when no Rydberg atoms are in its neighbourhood, is low⁸. But, when it does happen, an avalanche of excitations starts thanks to *facilitation*. Actually, that is not always true, because atoms can also spontaneously decay to the ground state. A competition between *facilitation* and spontaneous decay starts, and depending on the ratio of the rates of the two processes, the system can either saturate with Rydberg excitations or remain in a state with few Rydberg atoms, which do not manage to make the avalanche start. A more thorough explanation is provided below.

Absorbing-state phase transition

In [10] it was theoretically shown that such an atomic system governed by long-range interactions belongs to the universality class of directed percolation, where a system switches from an *absorbing* inactive to a fluctuating *active* phase. In [12] the signature of the *absorbing-state phase transition* was experimentally shown. In figure 4.4, I report a plot adapted from their work.

Figure 4.3 shows two simulations that I realized with the aim of intuitively introduce the *absorbing-state phase transition*. The figure show two Gaussian clouds (blue pixels), (top) and (bottom), that evolve respectively in the *active* and *absorbing* phases. When an atom is excited to the Rydberg state (red points) produces a region (dark grey rings) where the atoms (green points) can be *facilitated*. The light grey region around one Rydberg atom is the *blockaded* region. In this area, the energy shift due to interaction is higher⁹ than the driving laser detuning leading to a lower excitation rate.

In the *active* phase, until t_1 any excitation occurred. Then, with only one spon-

⁵We use as intermediate state the $|6p_{3/2}, F = 2\rangle$, which has a life-time of about 112ns [33].

⁶When we cool the atoms with the MOT, they have a mean velocity of about 0.1 m/s. For evolution of the system of few μ s we assume the atoms are at rest.

⁷The distribution of atoms in the MOT can be approximated by a 3D Gaussian.

⁸From expression 1.15, for large detunings the rate scales as Δ^{-2} .

⁹In the light grey region the shift is higher at least by the width of the Rydberg state resonance.

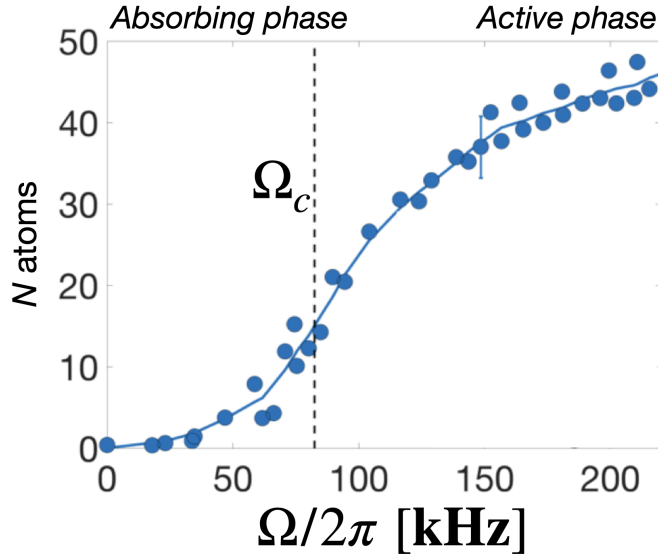


Figure 4.4: *Experimental evidence of the absorbing-state phase transition. Number of Rydberg atoms versus the Rabi frequency. Thermalization time 1.5 ms. Adapted from [12].*

taneous excitation, rapidly the avalanche of excitations saturates the space (t_2 , t_3). In the *absorbing* phase, instead, any attempt of triggering the avalanche fails, keeping the number of Rydberg atoms weakly fluctuating around zero.

In figure 4.4 an experimental evidence of the *absorbing-state phase transition* is shown. The experiment consisted in evolving the system for¹⁰ 1.5 ms, creating some seeds (~ 6) with the *excitation channel* in the first $0.3 \mu\text{s}$ and keeping always on only the *facilitation channel*. At the end, the counting of the number of Rydberg atoms, averaged on a sample of 100 repetitions, is collected and reported on the y-axis. The quantity which governs the rate of *facilitation* is the Rabi frequency Ω (first chapter),

$$\Gamma_{fac} \propto \Omega^2$$

Since the *dissipation channel* in this experiment was the spontaneous decay, which does not change in time, the ratio between the two processes depended only on Ω . So, the x-axis reports Ω .

The number of Rydberg atoms in the thermalized system are close to zero in the *absorbing phase*, and $N \sim (\Omega - \Omega_C)^\beta$ with an exponent $\beta = 0.31 \pm 0.04$ in the *active*

¹⁰The thermalization timescales for the system are governed by the lifetime of the Rydberg atoms, $\tau \sim 151 \mu\text{s}$ for 70s Rydberg state.

phase [12], with Ω_C the Rabi frequency of the critical point. Moreover, In [13] it was experimentally shown that in the *active phase* the system exhibits large fluctuations, or in other words a super-Poissonian behaviour ($Q > 0$). This means that a measurement of the fluctuations can be used to discriminate whether the system is in the *active phase* or not. In section 1.4 a model to intuitively understand this super-Poissonian behaviour is reported. Furthermore, I will show below an experiment we did in the present work, which aims to observe a *facilitation* signature by measuring the fluctuations of the number of Rydberg atoms.

4.1.1 A *facilitation* signature: the fluctuations

Figure 4.5 shows the pulses diagram for the experiment we did. Atoms are cooled to $\sim 120 \mu\text{K}$ with the MOT until point t_0 , reaching a typical density of $\sim 10^{10} \text{ cm}^{-3}$. In fact, differently from previous experiments (third chapter), here the density is crucial. We need higher densities to reach a regime where the van der Waals interaction between Rydberg atoms becomes important. To reach that density regime, we had to optimize the parameters of the MOT. The interval from t_0 to **A** is fixed to $1 \mu\text{s}$ such as to avoid any overlap between the MOT beams and the excitation beams, which could affect the experiment. Between point **A** and **B** all the physics we are interested in happens, we keep the *facilitation channel* on for $100 \mu\text{s}$. In **E**-**F** the electrostatic field field-ionizes only the Rydberg atoms, and then accelerates the resulting positive ions toward the detector. The detection process has a duration of $\sim 30 \mu\text{s}$. We repeated the experimental cycle shown in figure 4.5 100 times, and subsequently calculated the sample mean and the standard deviation. Figure 4.6 shows the number of Rydberg atoms (red points) detected, and the *Mandel-Q* parameter versus the detuning Δ_{IR} of the *facilitation channel*¹¹ (see figure 4.1).

The *Mandel-Q* parameter exhibits an asymmetry with respect to the peak of the Rydberg excitation resonance. The measured value of Q is super-Poissonian ($Q > 0$)¹² for positive detunings $\Delta_{IR} > 0$ and goes to a Poissonian ($Q \simeq 0$) for $\Delta_{IR} < 0$. The super-Poissonian distribution, as shown in section 1.4.1, can be due also to the presence of a jitter on the excitation laser source. The asymmetric trend of the *Mandel-Q* in the figure can be used to discriminate whether the super-Poissonian behaviour is an emergent signature due to *facilitation* or due to

¹¹Actually, when $\Delta_{IR} = 0$ the *facilitation channel* and the *excitation channel* are the same.

¹²We observe Q up to 3.5, which means that the observed variance is about 4 times the mean.

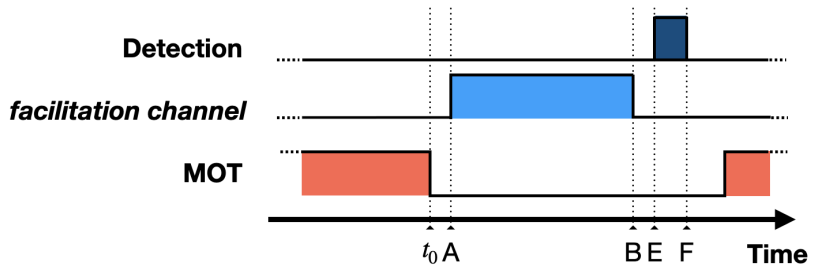


Figure 4.5: Pulses diagram for the facilitation experiment, the results of which are shown in figure 4.6.

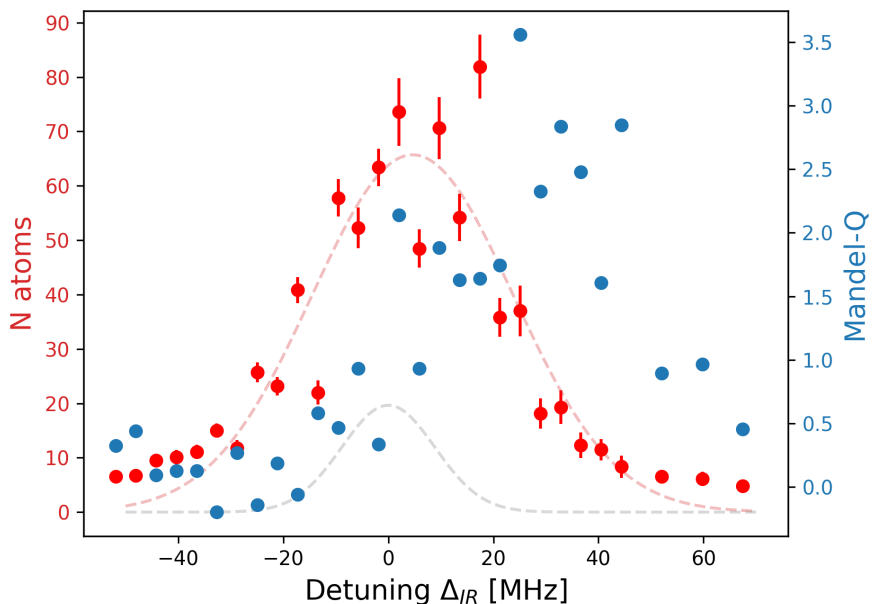


Figure 4.6: Experimental evidence of facilitation. Sample mean (red points) and Mandel-Q parameter (blue points) of 100 repetitions of the experiment, plotted versus the detuning of the facilitation channel (figure 4.1). The red dotted curve is a Gaussian fit as a guide to the eye. The grey dotted curve is the resonance observed in the single atom regime. A shift of the resonance is observed (~ 5 MHz) toward positive detunings. Other relevant parameters: $\Delta_{blue} = -222$ MHz, $\Omega_{2ph} = 500$ kHz. MOT density $d_{MOT} = 3 \cdot 10^{10} \text{ cm}^{-3}$. Evolution time 100 μ s. Data points are corrected with the detection efficiency.

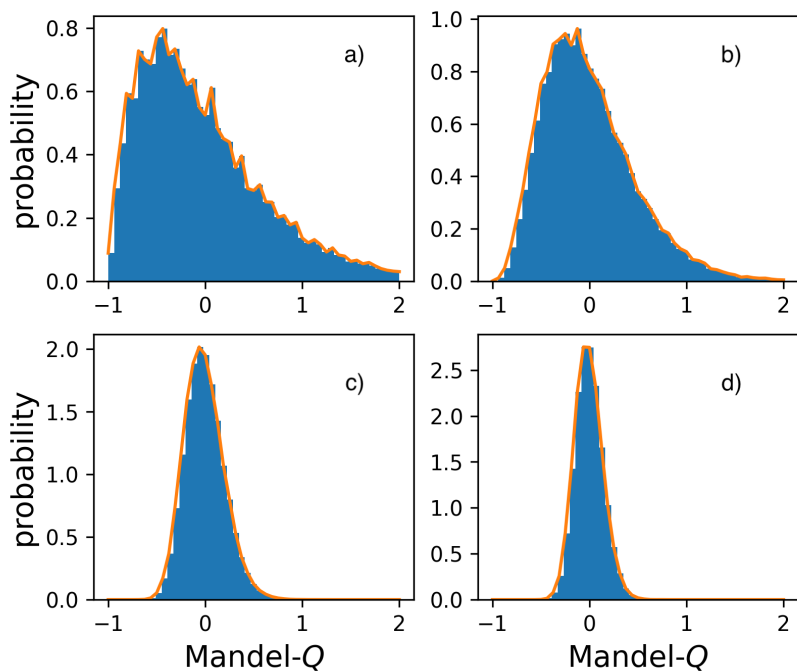


Figure 4.7: Distribution of the Mandel-Q by numerical approach, for different sample sizes. a) 5, b) 10, c) 50, d) 100. I extracted 10000 samples of size (5, 10, 50, and 100) from a Poisson distribution with mean $\mu = 10$, using python. For each sample I computed the Mandel-Q and than I plotted the histogram of it.

the laser jitter. In fact, the presence of a laser jitter should affect the experiment for both positive and negative detunings, independently. By this consideration we exclude that the observed fluctuations are due only to noise.

If figure 4.7 I plotted the distribution of the *Mandel-Q* for different values of the sample size, if the data are distributed with a Poisson distribution. When the sample size is 100, which is our case, the width of the distribution is $\Delta Q \simeq 0.3$. So to have $Q \simeq 3$ for a Poisson distribution it is very unlikely if the data are Poisson distributed.

As discussed at the beginning of this chapter, to speed up the dynamics (and make the black body transitions negligible) we set up an artificial *dissipation channel*. In the next section I will test it, showing some experimental results.

4.2 The artificial dissipation channel

Let's consider a Rydberg atom in a laser beam which resonantly couples the atom to an intermediate state, with a Rabi frequency Ω_{ED} (figure 4.8 reports a scheme). The rate for the atom to be deexcited to the intermediate state is equal to the rate for the inverse process. As shown in the introduction (section 1.3.4), in the incoherent regime, this rate is,

$$\Gamma_{dep} = \frac{\Omega_{ED}^2}{2\gamma}$$

where γ is the dephasing rate. When the atom is in the intermediate state, two processes can happen, either the atom absorbs a photon and is excited back in the Rydberg state or spontaneously decays to the ground (the spontaneous decay rate is Γ). If the spontaneous decay is much faster than the absorption rate ($\Gamma \gg \Gamma_{dep}$), then we assume instant the decay and the rate for the atom to end up in the ground state is equal to Γ_{dep} .

$$\Gamma_{r \rightarrow g} = \Gamma_{dep}$$

In this regime the dynamics reduces to a classical two-level system evolution, where the rate to be excited is Γ_{exc} and the decay rate is Γ_{dep} (figure 4.9). The

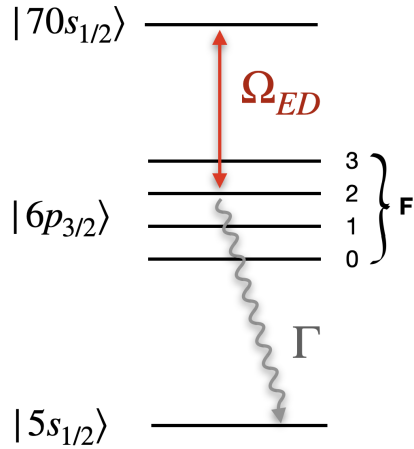


Figure 4.8: A scheme of the dissipation channel. A resonant laser beam couple the Rydberg state with the intermediate state, then the atom spontaneously decays to the ground state, with a rate Γ much grater than the incoherent deexcitation rate of the top transition.

evolution is given by the following system,

$$\frac{d\bar{p}}{dt} = \bar{p}A \quad ; \quad A = \begin{pmatrix} -\Gamma_{exc} & \Gamma_{exc} \\ \Gamma_{dep} & -\Gamma_{dep} \end{pmatrix}$$

which corresponds to

$$\begin{cases} \dot{\bar{p}_g} = -p_g\Gamma_{exc} + p_r\Gamma_{dep} \\ \dot{\bar{p}_r} = +p_g\Gamma_{exc} - p_r\Gamma_{dep} \end{cases}$$

where \bar{p} is the probability vector which describes the state

$$\bar{p} = \begin{pmatrix} p_g \\ p_r \end{pmatrix}$$

Using a frequentist approach I define these probabilities as,

$$p_g = \frac{N_g}{N} \quad ; \quad p_r = \frac{N_r}{N}$$

where N is the total number of atoms in the interaction volume, N_g and N_r are the number of atoms respectively in the ground and in the Rydberg states. Since in the interaction volume we estimated to have ~ 1000 atoms, and during the

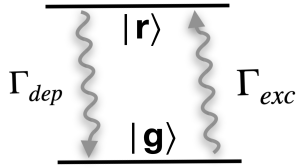


Figure 4.9: A scheme of the two level system in the incoherent regime.

experiments (figure 4.11) we excite less than 10 atoms, I assume that $N_g/N \simeq 1$. Multiplying both sides of the equation by N the evolution is approximated by the following equation

$$\frac{dN_r}{dt} = R - \Gamma_{dep}N_r \quad (4.1)$$

Where $R = \Gamma_{exc}N$ is a fixed rate and N_r is the number of Rydberg atoms. When only the *excitation channel* is on ($\Gamma_{dep} = 0$) and the initial condition is $N_r = 0$ the solution is

$$N_r(t) = Rt \quad (4.2)$$

else, when both the *excitation* and *dissipation* channels are on, the solution is,

$$N_r(t) = \frac{R}{\Gamma_{dep}} + Ce^{-\Gamma_{dep}t} \quad (4.3)$$

where C is a constant which can be computed imposing the initial conditions. Using $N_r = 0$ becomes,

$$N_r(t) = \frac{R}{\Gamma_{dep}} (1 - e^{-\Gamma_{dep}t}) \quad (4.4)$$

We can clearly see that the stationary state of the system is,

$$N_s = \frac{R}{\Gamma_{dep}} \quad (4.5)$$

The experimental results are shown and discussed in the section below.

4.2.1 Double dissipation experiment

Figure 4.10 reports the pulses diagram of the experiment. Similarly to the *facilitation* experiment, atoms are first cooled with the MOT. Then, the *excitation* and

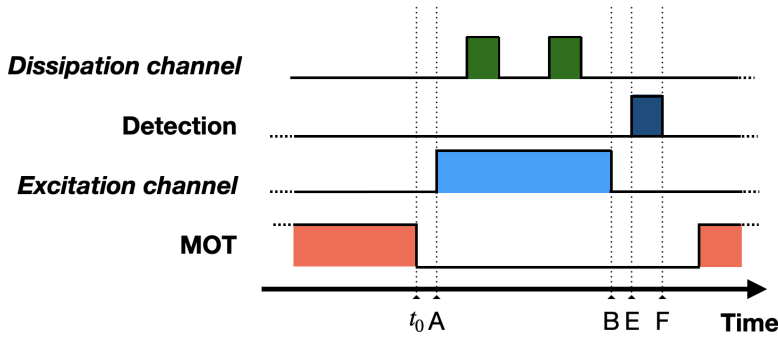


Figure 4.10: Pulses diagram for the dissipation experiment, the results of which are shown in figure 4.11.

dissipation channels are pulsed on, and at the end the Rydberg atoms are detected. The sample mean and the *Mandel-Q* parameter is computed for each point (of figure 4.11) with 100 repetitions of the experiment.

Figures 4.11 show the result of the experiments. We repeated twice the experiments with different parameters to show that we can control the speed of the dynamics playing with the two channels. Additionally, in order to demonstrate the reversibility and repeatability of the dynamics within the same evolution, we carried out a double dissipation in each experiment. In figure (top) the system evolves for $50 \mu\text{s}$ while in figure (bottom) for $25 \mu\text{s}$. The black points are obtained keeping always on both the *excitation* and *dissipation* channels, the violet points are obtained keeping always on the *excitation channel* and switching on the *dissipation* only in the negative slopes regions. The brown points (fig. 4.11 top) are obtained by keeping only the *excitation channel* on. The grey dotted curves are fits with either a linear (expression 4.2) or exponential (expression 4.3) model.

In each graph there are two linear fits and two exponential fits for the purple points, and an exponential fit for the black points. To determine R and Γ_{dep} , I calculated the mean of the rates estimated by the two pairs of fits. For the experiment reported in fig. 4.11 (top) the results are (expressed in MHz),

$$R = 0.123 \pm 0.005 ; \quad \Gamma_{dep} = 0.31 \pm 0.16$$

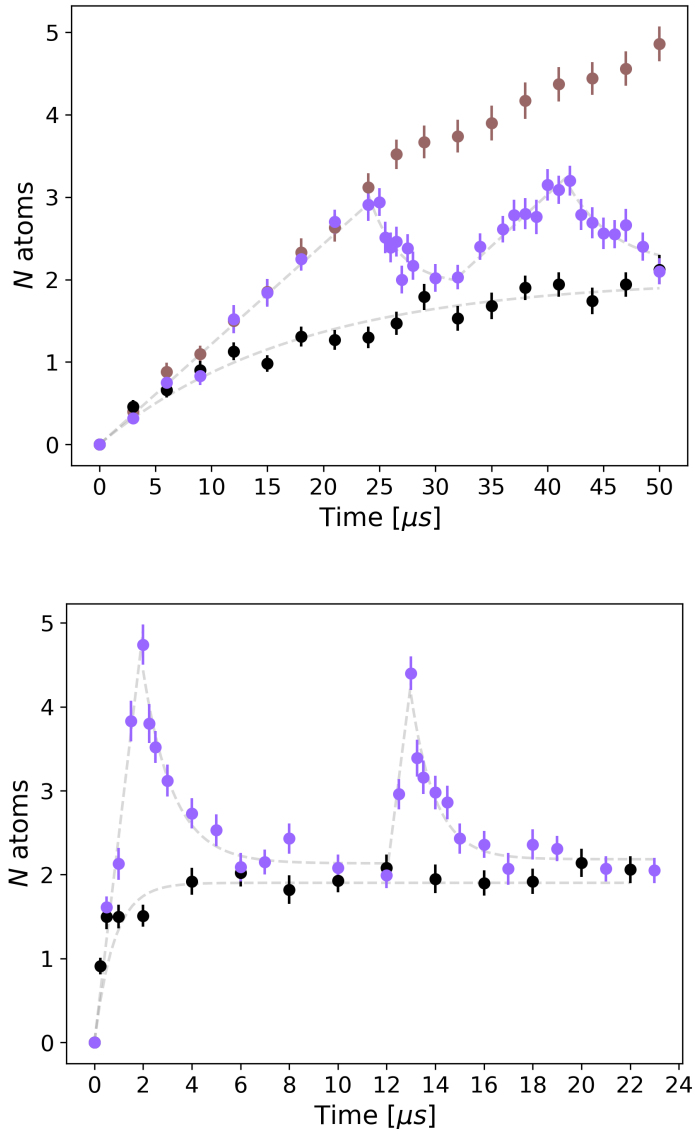


Figure 4.11: The double dissipation experiment. (top): excitation only (brown points), dissipation and excitation always (black points), and dissipation on in the intervals $[25, 30]$ and $[42, 50]$ (violet). (bottom) dissipation and excitation always (black points), dissipation on in the intervals $[2, 12]$ and $[13, 23]$ (violet). The dotted grey curves are fits with the linear models (expression 4.2) or the exponential models (expression 4.3). MOT density $d_{\text{MOT}} = 3 \cdot 10^9 \text{ cm}^{-3}$, data points are not rescaled by α .

while, for the experiment in fig. 4.11 (bottom) (expressed in MHz),

$$(\text{bottom}) \quad R = 2.4 \pm 0.2 \quad ; \quad \Gamma_{dep} = 0.90 \pm 0.21$$

So, using the engendered dissipation, we demonstrated that we were able to gain two orders of magnitude for the *dissipation* rate with respect to the spontaneous decay rate.

Closing remarks

In the last chapter, I introduced the three channels built with the aim of controlling the Rydberg current flow in an array of ^{87}Rb atoms: *excitation channel*, *facilitation channel*, and *dissipation channel*. In the first section the *absorbing-state phase transition* is introduced and an experimental evidence of *facilitation* in a many-body system, using the *facilitation channel* set up during this work, is reported. Then, in the last section also the *dissipation* has been tested in the two carried out experiments. After this work, the next experiment will consist of combining *facilitation* and *dissipation* with the aim of artificially controlling the critical point of the *absorbing-state phase transition*, resulting in faster dynamics.

Conclusions

The goal of this thesis was to experimentally prepare the basic tools and methods for a long-term project that aims to realize a simple Rydberg Atomtronics circuit. Before doing the experiments, we calibrated the detector by measuring the *detection efficiency* of the channeltron¹³, using the measurement of a CCD as reference signal (section 2.4.1). Moreover, I give an estimation of the *dead time* of the detector.

The first target in my thesis was to estimate the number of atoms trapped in the dipole trap. This was a challenging task because of the limits of the detection. During the detection, in fact, the atoms are photoionized (or field-ionized after Rydberg excitation), and the resulting ions are accelerated toward the detector by an electric field. When many atoms are ionized, they will repel each other, resulting in the loss of most of them (section 2.3.2) and an affected measurement. Moreover, the *dead time* of the detector (section 2.4.1) imposes a saturation limit for the detection, so even "non-interacting" ions can saturate the detection. Typically we observed a saturation at 30 – 40 ions measured per experiment, when photoionization readout is used. The method I proposed to measure the number of atoms trapped consists of performing multiple measurements on the dipole trap with a short photoionization pulse, with the purpose of emptying the trap piecemeal. Then, summing all the results, one can obtain the total number of atoms trapped. We repeated the experiment for different depths¹⁴ of the dipole trap, observing a value between almost 500 atoms for a depth of 1.6 mK to a few atoms for a depth of 0.3 mK (section 3.2). Finally, I provided a model to describe the obtained experimental data that consists of assuming that the density in the MOT is limited by the same processes that limit the density in the dipole trap.

¹³The channelton is a charge multiplier.

¹⁴The depth of a dipole trap is the minimum of the potential / the maximum of the intensity.

With this model we estimated the same order of magnitude for the number of atoms than the experimental results obtained for higher depths, while incompatible order of magnitudes were found for shallower traps.

The second task I completed aimed to characterize the loading time of the dipole trap (section 3.4). By experiment, I showed it to be on the order of magnitude of 10 ms. I proposed a continuous-time Markov chain to describe the dipole trap loading, and I used this model to estimate the order of magnitude of the quantities that govern the evolution. In fact, three rates can be defined: the loading rate R , the one-body losses rate γ (due to collisions with background gas atoms), and the two-body losses rate β (due to collisions between two trapped atoms) (section 3.4). Then, this result was used to collocate our set-up into a picture of the parameter space and discuss how a single atom could be trapped, using some results from the literature (section 3.4.3). Particularly, two-body collisions can be used to limit the number of atoms trapped to one. To achieve that, the two-body collision rate must be higher than our result ($\beta > 100$), which practically means that the waist¹⁵ of the dipole trap laser beam must be $w_0 \lesssim 1 \mu\text{m}$; in our case, by contrast, due to limitations imposed by our current setup we had $w_0 \simeq 5 \mu\text{m}$ and $\beta \sim 10 \text{ s}^{-1}$.

The last task was to set up and test the excitation laser system, composed simultaneously of three channels: *excitation*, *facilitation*, and *dissipation*. Starting from an already prepared laser source, I set up the optical path to reach the atoms (technical details are reported in section 2.3.2). Because of technical limitations (only one source for three independent channels), the *facilitation channel* can be detuned up to 30 MHz if one wants to use it simultaneously with the *dissipation channel*, otherwise 80 MHz is the upper bound. I conclude by showing some results obtained on a many-body disordered system, experimentally demonstrating that the above requirements can be satisfied in our setup. With the *facilitation channel*, I showed and discussed an experimental signature of *facilitation*. When the system is in the *active* phase, the fluctuations increase, resulting in a super-Poissonian statistics for the number of excited Rydberg atoms. The ratio variance/mean can be used to discriminate whether the system presents an emergent signature due to *facilitation*. A super-Poissonian statistics can be due also because of a noisy lasers source

¹⁵The waist is defined as the radial width of a Gaussian beam. Particularly, is the value of the radius where the intensity is $1/e^2$ the maximum, in the focal point of the beam.

(section 1.4.1), which should affect the experiment for both positive and negative detunings, independently. An asymmetric trend was observed for the *Mandel-Q* so we exclude that it is due only to the laser frequency noise.

In conclusion, with the *dissipation channel* we demonstrated to be able to reach $\sim 1 \text{ MHZ}$ of rate¹⁶. Reversibility and repeatability of the dynamics in a single evolution of the system were tested, performing a double excitation-dissipation experiment (section 4.2.1).

Outlooks

In upcoming experiments, the process of trapping a single atom is expected to be a relatively straightforward task. By making certain improvements to the current setup, such as reducing the waist of the dipole trap, we can potentially achieve successful trapping of a single atom. As discussed in the conclusions, It is particularly important to have a smaller waist; a value of $w_0 \lesssim 1 \mu\text{m}$, is necessary for this achievement. Before doing so, one could investigate the dynamics of systems of interacting Rydberg atoms trapped with a dipole trap rather than a MOT, momentarily deviating from the final goal of the project. The advantages would be having a smaller (hundreds compared to thousands) and colder ($\sim 10 \mu\text{K}$ instead of $\sim 100 \mu\text{K}$) set of atoms, which would make it possible to study many-body dynamics on a longer timescale.

Another important step will be to test the *facilitation* and *dissipation* channels simultaneously. This is also challenging because it will require tackling the technical problem of aligning all three channels with each other. The experiments on *facilitation*, in particular, required special attention in this aspect. If the laser is not well aligned with the highest density zones of the MOT, no emergent effects due to interactions are observed. After this, it will be possible to observe the *absorbing-state phase transition* with faster dynamics (i.e., shorter evolution time to reach thermalization), in which the black body radiation induced transitions will be negligible.

¹⁶The rate is a classical rate, since the system evolve in the inchoerent regime.

Bibliography

- [1] Y. H. Fung, P. Sompet and M. F. Andersen. Single Atoms Preparation Using Light-Assisted Collisions. 2016. DOI: [10.3390/technologies4010004](https://doi.org/10.3390/technologies4010004)
- [2] N. Schlosser, G. Reymond, and P. Grangier. Collisional Blockade in Microscopic Optical Dipole Traps. 2002. DOI: [10.1103/PhysRevLett.89.023005](https://doi.org/10.1103/PhysRevLett.89.023005)
- [3] Y. R. P. Sortais, A. Fuhrmanek, R. Bourgain, and A. Browaeys. Sub-Poissonian atom-number fluctuations using light-assisted collisions. 2012. DOI: [10.1103/PhysRevA.85.035403](https://doi.org/10.1103/PhysRevA.85.035403)
- [4] T. F. Gallagher. Rydberg Atoms. 1988. DOI: [10.1088/0034-4885/51/2/001](https://doi.org/10.1088/0034-4885/51/2/001)
- [5] J. Han, Y. Jamil, D. V. L. Norum, P. J. Tanner, and T. F. Gallagher. Rb nf quantum defects from millimeter-wave spectroscopy of cold ^{85}Rb Rydberg atoms. 2006. DOI: [10.1103/PhysRevA.74.054502](https://doi.org/10.1103/PhysRevA.74.054502)
- [6] N. Sibalic and C. S. Adams. Rydberg physics. 2018. DOI: [10.1088/978-0-7503-1635-4ch1](https://doi.org/10.1088/978-0-7503-1635-4ch1)
- [7] A. Browaeys, D. Barredo, and T. Lahaye. Experimental investigations of dipole-dipole interactions between a few Rydberg atoms. 2016. DOI: [10.1088/0953-4075/49/15/152001](https://doi.org/10.1088/0953-4075/49/15/152001)
- [8] M. Marcuzzi, J. Schick, B. Olmos and I. Lesanovsky. Effective dynamics of strongly dissipative Rydberg gases. 2014. DOI: [10.1088/1751-8113/47/48/482001](https://doi.org/10.1088/1751-8113/47/48/482001)
- [9] D. Manzano. A short introduction to the Lindblad Master Equation. 2020. DOI: [10.1063/1.5115323](https://doi.org/10.1063/1.5115323)

- [10] M. Marcuzzi, E. Levi, W. Li, J. P. Garrahan, B. Olmos and I. Lesanovsky. Non-equilibrium universality in the dynamics of dissipative cold atomic gases. 2015. DOI: [10.1088/1367-2630/17/7/072003](https://doi.org/10.1088/1367-2630/17/7/072003)
- [11] O. Morsch, I. Lesanovsky. Dissipative many-body physics of cold Rydberg atoms. 2018. DOI: [10.1393/ncr/i2018-10149-7](https://doi.org/10.1393/ncr/i2018-10149-7)
- [12] R. Gutierrez, C. Simonelli, M. Archimi, F. Castellucci, E. Arimondo, D. Ciampini, M. Marcuzzi, I. Lesanovsky, and O. Morsch. Experimental signatures of an absorbing-state phase transition in an open driven many-body quantum system. 2017. DOI: [10.1103/PhysRevA.96.041602](https://doi.org/10.1103/PhysRevA.96.041602)
- [13] C. Simonelli, M.M. Valado, G. Masella, L. Asteria, E. Arimondo, D. Ciampini, and O. Morsch. Seeded excitation avalanches in off-resonantly driven Rydberg gases. 2016. DOI [10.1088/0953-4075/49/15/154002](https://doi.org/10.1088/0953-4075/49/15/154002)
- [14] L. Amico *et al.* Roadmap on Atomtronics: State of the art and perspective. 2021. DOI: [10.1116/5.0026178](https://doi.org/10.1116/5.0026178)
- [15] P. M. Baker, J. A. Stickney, M. B. Squires, J. A. Scoville, E. J. Carlson, W. R. Buchwald, and S. M. Miller. Adjustable microchip ring trap for cold atoms and molecules. 2009. DOI: [10.1103/PhysRevA.80.063615](https://doi.org/10.1103/PhysRevA.80.063615)
- [16] C. Cohen-Tannoudji and D. Guéry-Odelin. Advances in Atomic Physics: An Overview. 2011. DOI: <https://doi.org/10.1142/6631>
- [17] Claude Cohen-Tannoudji, David Guéry-Odelin. ADVANCES IN ATOMIC PHYSICS.
- [18] I. H. Deutsch. Harnessing the Power of the Second Quantum Revolution. 2020. DOI: [10.1103/PRXQuantum.1.020101](https://doi.org/10.1103/PRXQuantum.1.020101)
- [19] M. Endres, H. Bernien, A. Keesling, H. Levine, E. R. Anschuetz, A. Krajenbrink, C. Senko, V. Vuletic, M. Greiner, and M. D. Lukin. Atom-by-atom assembly of defect-free one-dimensional cold atom arrays. 2016. DOI: [10.1126/science.aah3752](https://doi.org/10.1126/science.aah3752)
- [20] F. Perciavalle, D. Rossini, T. Haug, O. Morsch, L. Amico. Controlled flow of excitations in a ring-shaped network of Rydberg atoms. 2022. Corpus ID: 255096327 Preprint: arXiv:2212.12490

- [21] S. C. Caliga, C. J. E. Straatsma and D. Z. Anderson. Experimental demonstration of an atomtronic battery. 2017. DOI [10.1088/1367-2630/aa56d8](https://doi.org/10.1088/1367-2630/aa56d8)
- [22] J. G. Lee, B. J. McIlvain, C. J. Lobb and W. T. Hill. Analogs of Basic Electronic Circuit Elements in a Free-Space Atom Chip. 2013. DOI: [10.1038/srepo1034](https://doi.org/10.1038/srepo1034)
- [23] C. Ryu, P. W. Blackburn, A. A. Blinova, and M. G. Boshier. Experimental realization of Josephson junctions for an atom SQUID. 2013. DOI: [10.1103/PhysRevLett.111.205301](https://doi.org/10.1103/PhysRevLett.111.205301)
- [24] E. R. Elliott, M. C. Krutzik, J. R. Williams, R. J. Thompson, and D. C. Aveline. NASA's cold atom lab (CAL): system development and ground test status. 2018. DOI: [10.1038/s41526-018-0049-9](https://doi.org/10.1038/s41526-018-0049-9)
- [25] S. Palacios Alvarez, P. Gomez, S. Coop, and M. W. Mitchell. Single-domain Bose condensate magnetometer achieves energy resolution per bandwidth below \hbar . 2022. DOI: <https://doi.org/10.1073/pnas.2115339119>
- [26] L. Henriet, L. Beguin, A. Signoles, T. Lahaye, A. Browaeys, G. O. Reymond, and C. Jurczak. Quantum computing with neutral atoms. 2020. DOI: <https://doi.org/10.22331/q-2020-09-21-327>
- [27] R. Grimm, M. Weidemüller, and Y. B. Ovchinnikov. Optical dipole traps for neutral atoms. 1999. DOI: [https://doi.org/10.1016/S1049-250X\(08\)60186-X](https://doi.org/10.1016/S1049-250X(08)60186-X)
- [28] S. J. M. Kuppens, K. L. Corwin, K. W. Miller, T. E. Chupp, and C. E. Wieman. Loading an optical dipole trap. 2000. DOI: <https://doi.org/10.1103/PhysRevA.62.013406>
- [29] G. F. Knoll. Radiation Detection and Measurement. 1999. ISBN: 978-0-470-13148-0
- [30] V. Bécares and J. Blàzquez. Detector Dead Time Determination and Optimal Counting Rate for a Detector Near a Spallation Source or a Subcritical Multiplying System. 2012. DOI: [10.1155/2012/240693](https://doi.org/10.1155/2012/240693)
- [31] M. L. Larsen and A. B. Kostinski. Simple dead-time corrections for discrete time series of non-Poisson data. 2009. DOI: [10.1088/0957-0233/20/9/095101](https://doi.org/10.1088/0957-0233/20/9/095101)

- [32] M. Archimi, M. Ceccanti, M. Distefano, L. Di Virgilio, R. Franco, A. Greco, C. Simonelli, E. Arimondo, D. Ciampini, and O. Morsch. Measurements of blackbody-radiation-induced transition rates between high-lying S, P, and D Rydberg levels. 2022. DOI: [10.1103/PhysRevA.105.063104](https://doi.org/10.1103/PhysRevA.105.063104)
- [33] J. Marek and P. Munster. Radiative lifetimes of excited states of rubidium up to quantum number $n=12$. 1980. DOI: [10.1088/0022-3700/13/9/008](https://doi.org/10.1088/0022-3700/13/9/008)
- [34] H. Friedrich. Theoretical Atomic Physics. 2017. ISBN: 978-3-319-47769-5
- [35] S. Sevinçli and T. Pohl. Microwave control of Rydberg atom interactions. 2014. doi:[10.1088/1367-2630/16/12/123036](https://doi.org/10.1088/1367-2630/16/12/123036)
- [36] F. Bensch. Experimental setup and characterization of a dipole trap. Master's thesis, University of Pisa, 2023.
- [37] C. Simonelli. Dissipative and non-dissipative many-body physics with cold Rydberg atoms. PhD's thesis, University of Pisa, 2017.
- [38] G. Cichelli. Engineered dissipation for cold Rydberg atoms. Master's thesis, University of Pisa, 2022.
- [39] M. Archimi. Experimental studies of the blackbody induced population migration in dissipative Rydberg systems. PhD's thesis, University of Pisa, 2019.